

Distribution agreement

In presenting this thesis or dissertation as a partial fulfillment of the requirements for an advanced degree from Emory University, I hereby grant to Emory University and its agents the non-exclusive license to archive, make accessible, and display my thesis or dissertation in whole or in part in all forms of media, now or hereafter known, including display on the world wide web. I understand that I may select some access restrictions as part of the online submission of this thesis or dissertation. I retain all ownership rights to the copyright of the thesis or dissertation. I also retain the right to use in future works (such as articles or books) all or part of this thesis or dissertation.

Signature:

Paul Gregory Donlin-Asp

SMN functions as a molecular chaperone for mRNP assembly.

By

Paul Gregory Donlin-Asp
Doctor of Philosophy

Biochemistry, Cell and Developmental Biology

Dr. Gary J. Bassell, PhD
Advisor

Dr. Anita Corbett, PhD
Committee Member

Dr. Yue Feng, MD, PhD
Committee Member

Dr. Kenneth Moberg, PhD
Committee Member

Dr. James Q. Zheng, PhD
Committee Member

Accepted:

Lisa A. Tedesco, Ph.D.
Dean of the James T. Laney School of Graduate Studies

Date

SMN functions as a chaperone for mRNP assembly.

By

Paul Gregory Donlin-Asp

BS, University of Illinois Urbana-Champaign, 2009

Advisors: Gary J. Bassell, PhD

An abstract of

A dissertation submitted to the Faculty of the
James T. Laney School of Graduate Studies of Emory University
in partial fulfillment of the requirements for the degree of

Doctor of Philosophy

in Graduate Division of Biological and Biomedical Sciences
Biochemistry, Cell, and Developmental Biology

2016

Abstract

Spinal muscular atrophy (SMA) is a neuromuscular disease characterized by a specific degeneration of motor neurons. SMA results from a reduction in the survival of motor neuron (SMN) protein. We have previously shown specific defects in the axonal localization of poly A mRNA (including *β -actin* and *Gap43*) and mRNA-binding proteins (HuD, IMP1) in SMN-deficient motor neurons. Our findings led us to hypothesize that SMN plays a role in the assembly of messenger ribonucleoproteins (mRNPs), and that failure to assemble mRNA transport complexes leads to the reported mRNA localization defects in SMA motor neurons.

To test our hypothesis, we have established a trimolecular fluorescence complementation (TriFC) assay as a sensor for the association of mRNAs with RBPs. In motor neurons isolated from a severe SMA mouse model, as well as primary human fibroblasts from SMA patients, we readily detect a defect in the assembly of complexes containing IMP1 protein and *β -actin* mRNA. Furthermore, RNA immunoprecipitation experiments also show impairments in the association of IMP1 protein with *β -actin* mRNA. Through biochemical fractionation, we observe a consistent shift of IMP1-containing mRNPs toward smaller granules in SMA human fibroblasts. In SMA patient derived fibroblasts, IMP1 granules are consistently reduced in their volume relative to control lines, a phenotype consistent with both our TriFC and fractionation results. Finally, we can show a defect in the association of IMP1 with the cytoskeleton in the SMA patient fibroblasts, suggesting a mechanism to explain reduced mRNA localization reported in SMA motor neurons.

In summary, our results show that SMN plays a more general role in RNP assembly beyond the canonical role in snRNP assembly. Here, we demonstrate that SMN acts as a chaperone for the formation of transport-competent RNA granules, providing a mechanism for mRNA localization defects that may contribute to the motor neuron degeneration observed in SMA.

SMN functions as a chaperone for mRNP assembly.

By

Paul Gregory Donlin-Asp

BS, University of Illinois Urbana-Champaign, 2009

Advisor: Gary J. Bassell, PhD

A dissertation submitted to the Faculty of the
James T. Laney School of Graduate Studies of Emory University
in partial fulfillment of the requirements for the degree of
Doctor of Philosophy
in Graduate Division of Biological and Biomedical Sciences
Biochemistry, Cell, and Developmental Biology
2016

Acknowledgements

The work detailed in this thesis could not have been completed without the support of a number of individuals during my time in graduate training.

I would like to thank both of my advisors on this project, Dr. Gary Bassell and Dr. Wilfried Rossoll, for the support and guidance they have given me during my thesis studies. Additionally for the willingness and encouragement for my participation and attendance at a number of training courses and conferences which expanded my understanding of the field.

I would also like to thank Dr. Claudia Fallini, who was the individual who first trained me and guided me on the start of this project and continued to offer ideas and critical assessment after leaving the lab.

I would like to also thank my thesis committee, Dr. Anita Corbett, Dr. Yue Feng, Dr. Ken Moberg and Dr. James Zheng, for all of the helpful comments and guidance they have provided during the development of my project. Additionally I would like to especially thank Dr. Anita Corbett for the encouragement and support in the pursuit of funding (NIH NRSA and ARCS foundation award) and attendance at the 64th Annual Lindau Nobel Laureate meeting.

Additionally I would like to thank Dr. Katie Williams, Kristen Thomas, Lian Li, Shirley Huang, Jeremy Rouanet and Jazmin Campos for excellent technical and experimental protocol support over the years.

This work was supported by the Muscular Dystrophy Association (MDA) and Weissman Family Foundation to GJB; the US National Institute of Health (NIH) Grant NS091749 to WR; the National Research Service Award (NRSA) training award F31NS084730-01 and ARCS Fellowship Roche Foundation award to PGDA. This research project was supported in part by the Emory University Integrated Cellular Imaging Microscopy Core of the Emory Neuroscience NINDS Core Facilities grant, P30NS055077. This study used samples from the NINDS Cell Line Repository (<http://ccr.coriell.org/ninds>), as well as clinical data. NINDS and NIGMS Repository sample numbers corresponding to the samples used are: ND29178, ND29179, GM09677, and GM00232.

Table of Contents

1. A role for the survival of motor neuron protein in mRNP assembly and transport.....	1
Abstract	2
Introduction.....	3
Spinal Muscular Atrophy is characterized by axonal and synaptic defects	5
The SMA disease protein SMN has an essential role in splicesomal snRNP assembly	6
SMN is actively transported in axons during development.....	8
SMN is required for the axonal delivery of mRNPs	9
SMN is involved in translational regulation	12
Does SMN regulate the assembly of mRNP granules?.....	13
Conclusion	14
Figures.....	16
Figure 1. Mechanisms of axonal mRNA localization and local translation	16
Figure 2. Model for the mislocalization of mRNA observed in SMA motor neurons.....	18
Figure 3. SMN in mRNP assembly and axonal mRNA localization ...	20

2. Spatially and temporally regulating translation via mRNA binding proteins in cellular and neuronal function	22
Abstract	23
Introduction.....	24
1. Polarity- from the basal to apical membranes and beyond.	25
2. Translational regulation in neuronal function.....	28
2.1 Dendrites	28
2.2 Axons	29
3. Dysregulation of local translation in disease	30
3.1 Neurodevelopmental diseases	30
3.2 Neurodegenerative diseases	32
3.3 Axonal injury and repair	35
4. Studying translation regulation: the ever expanding toolbox	35
4.1 Determining where mRNA is in space and time	36
4.2 Defining what are mRNA binding proteins and what mRNAs they bind	38
4.3 Defining what transcripts are being translated and where translation occurs	40
Conclusions and future directions	43
Figures.....	44
Figure 1. Translation Repression in RNA localization.....	44
Figure 2. Local translation in cellular polarity.....	46
Figure 3. Local translation in neuronal function	48
Figure 4. Dysregulation of local translation in disease.....	50

3. The survival of motor neuron protein acts as a molecular chaperone for mRNP assembly	52
Summary	53
Highlights.....	55
Background	56
Results.....	57
Association of IMP1 protein with β -actin mRNA is impaired in cultured motor neurons from a SMA mouse model	57
IMP1 mRNP granules show assembly defects and reduced size in SMA patient fibroblasts	60
IMP1 containing mRNP granules are reduced in volume in SMA patient fibroblasts	62
IMP1 mRNP granules show decreased association with the cytoskeleton in SMA patient fibroblasts	62
Discussion	64
Experimental Procedures	69
Acknowledgments	75
Figures & Tables	77
Figure 1. Trimolecular Fluorescence Complementation (TriFC) allows visualization of RNA and protein association <i>in situ</i>	78
Figure 2. IMP1 and β -actin association is reduced in an SMA mouse model	81
Figure 3. IMP1 and β -actin association is reduced in SMA patient fibroblasts.....	83
Figure 4. IMP1 association with mRNA is impaired in SMA patient fibroblasts.....	85

Figure 5. IMP1 granules show reduced complexity in SMA patient samples	88
Figure 6. IMP1 granules are reduced in size in SMA patient samples and can be rescued by restoring expression of SMN	90
Figure 7. IMP1 complexes show reduced association with the cytoskeleton in SMA fibroblasts	93
Figure 8. SMN functions as a chaperone for IMP1- <i>β-actin</i> granule assembly	97
Supplementary Figure 1. Cytoskeletal proteins show unaltered distributions in SMA fibroblasts	99
Supplementary Figure 3. PABPC1 granules show reduced complexity in SMA patient samples	101
Supplementary Table 1. Statistical comparisons for figure 1D	103
Supplementary Table 2. Statistical comparisons for figure 1E	105
Supplementary Table 3. Statistical comparisons for figure 3B	107
Supplementary Table 4. Statistical comparisons for figure 4B, IMP1 steady state protein levels	110
Supplementary Table 5. Statistical comparisons for figure 4B, SMN steady state protein levels	113
Supplementary Table 6. Statistical comparisons for figure 4E	116
Supplementary Table 7. Statistical comparisons for figure 6D	123
Supplementary Table 8. Statistical comparisons for figure 6F	126
Supplementary Table 9. Statistical comparisons for figure 7B	131
Supplementary Table 10. Statistical comparisons for figure 7D	134
Supplementary Table 11. Statistical comparisons for figure 7E	137
Supplementary Table 12. Statistical comparisons for figure 7G	139
Supplementary Table 13. Statistical comparisons for figure 7I	141
4. Conclusions and future directions	148.
Overview	149
SMN as a chaperone for RNP assembly	150

What mRNA binding proteins are altered in their association with mRNA in SMA?	152
What RNP complexes show alterations in their assembly in SMA? ...	153
What extent <i>in vivo</i> does non-splicing related RNP changes contribute to pathology in SMA?	154
Are defects seen in SMA mouse motor neurons are conserved in patient derived samples?.....	156
Future directions for SMA therapy	157
Why are motor neurons affected in SMA?.....	160
Materials and methods	161
Figures.....	164
Figure 1. Widespread RNA dysfunction likely contributes to SMA pathology and motor neuron death	164
Figure 2. SMN in RNP biogenesis	166
Figure 2. RNA interactome capture to assess mRNP granule composition in SMA patient samples	168
Figure 3. RNP gradient isolation to assess widespread changes in RNP granule size and complexity in SMA patient samples	170
Figure 4. SMA iPSC motor neuron cultures show defects seen in SMA mouse motor neurons	172
Figure 5. Manipulating mRNA levels as a therapeutic strategy in SMA	174
Figure 6. RG3039 increases TriFC signal in cell culture.....	176
Figure 7. RG3039 increases poly(A) RNA signal in treated cells ...	178
Figure 8. Hypo vs Hyper RNP assembly in disease	180

5. Appendix	182
mRNAs are mislocalized from axonal compartments with SMN deficiency	183
GAP43 protein is reduced in SMA growth cones	183
Overexpression of IMP1 and HuD rescues GAP43 axonal deficiency	184
SMN deficiency affects translation at the growth cone.....	185
Materials and methods	187
Figures.....	192
Figure 1. Gap43 and <i>β-actin</i> mRNAs are reduced in axons and growth cones of SMN deficient motor neurons.....	192
Figure 2. GAP43 protein levels are reduced in axonal growth cones of SMA motor neurons	194
Figure 3. SMN deficiency causes reduced local protein synthesis in axonal growth cones	196
Figure 4. Overexpression of HuD and IMP1 restores GAP43 protein and transcript levels in growth cones, as well as axon outgrowth of SMA motor neurons	198
6. References	200

**Chapter 1:
A role for the survival of motor neuron protein in mRNP assembly
and transport**

Paul G Donlin-Asp¹, Gary J Bassell^{1,2} & Wilfried Rossoll¹

¹ Department of Cell Biology, Emory University School of Medicine,
Atlanta, Georgia, USA

² Department of Neurology, Emory University School of Medicine, Atlanta,
Georgia, USA

Current Opinion in Neurobiology, Volume 39 pages 54-61

Co-corresponding authors:

Wilfried Rossoll, Ph.D. and Gary J. Bassell, Ph.D.

Emory University School of Medicine

Whitehead Biomedical Research Building, Room 415

615 Michael St NE

Atlanta, GA. USA 30322

email: wrossol@emory.edu and gbassel@emory.edu

Tel: (404) 727-0668

FAX: (404) 727-0570

Abstract:

Localization and local translation of mRNA plays a key role in neuronal development and function. While studies in various systems have provided insights into molecular mechanisms of mRNA transport and local protein synthesis, the factors that control the assembly of mRNAs and mRNA binding proteins into messenger ribonucleoprotein (mRNP) transport granules remain largely unknown. In this review we will discuss how insights on a motor neuron disease, spinal muscular atrophy (SMA), is advancing our understanding of regulated assembly of transport competent mRNPs and how defects in their assembly and delivery may contribute to the degeneration of motor neurons observed in SMA and other neurological disorders.

Introduction:

Neurons with their highly elaborate branched and elongated structures are the epitome of a functionally and morphologically polarized cell. It has remained a key question how neurons maintain the functional domains of the axon, soma and dendrites to facilitate normal neuronal function across large distances. Pioneering work from the 1960s has demonstrated local protein synthesis in purified synaptosomal preparations (Autilio et al., 1968; Morgan and Austin, 1968) and in isolated mammalian axons (Edstrom and Sjostrand, 1969; Koenig, 1967). These observations gave rise to the hypothesis that localization and local translation of mRNA may provide nerve terminals with an autonomous spatiotemporal control of the local proteome (Holt and Schuman, 2013). While local translation in dendrites has been widely accepted since the identification of polyribosomes at the base of dendritic spines (Steward and Levy, 1982), a lack of easily identifiable polysomes in mature axons has led to the view that local protein synthesis may be a specific feature of dendrites. Recent work demonstrates that translational machinery in axons directly associates with the plasma membrane (Tcherkezian et al., 2010), providing an explanation why it has been difficult to visualize ribosomes in axonal compartments by electron microscopy. Studies from several labs have clearly demonstrated a role for local translation for axonal outgrowth and pathfinding during development (Yoon et al., 2009), as well as in axon

regeneration after nerve injury and in neurodegenerative disease (Baleriola and Hengst, 2015; Baleriola et al., 2014).

We know that, as in all aspects of post-transcriptional regulation of mRNA, protein and mRNA interactions are essential for achieving proper regulation. While basic principles of localization are understood (Figure 1), how proper mRNA-protein associations are regulated *in vivo*, and the very structure of the mRNA transport complexes have remained elusive, and highlight an important gap in our knowledge. Recent work on a motor neuron disease, spinal muscular atrophy, may provide insight into these outstanding questions.

Spinal muscular atrophy (SMA) is caused by reduced levels of survival motor neuron (SMN) protein (Burghes and Beattie, 2009). While SMN has been shown to play an essential role in spliceosomal snRNP assembly (Battle et al., 2006; Gubitzi et al., 2004), work from several labs has demonstrated additional SMN-dependent defects in the localization and local translation of axonal mRNAs (Burghes and Beattie, 2009; Fallini et al., 2012b; Jablonka et al., 2014; Rossoll and Bassell, 2009a). In response to these studies, a more general role for SMN in RNP complex assembly that goes beyond its well characterized function in snRNP assembly and splicing has now been widely accepted (Li et al., 2014b; So et al., 2016). Taken together, it suggests that SMA can be described as a disease of defective RNP assembly, affecting various pathways that regulate mRNA splicing, stability, and localization.

It is the aim of this review, to summarize evidence for a role of SMN in the assembly and delivery of axonal mRNPs, thus linking basic mechanisms in RNP assembly, mRNA localization, and local translation to neurodegenerative disease.

Spinal Muscular Atrophy is characterized by axonal and synaptic defects

Spinal muscular atrophy (SMA) is the leading genetic cause of infant mortality, and the second most common fatal autosomal recessive genetic disorder world-wide (Prior, 2010). SMA is a neurodegenerative disease characterized by progressive denervation of skeletal and intercostal muscles, muscle weakness, paralysis, and eventual death due to respiratory failure . The primary pathology in SMA is a developmental neuromuscular junction (NMJ) synaptopathy (Kariya et al., 2008) followed by degeneration of motor neurons, although there is growing evidence for the involvement of other tissues and cell types in severe cases (Gogliotti et al., 2012; Shababi et al., 2013). Axonal degeneration precedes motor neuron cell death (Cifuentes-Diaz et al., 2002; Monani et al., 2000) and defects at the NMJ are the earliest events detected in SMA mouse models (Goulet et al., 2013; Ling et al., 2012). NMJs are established at a normal rate, followed by structural as well as functional perturbations and maturation defects on the morphological and molecular level (Bowerman et al., 2012; Kariya et al., 2008; Kong et al., 2009), loss of NMJs,

denervation, and onset of muscle atrophy in a subset of specifically sensitive muscles (Fallini et al., 2012b; Goulet et al., 2013). The reason of the specific vulnerability of motor neurons and NMJs in SMA is still largely unknown.

The genetic causes of SMA are mutations or more commonly deletions in the survival of motor neuron (SMN) encoding gene, *SMN1*. Due to an ancient gene duplication, humans carry a single copy of the telomeric *SMN1* gene, and a variable number of centromeric *SMN2* genes. *SMN2* cannot fully compensate for the loss of *SMN1*, since it harbors a human-specific splice-site mutation that inhibits the inclusion of exon7 and results in low levels of full length SMN transcript (Lorson et al., 1999a). SMN is ubiquitously expressed, and is vital for normal cellular function with complete loss of SMN resulting in early embryonic lethality in mice (Schrank et al., 1997).

These findings raised the question how reduced levels of the essential SMN protein can cause the specific pathology observed in SMA.

The SMA disease protein SMN has an essential role in spliceosomal snRNP assembly

SMN localizes to both the cytoplasm and the nucleus where it is assembled in an unknown manner with eight other proteins (Gemins2–8 and Unrip) to form a large macromolecular complex (Li et al., 2014b). SMN and all gemins tested so far are essential for viability, indicating an

important role in a basic cellular function. SMN and its associated proteins is that of a molecular chaperone for spliceosomal snRNP assembly (Grimmler et al., 2005; Li et al., 2014b; Otter et al., 2007; Pellizzoni et al., 2002) (Burghes and Beattie, 2009). The SMN complex assists in the assembly of heptameric member ring of spliceosomal Sm proteins on the uridine rich stretch found in all snRNAs, to ensure specificity in the assembly of the snRNP particles (Meister et al., 2001; Pellizzoni et al., 2002). In addition to the classical snRNP biogenesis pathway, SMN has also been found to directly function in the maturation of the U7 snRNP, which functions in the 3'-end processing of histone mRNAs (Marzluff et al., 2008). It will be of interest if future studies can determine that the SMN complex is also required for the assembly of related LSm2–8 and LSm1–7 complexes regulating snRNP formation and mRNA decay (Li et al., 2014b).

Consistent with the role of SMN in snRNP assembly, splicing defects occur in all SMA models characterized thus far (Gabanella et al., 2007; Zhang et al., 2008). However, these defects occur ubiquitously throughout various tissues, and the majority of splicing changes occur in later stages of SMA and may represent a secondary non-specific effect of neurodegeneration (Baumer et al., 2009). Recent work identified a specific minor spliceosomal target being affected in SMA motor neurons (Imlach et al., 2012; Lotti et al., 2012), however the role of this splicing defect and the function of the protein encoded remains to be fully elucidated.

The idea that SMN may have distinct and localization-dependent functions in the cell apart from mRNP assembly came mainly from two observations: firstly, SMN interacts with several mRNA-binding proteins that are not associated with snRNPs and secondly, SMN can localize to mobile RNA granules in axons. Taken together, these findings led to the hypothesis that SMN may have a non-canonical role in axonal mRNA metabolism that may explain the vulnerability of motor neurons to reduced SMN protein levels (Briese et al., 2005; Fallini et al., 2012b; Rossoll and Bassell, 2009a).

SMN is actively transported in axons during development

Early immunohistochemical studies in rats have localized SMN in dendrites and axons of spinal cord motor neurons *in vivo* (Bechade et al., 1999; Pagliardini et al., 2000). These immuno-EM analyses also depicted SMN on cytoskeletal filaments and associated with polyribosomes. Several immunofluorescence studies have detected SMN in neurites of cultured P19 cells (Fan and Simard, 2002), and axons of cultured motor neurons (Rossoll et al., 2002). Live cell imaging in cortical and motor neurons showed that SMN granules are actively transported into neuronal processes and growth cones in a microtubule-dependent manner at rates over one micron per second, consistent with fast axonal transport (Fallini et al., 2010; Zhang et al., 2003). SMN granules colocalized with Gemin

proteins but not spliceosomal Sm proteins in primary and stem cell-derived motor neurons, and SMN-Gemin2 complexes were actively co-transported in axons of cultured primary cortical and motor neurons (Fallini et al., 2011; Zhang et al., 2006).

Axonal localization of SMN *in vivo* has been observed in zebrafish during motor axon outgrowth (Hao et al., 2015) and in neuromuscular junctions in the embryonic and early postnatal mouse diaphragm (Dombert et al., 2014). In adult vertebrates, axonal localization of SMN is very low or absent, suggesting that its presence in transport granules is primarily required during early developmental stages of axonal outgrowth, arborization, and presynaptic differentiation.

While a recent study reports the presence of SMN and SmB-containing transport vesicles in neurites of cultured neuronal cells (Prescott et al., 2014), SmB has been shown to also regulate mRNA localization (Gonsalvez et al., 2010) and there is currently no plausible role for SMN in intra-axonal snRNP assembly. These data suggest that SMN plays an important role in axon and synapse growth and maintenance, in a splicing-independent function.

SMN is required for the axonal delivery of mRNPs

Reduced axonal localization of *β-actin* mRNA in SMA motor neurons was the first example of a mislocalized mRNA in SMA (Rossoll et al., 2003). Since then, SMN has been found to regulate the localization of

several mRNAs in axons (Akten et al., 2011; Fallini et al., 2013; Fallini et al., 2011; Hubers et al., 2011; Sanchez et al., 2013). Defects in mRNA localization are accompanied by similar decrease in the axonal levels of the SMN-interacting mRNA binding proteins HuD and IMP1 (Fallini et al., 2014; Fallini et al., 2011). IMP1, also known as zipcode binding protein 1 (ZBP1), is a KH domain RNA-binding protein essential for the localization and regulated translation of a number of mRNAs, including *β -actin* and *growth-associated protein 43 (Gap43)* mRNA (Donnelly et al., 2011). IMP1 associates with transporting RNA granules along with the ELAV-like RNA-binding protein HuD, and regulates the stability and axonal localization of *Tau*, *neuritin/cpg15*, and *Gap43* mRNA (Atlas et al., 2007; Yoo et al., 2013). SMN deficiency has been shown to cause mislocalization of the *cpg15* transcript in SMA neurons (Akten et al., 2011). These observations lead to the hypothesis that SMN may function as a chaperone for mRNA and protein interaction and association with transport machinery (Figure 2 & Figure 3a).

Although elegant work has demonstrated that the local translation of *β -actin* and *Gap43* mRNA is important for axon branching and outgrowth (Donnelly et al., 2013), and their mislocalization may explain axonal outgrowth defects in SMA motor neurons, it appears likely that a deficiency of multiple mRNAs contributes to SMA pathogenesis. This would be consistent with a general mislocalization of polyA mRNA in the axons of SMN-depleted motor neurons (Fallini et al., 2011), and the wide

spectrum of transcripts associated with axon growth and synaptic activity that were found down-regulated in axons of SMN-deficient motor neurons (Saal et al., 2014).

SMN is co-transported with the mRNA binding proteins, HuD and IMP1, in primary motor neuron axons, demonstrating its association with axonal mRNP granules (Fallini et al., 2011). Currently, the role of SMN in these mRNP granules is unknown, however it may be involved directly with axonal transport (Figure 3b). Recent work has demonstrated the association of SMN with COP1 (Peter et al., 2011) and that this association is important for axonal outgrowth (Li et al., 2015). Taken together with studies showing RNA association with COP1 complex (Todd et al., 2013), SMN may function as a bridge connecting mRBPs and COP1 vesicles transporting in the axon (Figure 3c), mediated by SMNs YG repetitive domain which functions in the assembly of oligomer complexes of SMN (Gupta et al., 2015; Martin et al., 2012). The capacity to form oligomers and associate with RNA binding proteins may also be linked to reports of SMN in the regulation of stress granule assembly (Hua and Zhou, 2004; Zou et al., 2011), and may also play a role in formation of additional 'higher order' granules as have been proposed for the SMN-associated protein FUS (Elbaum-Garfinkle and Brangwynne, 2015; Groen et al., 2013; Murakami et al., 2015; Sun et al., 2015; Yamazaki et al., 2012).

SMN is involved in translational regulation

Since SMN is a component of axonal mRNP transport granules, it may also function in posttranscriptional regulation at the axon terminal. SMN has been found to associate with polyribosomes and act as a repressor of translation *in vitro*, potentially regulating the homeostasis of translationally active and translationally quiescent mRNA molecules at the axon terminus (Sanchez et al., 2013). One of its targets is the arginine methyltransferase CARM1, which can act as a mediator of nonsense-mediated mRNA decay (NMD) and is abnormally up-regulated in SMA, adding exacerbated degradation of specific mRNAs to the molecular defects associated with SMN deficiency (Sanchez et al., 2015).

Additionally, the SMN-associated protein Gemin5, which directly binds RNA, has been implicated in several mechanisms of translation regulation (Pineiro et al., 2013; Pineiro et al., 2015; Workman et al., 2015). Consistent with regulating translational homeostasis, recent reports point to disruptions in mTOR regulated axonal translation (Kye et al., 2014). Furthermore, depleting PTEN in SMN deficient motor neurons rescued axonal length (Ning et al., 2010) and depleting PTEN at the NMJ in a SMA mouse model modestly improved survival (Little et al., 2015), demonstrating that mTOR regulation of local translation may be an attractive therapeutic target.

SMN has been reported to regulate membrane remodeling and anchoring of components of the protein synthesis machinery that is

required for the motility of fibroblasts (Francesca et al., 2016), similar to processes that connect the translational machinery to the plasma membrane in neuronal processes (Tcherkezian et al., 2010).

Does SMN regulate the assembly mRNP granules?

Recent studies have shown that beyond its role in snRNP assembly, SMN may function as a chaperone for the assembly of multiple ribonucleoprotein (RNP) complexes (Azzouz et al., 2005; Boulisfane et al., 2011; Brahms et al., 2001; Friesen and Dreyfuss, 2000; Li et al., 2014b; Lotti et al., 2012; Pellizzoni, 2007) (Figure 2 & 3a). Since SMN itself has not been identified as an mRNA-binding protein, SMN complex associated proteins are more likely to mediate the interaction with mRNA. Recent evidence has demonstrated that a number of these SMN core complex components, specifically Gemin5 and Unrip, directly bind mRNAs despite their lack of canonical RNA-binding domains (Castello et al., 2013, 2016b). SMN, through interactions with mRNA binding proteins and its complex members associating with mRNA may function to directly assemble messenger ribonucleoprotein (mRNP) complexes through increasing the affinity of mRNA binding proteins for their target mRNAs, which is analogous to the function of SMN in snRNP assembly. Additionally, this may explain its reported polyribosomal association (Sanchez et al., 2013), as mRNA binding proteins associated with SMN

such as FMRP (Piazzon et al., 2008) are known to be polyribosome associated (Bassell and Warren, 2008).

Conclusion

Despite considerable progress in understanding the processes of mRNA localization and local translation in axons, the molecular mechanisms that govern the assembly of mRNAs and mRBPs into mRNP transport granules are poorly understood. A recent study on the interactome of two distinct neuronal RNA granule shows that they share only a third of the identified proteins, suggesting that specific mRBP-associated transport granules are much more heterogeneous than previously anticipated (Fritzsche et al., 2013). The molecular machinery that assembles transcripts with a specific set of proteins that regulate their translocation process along microtubules, and their dissociation from the mRNPs, resulting in the mRNA being translated by ribosomes, remains unknown.

The neurodegenerative disease SMA, once considered a splicing disease, may provide insight into these processes. Multiple studies point to a general role for the SMA disease protein in the assembly of not only spliceosomal snRNP complexes, but also RNPs that regulate mRNA stability and localization . It will be interesting to see what other components of the SMN core complex are involved in these processes.

As most of the current work on mislocalization of mRNA in SMA has been performed mainly *in vitro*, it remains an important question what

mRNA localization defects are present in vertebrate models of SMA *in vivo*, and whether rescue of these defects can mitigate the disease phenotype. If SMA is disease of defective RNP assembly, one can expect a wide array of downstream effects on posttranscriptional regulation, including mRNA splicing, localization, and local translation. Future work will need to show which defects are most relevant for the SMA pathogenesis and are expected to provide insight into potential disease mechanism targeted therapeutic strategies.

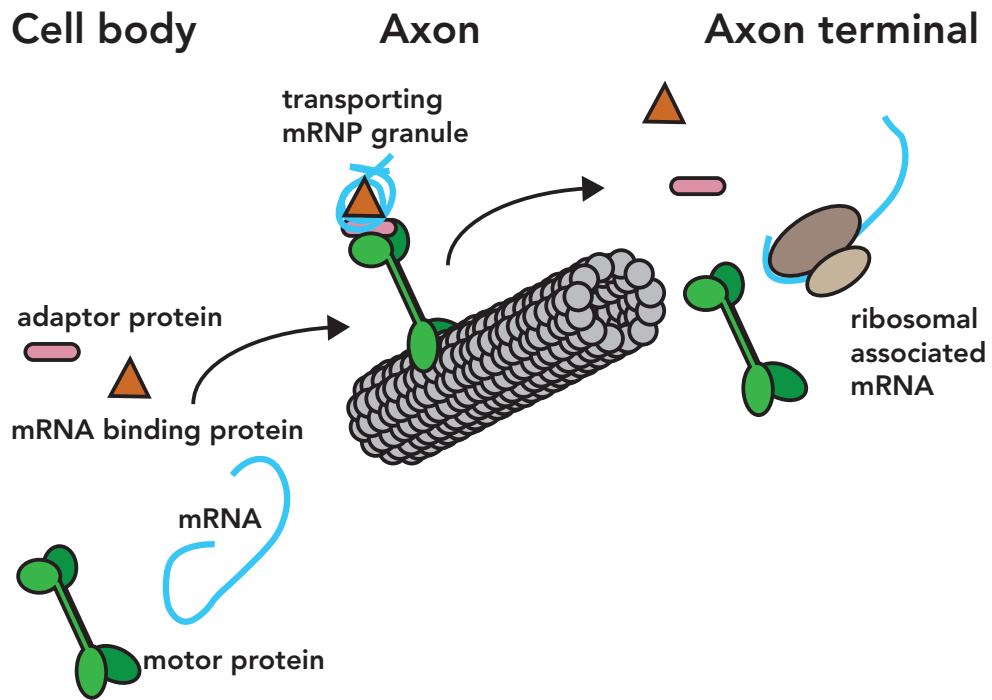
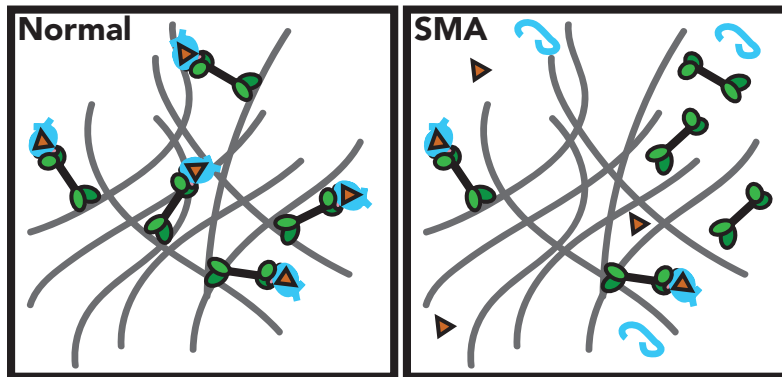


Figure 1: Mechanisms of axonal mRNA localization and local translation.

Shown is a simplified model for how mRNA localization is accomplished. mRNA and mRNA-binding proteins (mRBPs) associate, forming higher order complexes that can associate either directly or indirectly through adaptor proteins with molecular motors such as kinesins and dynein. These mRNA transport granules are believed to be predominately non membrane bound, and are localized through fast axonal transport along microtubules. Upon reaching the axonal terminals, post translational modifications of mRNA binding proteins alter their affinity for their mRNA targets, allowing binding of ribosomal subunits and translation to occur in a spatially and temporally regulated fashion.

Mislocalization of mRNA in SMA



Key:

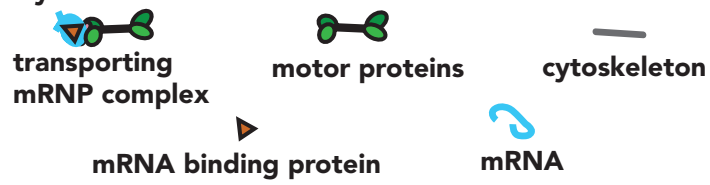


Figure 2: Model for the mislocalization of mRNA observed in SMA motor neurons:

Upon being assembled in the cell body, mRNP complexes associate with motor proteins to achieve subcellular localization via both the microtubule and actin cytoskeleton for long- and short-range transport, such as into both axonal and dendritic compartments. Defects in the assembly of mRNAs with mRNA binding proteins, due to insufficient levels of SMN, leads to decreased numbers of mRNP complexes interfacing with motor proteins, and thus the cytoskeleton, resulting in a net decrease in the amount of transported mRNA.

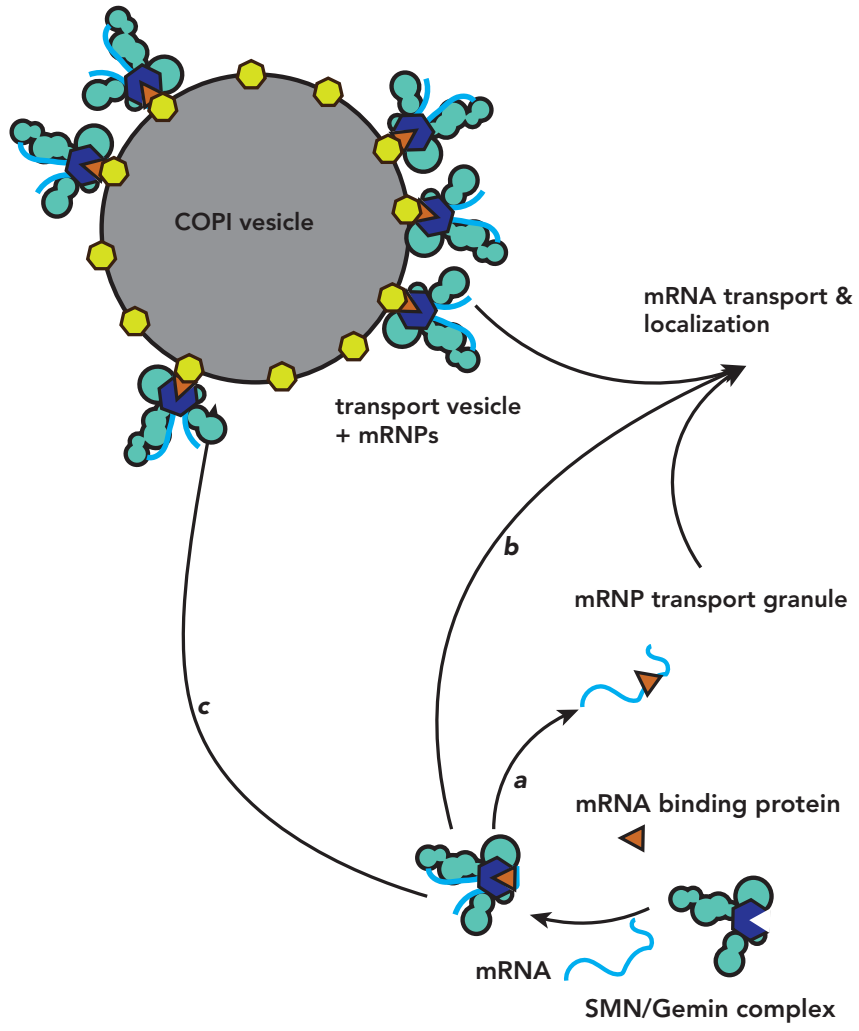


Figure 3: SMN in mRNP assembly and axonal mRNA localization.

SMN and its associated Gemin proteins may regulate mRNA and mRNA protein association. Similar to the spliceosomal snRNPs, Gemins likely directly interface with mRNA while SMN through its tudor domain associates with mRNA binding proteins. The concerted action of the SMN complex facilitates the assembly of mRNA and proteins into mRNP granules which can be transported without associated SMN complexes (a), or through the oligomerization properties of SMN's YG repeat domain, may form SMN complex-containing mRNPs for high levels of axonal transport in developing axons (b). Additionally, through association with COPI vesicles, SMN may bridge mRNPs and transporting vesicles, allowing mRNAs to utilize vesicular transport mechanisms (c).

**Chapter 2:
Spatially and temporally regulating translation via mRNA binding proteins
in cellular and neuronal function**

P.G. Donlin-Asp¹, W. Rossoll^{1,2}, G.J. Bassell^{1,2,3}

¹Department of Cell Biology

²Center for Neurodegenerative Disease

³Department of Neurology

Emory University School of Medicine,
Atlanta, GA 30322

Corresponding authors:

Gary J. Bassell
Dept. Cell Biology WBRB 415
Emory University School of Medicine
615 Michael St NE
Atlanta, GA. USA 30322
email: gbassel@emory.edu
Tel: (404) 727-0668
FAX: (404) 727-0570

Invited review article, FEBS letters

Abstract

Coordinated regulation of mRNA localization and local translation are essential steps in cellular asymmetry and function. Increasingly, it is evident that mRNA binding proteins play critical functions in the controlling the fate of mRNA, including when and where translation occurs. In this review, we will discuss the increasingly robust and complex roles that mRNA binding proteins play in regulation of local translation that impact cellular function in vertebrates. First we will discuss the role of local translation in cellular polarity and possible links to vertebrate development and patterning. Next, we will discuss the expanding role for local protein synthesis in neuronal development and function, with special focus on how a number of neurological diseases have given us insight into the importance of translational regulation. Finally, we will discuss the ever-increasing set of tools to study regulated translation and how these tools will be vital in pushing forward and addressing the outstanding questions in the field.

Introduction

In the past few decades, spatial restriction of protein accumulation through translational repression and mRNA localization has emerged as key regulators in eukaryotic biology. While initially viewed as restricted to handful of mRNAs, recent work has demonstrated that the vast majority of mRNAs in the *Drosophila* embryo show distinctive localization patterns corresponding to their protein distributions (Lecuyer et al., 2007) and additionally it has emerged that regulation of translation is a highly regulated step in controlling protein homeostasis in the cell. These studies highlight the importance of understanding the mechanisms underlying regulation of local translation.

Localization of mRNA and translational repression are intricately linked to spatially restrict protein accumulation and prevent ribosomal association from impeding processive transport of mRNA (Figure 1). It has long been speculated that polyribosomal association would impair dynamics of mRNA, and also fail to spatially restrict protein accumulation. Recent experimental evidence has demonstrated mRNA that is undergoing translation shows reduced dynamics in the cytoplasm (Katz et al., 2016) (Figure 1A-B) relative to translationally repressed mRNA (Figure 1C-E). By coupling these two processes, not only does the cell have more efficient transport of the mRNA, but also can respond to extracellular cues that allow rapid on-site, on-demand translation of key proteins in response to these cues, such as in growth cone turning and guidance (Lin and Holt, 2007). However, it is increasingly clear that the mechanisms of both localization of mRNA and regulation of translation are highly diverse and essential processes regulating everything from synaptic plasticity to organismal patterning.

In this review we will discuss regulation of local translation and mRNA localization in normal cellular and neuronal function and how dysregulation of these processes underlies a number of disease states. Additionally, we will address emerging technologies, which will further enhance the studies of these processes.

1. Polarity- from the basal to apical membranes and beyond.

The first descriptions of local protein synthesis, was that of translation at the rough endoplasmic reticulum (RER) (Figure 2A). The majority of this localization is in fact dependent on translation, utilizing the signal recognition particle (SRP) dependent pathway (Schwartz, 2007). However, recent work has started to characterize a number of cases of SRP-independent mechanisms targeting mRNAs to the ER (Chartron et al., 2016; Kraut-Cohen et al., 2013; Pyhtila et al., 2008), including mRNA binding protein dependent localization, including the muscleblind family of mRNA binding proteins (Wang et al., 2012). Integrating both genome wide RNAseq and subcellular fractionation, identified the local rough ER associated transcriptome, along with additional subcellular compartments. Their results demonstrate MBNL proteins to bind 3'UTR sequences and regulate the cytoskeletal dependent targeting of hundreds of mRNAs to the rough endoplasmic reticulum. More recently, MBNL protein binding to 3'UTR sequences was shown to play a role in gene-distal polyadenylation and RNA localization to neuronal processes of cultured neurons (Taliaferro et al., 2016), indicating that the same protein may function to direct and regulate RNAs to multiple subcellular locations.

The ER in addition to being a site of local protein synthesis also may serve as a location of translational regulation as well (Kim et al., 2014). ER is not

the only membrane-bound organelle enriched for mRNA and translation, mitochondria (Eliyahu et al., 2010; Lesnik et al., 2015) which have their own ribosomes and RNA, do require localization of a number of nuclear encoded transcripts (Figure 2B).

The earliest report of vertebrate mRNA which was localized and locally translated, was for the transcript *β-actin* (Shestakova et al., 2001). Being first described to localize at the leading edge of migrating fibroblasts (Latham et al., 1994; Ross et al., 1997), it is also widely detected in a number of protrusions of the membrane and cytoskeleton such as in axonal growth cones (Donnelly et al., 2013; Merianda et al., 2013; Nagaoka et al., 2012; Willis and Twiss, 2010; Yoo et al., 2013) and dendritic spines (Buxbaum et al., 2014; Eom et al., 2003; Klein et al., 2013). Recent work has also identified *β-actin* as an important component of the basal membrane, specifically localizing at focal adhesions (Gu et al., 2012; Katz et al., 2016; Katz et al., 2012) (Figure 2C). Studying the mRNA binding protein responsible for the localization of *β-actin*, IMP1/ZBP1, the authors demonstrate, using MEFs derived from knockout mice, that IMP1/ZBP1 is required for *β-actin* mRNA localization to the focal adhesions, and that focal adhesion strength is substantially impaired in IMP1 depleted cells. Furthermore, by directly tethering *β-actin* mRNA, utilizing the MCP-MS2 system fused with vinculin, they were able to show that localized *β-actin* mRNA regulates both the size and lifetime of focal adhesions. Apart from mRNA localization at the basal membrane, increasing evidence has demonstrated localization of mRNAs as important at a number of lateral membrane structures, including the tight junction (Nagaoka et al., 2012) and the desmosome (Jakobsen et al., 2013) (Figure 2D-F).

With an increasingly evident role of mRNA localization at the basal and lateral cellular membranes, it has remained likely that similar roles exist for the apical membrane as well. Increasing reports of a number of extracellular microvesicles and exosomes, which originate from the apical surface, have described them as being enriched in a number of RNAs, including mRNAs (Eirin et al., 2014; Tkach and They, 2016). Work remains to be done to address how RNAs are delivered to the apical region and incorporated into these extracellular membrane structures (Figure 2G), however it remains likely that it is similar in nature to RNA delivery into cellular protrusions. In a study on the composition of membrane protrusions it was found that the microtubule binding protein adenomatous polyposis coli (APC), which is also an mRNA binding protein (Mili et al., 2008; Preitner et al., 2014; Yasuda et al., 2013), is enriched for a number of transcripts within membrane protrusions (Mili et al., 2008). Additionally, recent work has identified local translation as an essential regulator of cellular protrusions (Mardakheh et al., 2015). Aside from cellular protrusions the primary cilia, which is important in regulation of cellular polarity and proper signaling during development (Goetz and Anderson, 2010), and resides at the apical surface of most cells during some point in their development, may be regulated through regulation of translation. In a recent high throughput siRNA screen a number of translational repressors, were found to be essential regulators of cilia development (Wheway et al., 2015). Given that centrosomes, which form the base of primary cilia, are known to be mRNA associated (Lambert and Nagy, 2002), these data suggest that essential localized regulation of translation, likely regulate establishment and maintenance of cellular polarity and function.

A vital question moving forward is to address the role of mRNA localization and local translation in vertebrate development, polarity and

patterning. These processes, extensively studied in *Drosophila* (Kugler and Lasko, 2009; Lasko, 2012; Lecuyer et al., 2007), have remained elusive in vertebrates. Given that a knockout of the zipcode binding protein 1 (ZBP1/IMP1/IGF2BP1/Vg1RBP/VICKZ) results in widespread phenotypes such as kidney defects and dwarfism (Hansen et al., 2004) and a knockout of another translational repressor Mex3b demonstrate reduced body weight and impaired gamete development (Le Borgne et al., 2014), it is clear that a similar role of posttranscriptional regulation governing development exists in vertebrates as in *Drosophila*.

2. Translation regulation in neuronal function.

Neurons epitomize functional and morphological polarity, with highly elaborate branched axonal and dendritic compartments, and both these structures require local translational regulation for their function. As early as the 1960's, local protein synthesis was detected in synaptic preparations (Autilio et al., 1968; Morgan and Austin, 1969) and in axons (Edstrom and Sjostrand, 1969; Koenig, 1967). Additionally, with an increasing understanding of the requirement of new protein synthesis for long-term memory (Klann and Sweatt, 2008), it has become clear that local translation of mRNA may underlie key aspects of neuronal function and activity (Alvarez et al., 2000; Holt and Schuman, 2013).

2.1 Dendrites.

Local protein synthesis in dendritic compartments is appreciated to play important roles in neuronal development and synaptic plasticity, which may go awry in several neurological diseases (Swanger and Bassell, 2013). Early studies utilizing electron microscopy (EM) visualized polyribosomes localized to the base

of dendritic spines, and it is these localized polysomes which are believed to play a vital role in protein synthesis-dependent synaptic plasticity (Steward and Schuman, 2001), and an increasingly diverse set of mRNAs have been detected in dendrites (Bramham and Wells, 2007; Cajigas et al., 2012). Local protein synthesis has been characterized as coupled to NMDA dependent long-term potentiation (LTP) (Miller et al., 2002)(Figure 3A) and mGluR-dependent long-term depression (LTD) (Huber et al., 2000), and is postulated to occur at subsynaptic sites within dendritic spines (Steward and Worley, 2001). A number of mRNA binding proteins regulating translation localize to dendrites, such as FMRP (Richter et al., 2015), and are connected to neurodevelopmental disorders such as Fragile X Syndrome and Autism Spectrum Disorders (discussed in section 3.1).

2.2 Axons.

Local translation has been widely demonstrated in developing axons (Leung et al., 2006; Zivraj et al., 2010) where it regulates axonal outgrowth and pathfinding during axonal development (Yoon et al., 2009). A number of studies have demonstrated the importance of regulated local translation and translation repression to allow stimulus-induced translation in the growth cone (Figure 3B). Growth factors such as BDNF and netrin (Leung et al., 2006; Sasaki et al., 2010; Welshhans and Bassell, 2011; Willis et al., 2007; Yao et al., 2006) can induce translation to occur in a spatially restricted fashion to facilitate growth cone turning and branching toward guidance cues. One of the best-studied mRNA binding proteins in this process, and also highly conserved proteins, has been the mRNA binding protein ZBP1/IMP1/IGF2BP1/VICKZ/Vg1RBP (Gaynes et al., 2015; Kalous et al., 2014; Medioni et al., 2014; Welshhans and Bassell, 2011).

Mechanistically acting as a translational repressor and localizing factor for mRNA, the ZBP1 family of proteins keeps messenger RNA quiescence until it reaches its destination, where stimulus-induced Src kinase phosphorylation (Huttelmaier et al., 2005) of the protein relieves translational repression and allows local protein synthesis. While traditionally linked to axonal guidance cues such as BDNF and netrin, recent work has also demonstrated that local release of ZBP1-mediated translational silencing is induced by Sonic Hedgehog (Shh) signaling in the axons (Lepelletier et al., 2017).

While local translation in dendrites and developing axons is widely accepted, it has been far more controversial in mature axons. In part, this has been due to difficulties in detecting polyribosomes in the axon, and recent work suggests this may be due to translational machinery associating directly with the plasma membrane (Tcherkezian et al., 2010), masking ribosomes from view by electron microscopy. Recent profiling of ribosome-associated transcripts provides further support for local protein synthesis in adult axons (Shigeoka et al., 2016). Future work will be needed to further probe axonal compartments to fully define and characterize the mRNAs being translated in the axon, and how neuronal function is mediated by and influenced by these transcripts during activity.

3. Dysregulation of local translation in disease.

Given the widespread nature of local translation in neurons and other cell types, it is unsurprising that dysregulation of these processes underlies a number of neurological and neurodegenerative diseases (Wang et al., 2016b).

3.1 Neurodevelopmental diseases.

Given the widespread requirement of localized translation in *Drosophila* development (Lecuyer et al., 2007), it is not surprising that a similar requirement exists within vertebrate development as well. A number of neurodevelopmental disorders, such as fragile x syndrome and autism have substantial pathological features that may result from dysregulation of local protein synthesis (Figure 4A,B).

Fragile X syndrome (FXS), which results from the inherited loss of the Fragile X Mental Retardation Protein (FMRP), is the most common form of inherited intellectual disability and the leading monogenetic cause of autism (Penagarikano et al., 2007). FMRP functions as a translational repressor, binding to many target mRNAs encoding proteins that play key roles at the synapse (Huynh et al., 2015; Santoro et al., 2012). FMRP binding to mRNA is involved in ribosome stalling, as a general mechanism to repress translation of numerous target mRNAs (Darnell and Klann, 2013; Darnell et al., 2011). Furthermore, recent evidence points to FMRP binding to the ribosome itself to regulate translation (Chen et al., 2014). Given its role as a translational repressor, excessive protein synthesis is a well-established feature of FXS (Bolduc et al., 2008; Gross et al., 2010; Gross et al., 2011; Osterweil et al., 2010). Recent work has also demonstrated local translational regulation is also impaired in FXS (Ifrim et al., 2015; Tatavarty et al., 2012), as FXS mice show elevated baseline protein synthesis that is unresponsive to mGluR stimulation (Figure 4A).

Given the overlap of FMRP target mRNAs that are linked to autism (Darnell et al., 2011; De Rubeis et al., 2014), it is very likely that similar underlying disease mechanisms are shared between these two diseases. This is supported by a growing body of work that have identified a number of translation regulating proteins, such as eIF4E (Gkogkas et al., 2013; Huber et al., 2015;

Huynh et al., 2015; Santini and Klann, 2014), as factors associated with and altered in autism. Additionally, a number of reports have demonstrated multifunctional roles for various mRNA binding proteins associated with autism, such as Rbfox1 (Bill et al., 2013; Ray et al., 2013; Weyn-Vanhentenryck et al., 2014), which has a well-described function in splicing. In a recent study (Lee et al., 2016), it was found cytoplasmic Rbfox1 associates with 3'UTRs of a number of autism related transcripts and blocks miRNA association. Loss of cytoplasmic Rbfox1 (Figure 4B) leads to miRNA mediated repression and silencing of these transcripts that are relevant to autism and synaptic development relevant, which could not be rescued by nuclear Rbfox1.

These studies underscore the importance of translational regulation in both neuronal homeostasis and plasticity. Furthermore, the heterogeneity especially within Autism highlights that further RNA binding proteins and translational regulating proteins remain to be identified which regulate synaptic plasticity.

3.2 Neurodegenerative diseases.

In addition to neurodevelopmental disorders, perturbations in mRNP regulated translation occur in a number of neurodegenerative disorders, including spinal muscular atrophy (SMA), amyotrophic lateral sclerosis (ALS) and Alzheimer's disease (AD).

Spinal muscular atrophy (SMA) is a motoneuron disease caused by reduced levels of survival motor neuron (SMN) protein due to mutations in the *SMN1* gene (Burghes and Beattie, 2009; Monani, 2005). SMA is characterized by axonal degeneration and synaptic defects in the spinal motor circuitry, including maturation defects and degeneration at the neuromuscular junctions

(Donlin-Asp et al., 2016; Fallini et al., 2012b; Rossoll and Bassell, 2009b). While SMN has an essential role in spliceosomal snRNP assembly (Battle et al., 2006; Gubitza et al., 2004), work from several labs has demonstrated additional SMN-dependent defects in the localization and local translation of axonal mRNAs (Burghes and Beattie, 2009; Fallini et al., 2012b; Jablonka et al., 2014; Rossoll and Bassell, 2009a; Saal et al., 2014) (Figure 4C). Recent studies have identified SMN in polysomal fractions (Sanchez et al., 2013) and reduced translation in distal axonal compartments of SMN depleted neuronal cultures (Fallini et al., 2016). The underlying mechanisms behind the local translation defects in SMA may stem from impaired mRNP assembly and localization, or direct defects in translational regulation in SMA. This indicates a more general role for SMN in RNP complex assembly beyond its very well characterized function in snRNP assembly and splicing regulation (Li et al., 2014b; So et al., 2016). This would suggest that SMA can be characterized as a disease of 'RNP hypoassembly' (Donlin-Asp et al., 2016; Shukla and Parker, 2016), SMN has also been shown to regulate miR-183 levels in neurites, thus regulating axonal translation of mTor via direct binding to its 3' UTR (Kye et al., 2014), highlighting the multitude of defects, including defective regulation of translation, resulting from alterations in mRNP assembly.

Myotonic Dystrophy (DM) while traditionally viewed as a muscle disease, a number of neuronal associated phenotypes are present (Caillet-Boudin et al., 2014), indicating a much more complex pathophysiology. Similar to SMA, DM has been predominantly viewed as a splicing disease (Meola and Cardani, 2015), however this view has been recently challenged with the identification of MBNL proteins, which are involved in the pathophysiology of the disease, being involved in subcellular localization of mRNAs to the rough ER (Wang et al.,

2012). This study identified numerous mRNAs that had impaired localization in cell culture models of myotonic dystrophy and, again similar to SMA, indicates that mRNA mislocalization and therefore mislocalization of local translation as a disease mechanism in myotonic dystrophy.

Amyotrophic lateral sclerosis (ALS) is the most common form of adult onset neurodegenerative disease of the motoneurons (Renton et al., 2014). It shows a significant overlap in genetics, histopathology, and clinical features with frontotemporal dementia (FTD), the most common form of presenile dementia, suggesting that both diseases are part of a disease spectrum (Ling et al., 2013). ALS has a number of genetic causes (Renton et al., 2014) and complex pathology involving non-cell-autonomous toxicity of glia, ER stress, impaired protein degradation, disruption of axonal transport, and defects in RNA metabolism [Taylor, Brown, Cleveland Nature 2016]. A number of the genes causing ALS encode mRNA binding proteins, which regulate translation such as FUS/TLS (Luo et al., 2015; Sharma et al., 2016; Yasuda et al., 2013) and TDP-43 (Freibaum et al., 2010; Guo et al., 2011; Romano et al., 2016). Recent work has characterized a role for TDP-43 in concert with FMRP in translational regulation (Coyne et al., 2015; Majumder et al., 2016), which may also affect local translation in dendrites and axons (Wang et al., 2008b) (Ishiguro et al., 2016). TDP-43 and FUS/TLS form multimers through low-complexity prion-like domains, which facilitates the assembly of membrane less organelles such as RNA stress granules, which are sites of translational suppression under stress conditions (Li et al., 2013). “RNP hyperassembly” into insoluble aggregates may be a common dysfunction in the disease (Shukla and Parker, 2016).

Another emerging disease of interest for dysregulated local translational regulation is Alzheimer’s disease (AD). In a recent study (Baleriola et al., 2014), it

was found that local A β 1-42 treatment induced the translation of the axonally localized activating transcription factor 4 (ATF4) mRNA , resulting in long-range retrograde transport of newly synthesized ATF4 and induction of cell death. This retrograde transport of ATF4 and subsequent cell death may explain the spread of AD pathology across the brain.

3.3 Axonal injury and regeneration.

One additional area of interest for alterations in translation in neurons is in axonal repair after injury (Doron-Mandel et al., 2015; Kalinski et al., 2015; Michaelevski et al., 2010; Rishal and Fainzilber, 2014; Sachdeva et al., 2016). Unlike diseases such as FXS or SMA, alterations in local translation, specifically in enhanced localization of mRNA and translation, allows for robust axonal growth and peripheral nerve regeneration (Figure 4E). This upregulation of local translation is believed to require enhanced transport of mRNAs into the injured axons , translation of existing mRNAs in mature axons (Merianda et al., 2015), and depends on proper growth and signaling cues for proper axonal regeneration (Kalinski et al., 2015). Ongoing work seeks to understand how these processes might be better harnessed and enhanced for both peripheral axonal injury and spinal cord injury treatment (Twiss et al., 2016).

4. Studying local translational regulation: the ever-improving toolbox.

Coincident with the expansion of studies examining local translational regulation has been a renaissance in the development of increasingly sophisticated and sensitive set of tools to address localized translation and the processes that regulate it. Here we will discuss current technologies in the field and the outstanding questions in the field that are being addressed with them.

4.1 Defining where mRNA is in space and time.

Perhaps one of the most important innovations in our understanding of posttranscriptional regulation has been deciphering where mRNA is localized within the cell. Major breakthroughs into understanding RNA distribution in the cell have come from single molecule *fluorescent in situ hybridization* (FISH) studies, visualizing mRNA distribution in the cell. This has led to not only widespread characterization of where single transcripts are localized (Femino et al., 2003; Levsky and Singer, 2003), but with the development of innovative multiplexed versions of FISH (Chen et al., 2015; Moffitt et al., 2016) it is possible to quantify the numbers and locations of thousands of RNA species in (Chen et al., 2016) intact cellular structures. Work has also demonstrated the compatibility of RNA FISH with expansion microscopy, allowing even greater insight into the subcellular localization of RNA transcriptions. Additionally, further refinements and coupling with clearing procedures such as CLARITY (Sylwestrak et al., 2016) have allowed enhanced resolution of RNA localization in intact tissues with high spatial resolution. Despite the power and versatility of FISH, its major drawback has always been that it is in fixed cells or tissues; meaning dynamic information is out of reach.

To quantify mRNA dynamics in living cells a number of approaches have been successfully utilized, including the use of molecular beacons (Chen et al., 2011) and the MS2 tagging approach (Bertrand et al., 1998). Molecular beacons are self-quenching oligonucleotide hybridization probes that remain in a quenched “dark state” when not hybridized to their specific target. Their strength lies in both the strength of the signal that they produce, since they rely on fluorescent dyes rather than proteins, and that they target endogenous RNA

rather than relying on a reporter based system. While a number of elegant studies have successfully employed them (Alami et al., 2014) the delivery into the cell remains a serious drawback.

The most widely used method of RNA tracking in live cells is the MS2 tagging approach (Aguilhon et al., 1998). This system employs the MS2 bacteriophage coat protein (MCP) fused to fluorescent proteins along with a modified RNA of interest. This RNA of interest contains the hairpin loop structures that MCP recognizes, and allows direct fluorescent labeling of RNA in living systems. This system has been widely applied to a number of biological systems successfully, as all one requires is a means to transfect plasmids encoding the RNA of interest and MCP. Additionally with the implementation of similar bacteriophage-stem loop combinations (PP7 and λ N22) multiplexing and tracking of a number of different RNA species is possible (Hocine et al., 2013; Ma et al., 2016). However, unless the endogenous genomic locus encoding the RNA of interest is modified to encode the MS2/PP7/BoxB stem loops (Lionnet et al., 2011; Ma et al., 2016), it is impossible to resolve endogenous RNA dynamics. Additionally, there have been some reports that the MS2 system may alter the stability and dynamics of mRNA (Garcia and Parker, 2016).

Recent work has attempted to create novel RNA labeling strategies outside of the MS2 and molecular beacon approaches. One recent study takes advantage of innovations the CRISPR/Cas9 system, which has recently been shown to be able to target RNA in vitro (O'Connell et al., 2014), to label endogenous RNA in live cells (Nelles et al., 2016). In this approach, RNA-targeting Cas9 (RCas9) is labeled with a fluorescent protein and expressed alongside the guide RNA and an oligonucleotide PAMer that recognizes the RNA(s) of interest. While only one study so far has used this approach, the

possibility of direct visualization of endogenous RNA targets is extremely promising. Additionally, with recent work improving the ability to deliver RNA into cells and tissues (McKinlay et al., 2017), delivering directly modified mRNAs is increasingly a viable strategy especially *in vivo*.

4.2 Defining what are mRNA binding proteins and what mRNAs they bind.

A crucial aspect to understanding translational regulation of mRNA, is characterizing what proteins bind to mRNA and where in the mRNA these proteins bind. Recent innovations have enabled characterizing not only what proteins are bound to RNA, but also what domains of proteins bind to RNA.

RNA interactome capture (Castello et al., 2013), which applies UV crosslinking, to irreversibly capture RNA-protein interactions, followed by oligo(dT) bead pulldown of mRNA, gives a transcriptome wide view of all proteins interacting with mRNA in a cell population. Interestingly, this approach has uncovered a number of unconventional RNA-protein associations, increasing the repertoire of known RNA binding proteins (Castello et al., 2015). Additionally, a modification of this approach allows for mapping of domains that are associated with RNA, further expanding our understanding of RNA binding domains (Castello et al., 2016a). Work has also attempted to understand the proteomic network of mRNP granules (Fritzsche et al., 2013), which will shed light onto how translational repression and localization are achieved. Early studies have relied on biochemical isolation and pull down to identify proteomic networks, but with BioID (Roux et al., 2013) and APEX2 (Lam et al., 2015) labeling, it will be increasingly easy to address these questions for a number of mRNA binding proteins.

Characterizing transcripts bound by RNA binding proteins has also increasingly become routine. Initial attempts utilized RNA immunoprecipitation (Keene et al., 2006; Peritz et al., 2006), adapting standard protein immunoprecipitation followed by isolation and amplification of RNA that was isolated and detection by quantitative RT-PCR for detection of specific RNAs. These protocols were readily adapted for both microarray and RNA-sequencing for a global view of the RNAs bound by specific proteins. While powerful, these approaches were plagued by evidence that RNAs interacting with proteins being IP'ed could be altered following cell lysis and pull down, bringing into question the accuracy of the targets identified. Furthermore, these approaches as gave a low-resolution view of where the RNA binding protein associated with the mRNA, making it nearly impossible to define sequence motifs. Identical to RNA interactome captures use of UV crosslinking, Crosslinking and Immunoprecipitation (CLIP) (Darnell, 2010; Ule et al., 2005) based approaches have increased the stringency of our understanding of what RNA and protein interactions are occurring *in vivo* and more importantly with the advent of approaches such as iCLIP (Huppertz et al., 2014; Konig et al., 2010, 2011), its become possible to map at nucleotide resolution where mRNA and protein associations occur, making it possible to identify sequence motifs within target mRNAs. One major limitation of CLIP based approaches thus far, is that tissue specific profiling of RNA-protein association has yet to be accomplished, due to the relatively high amount of protein material required. With increasingly efficient and sensitive sequencing methodologies, this is a bridge likely soon to be crossed.

While CLIP and other IP based approaches have been the gold standard in the field, attempts at devising labeling strategies for RNA similar to that of

BioID and APEX2 for protein labeling remain tantalizing, given the ease for scaling up and performing much more high throughput analysis of mRNA-protein association it would afford. One such attempt, using the catalytic domain of the RNA editing enzyme ADAR fused to an RNA binding protein of interest (McMahon et al., 2016), demonstrated the feasibility of such a metabolic labeling approach. Further refinements will have to be made, as of yet it gives a far lower resolution view of RNA-protein association than CLIP. Additionally, ADAR based modification to identify associated transcripts may lead to widespread alterations in the behavior of RNA, complicating the interpretation.

4.3 Defining what transcripts are being translated and where translation occurs.

Tools to profile the translome have undergone rapid innovation in the past few years. The first important innovation was the development of the Translating Ribosome Affinity Purification (TRAP) mouse models based on a series of bacterial artificial chromosome (BAC) transgenic mice that express EGFP-tagged ribosomal protein L10a from CNS cell-type specific promoters in defined cell populations (Doyle et al., 2008; Heiman et al., 2008). The related RiboTag mouse model (Sanz et al., 2009) uses a more general approach that takes advantage of the large number of available tissue-specific Cre mice and an HA tagged exon inserted into the gene encoding for a ribosomal protein L22 (RPL22), which is flanked by loxP sites allowing for Cre mediated recombination. Since all ribosomes contain the HA-modified protein, one can isolate all ribosomes from specific tissues and profile where on all mRNA transcripts ribosomes are located. While powerful on its own (De Gendt et al., 2014; Lesiak et al., 2015; Sanz et al., 2013), recent adaptations have further refined this

protocol for isolation of ribosomes from axons in mature circuits (Shigeoka et al., 2016), providing the first direct evidence of widespread translation in mature axons.

These techniques of profiling translation, while powerful, do not address being able to visualize and quantify translation in intact cellular structures. A number of metabolic labeling techniques, inspired by earlier pioneering work using radioisotope labeled methionine (Browder et al., 1992), have allowed us to visualize where translation occurs in cells. These include techniques such as Fluorescent Non-Canonical Amino acid tagging (FUNCAT) (Dieterich et al., 2010; Tom Dieck et al., 2012), which uses a methionine analog, and puromycin labeling (David et al., 2012; Graber et al., 2013; Schmidt et al., 2009) to visualize newly synthesized proteins. Recent work has demonstrated that coupling the proximity ligation assay with either FUNCAT or puromycin labeling allows visualization of specific protein translation events (tom Dieck et al., 2015). Using this approach, it was shown that the mRNA binding protein hnRNPQ regulates the translation of Gap43 mRNA (Williams et al., 2016). Additionally a novel labeling strategy also will likely allow cell type specific protein labeling *in vivo* (Mahdavi et al., 2016). Utilizing a modified version of methionyl-tRNA synthetase that can charge tRNA to a non canonical amino acid azidonorleucine, this study was able to demonstrate robust protein labeling in cultured cells, opening the door to possible tissue specific expression and cell type specific labeling of proteins *in vivo*.

The last area of active interest, is not only being able to see where in cells translation occurs- but to be able to see it in real time. Initial work focused on utilizing either bleaching or photocoverion of fluorescent proteins (Leung and Holt, 2008) and while some truly pioneering work was accomplished using these

reporters, they were unable to resolve single translation events. To address this, a number of new approaches have been utilized. In one such approach, the yellow fluorescent protein Venus is used. Venus, which is exceptionally bright, has a fast maturation time and rapidly bleaches, is ideal for quantifying single translation events in real time. Single molecule venus translation studies have been used to quantify translational dysregulation of both Arc (Tatavarty et al., 2012) and PSD95 (Ifrim et al., 2015) mRNAs in mouse hippocampal neuronal cultures from a fragile x syndrome model. This technique is exceptionally powerful, however its major drawback is the inability to track the dynamics of newly synthesized proteins overtime. This point has presented significant challenges, due to the inherent photobleaching properties of fluorescent proteins, and until recently unlike the signal amplification that one can achieve with mRNA labeling with the MS2 system with multiple hairpin loop binding sites, it has been impossible to amplify fluorescent protein labeling on single proteins. Recent work has developed a novel tagging strategy, SunTag (Tanenbaum et al., 2014). This labeling strategy uses co-expression of a fluorescently tagged single-chain variable fragment (scFv) antibodies fused to a fluorescent protein along side a protein of interested tagged with 24 repeats of the peptide motif recognized by the scFv. The amplification afforded by this tag allows single particle imaging of proteins in living cells. Recently this labeling strategy has been successfully utilized, along side the MS2 system, to quantify single translation events in live cells (Morisaki et al., 2016; Pichon et al., 2016; Wang et al., 2016a; Wu et al., 2016; Yan et al., 2016). Application of this technique *in vivo* will be challenging, due two-part system for imaging. However, the spectacular signal-to-noise ratio will likely make this the best method for resolving translational dynamics of endogenous proteins.

5. Conclusions and future directions.

Pioneering work in a number of cellular models, many discussed in this review, have expanded our understanding of how mRNA translation is regulated locally by mRNA binding proteins in space and time. From neuronal activity to cellular polarity, the list of functions regulated by subcellular localization of translation continues to expand year by year. Increasingly it is evident that a role for local translation in processes such as polarization and development, first identified in invertebrate models such as *Drosophila*, are conserved in vertebrate systems. Since the revelation of how widespread subcellular localization of mRNAs are (Lecuyer et al., 2007), the future of the field is clear- a push *in vivo*. Only by studying these processes in intact and complete systems, will it be possible to truly unravel the complexities and intricacies of how localized translation regulates cellular function. In fact, had it not been by exploiting an *in vivo* approach, the recent revelation of mature axonal translation (Shigeoka et al., 2016) would not have been possible. By looking *in vivo* it will be possible to not only quantify the extent of local translation as it pertains to neuronal function and activity, but indeed also how it contributes to development, function and is dysregulated in disease. The insights afforded by such focus, will expand our understanding of the extent of localized translation and keep the field busy for decades to come.

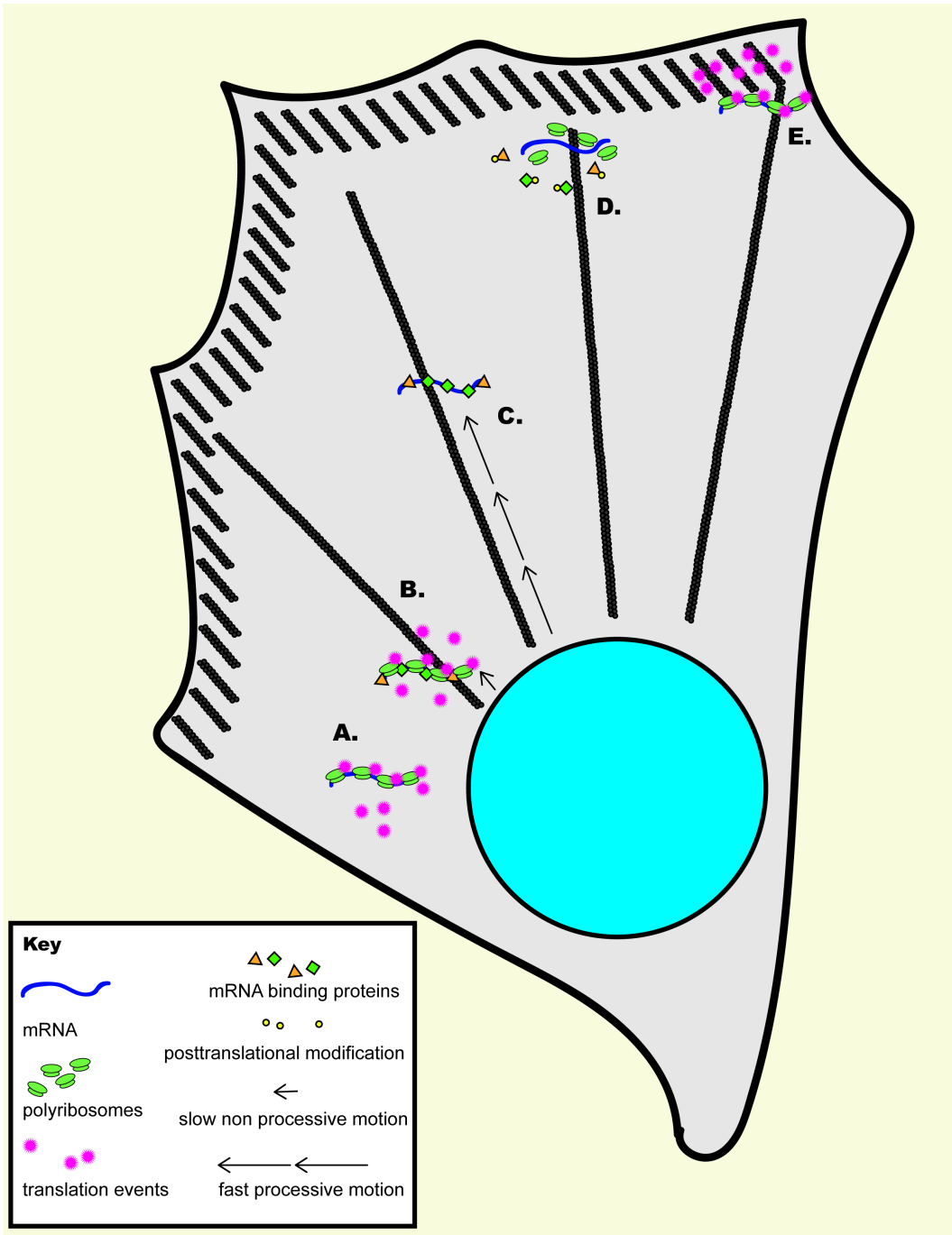


Fig. 1. Regulation of local translation in mRNA localization.

Coupling of translational repression through mRNA binding protein association functions to spatially restrict protein accumulation and accelerate the dynamics of transporting mRNA. Non localizing mRNA that is undergoing translation is coated with polyribosomes (A) limiting and slowing its movement in the cytoplasm. If translating mRNA were to be transported, the bulk of the ribosome association would impede its rapid and processive movement through the cytoplasm along cytoskeletal tracts (B). However, translationally repressed mRNA with limited ribosomal association will rapidly be transported through the cytoplasm to distal sites (C) and when the mRNA reaches its target destination, changes in the posttranslational modification profile of the mRNA binding proteins will relieve translational repression (D) and allow rapid local translation and protein accumulation (E).

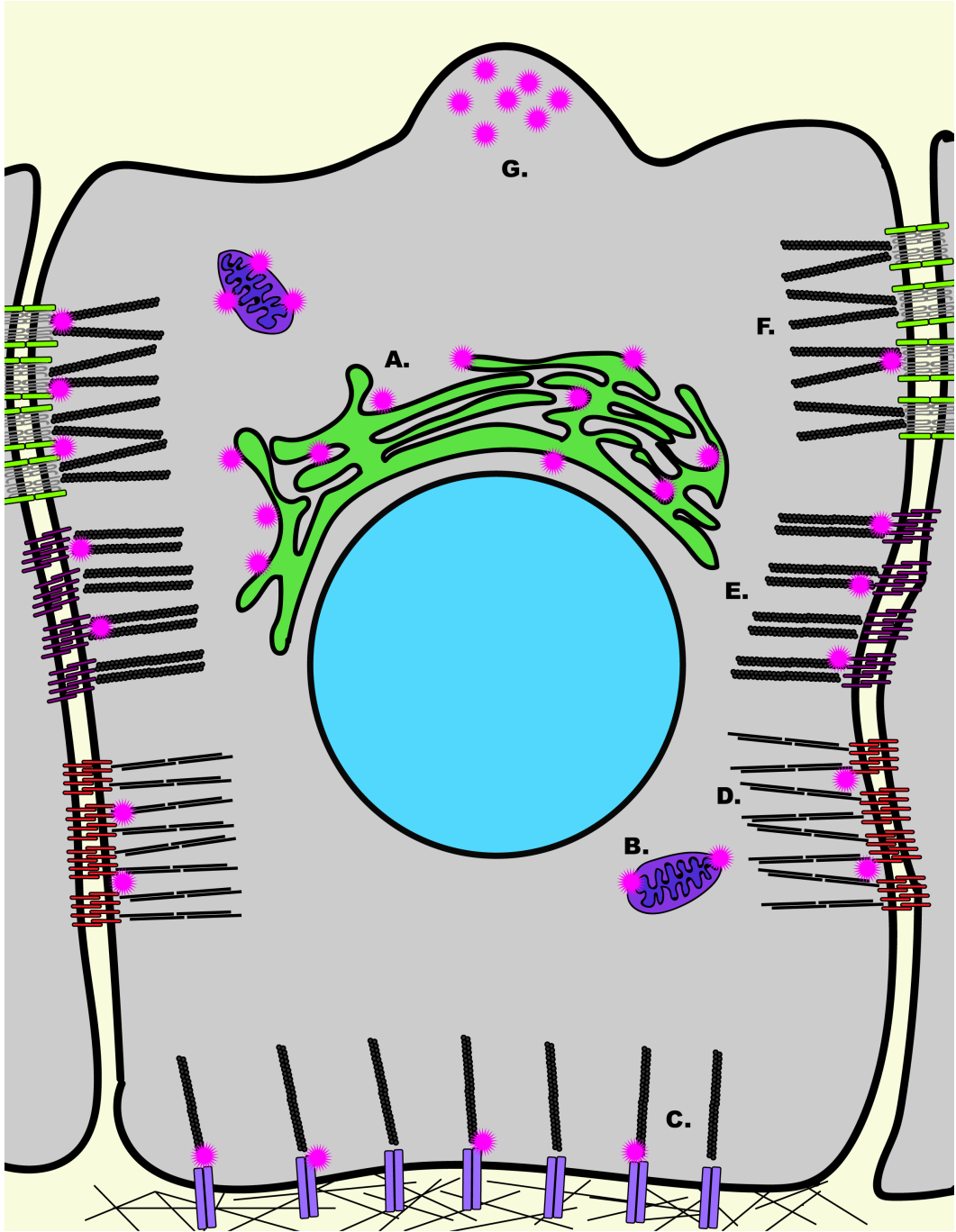


Fig. 2. Regulation of local translation in cellular polarity.

Local translation is abundant in polarized cells. Local translation (pink stars), both SRP signaling particle dependent and independent translation is widespread at the endoplasmic reticulum (A). Mitochondria are also sites of abundant localized translation (B). None membrane bound structures are also sites of highly abundant localized translation. At the basal membrane, actin interacting focal adhesions (C), local translation helps to function in mediating adhesion lifetime and strength. At the lateral membrane, local translation is observed at the keratin associated desmosomes (D), and actin association adherens junctions (E) and tight junctions (F). Additionally, membrane protrusions are also sites of widespread local translation (G).

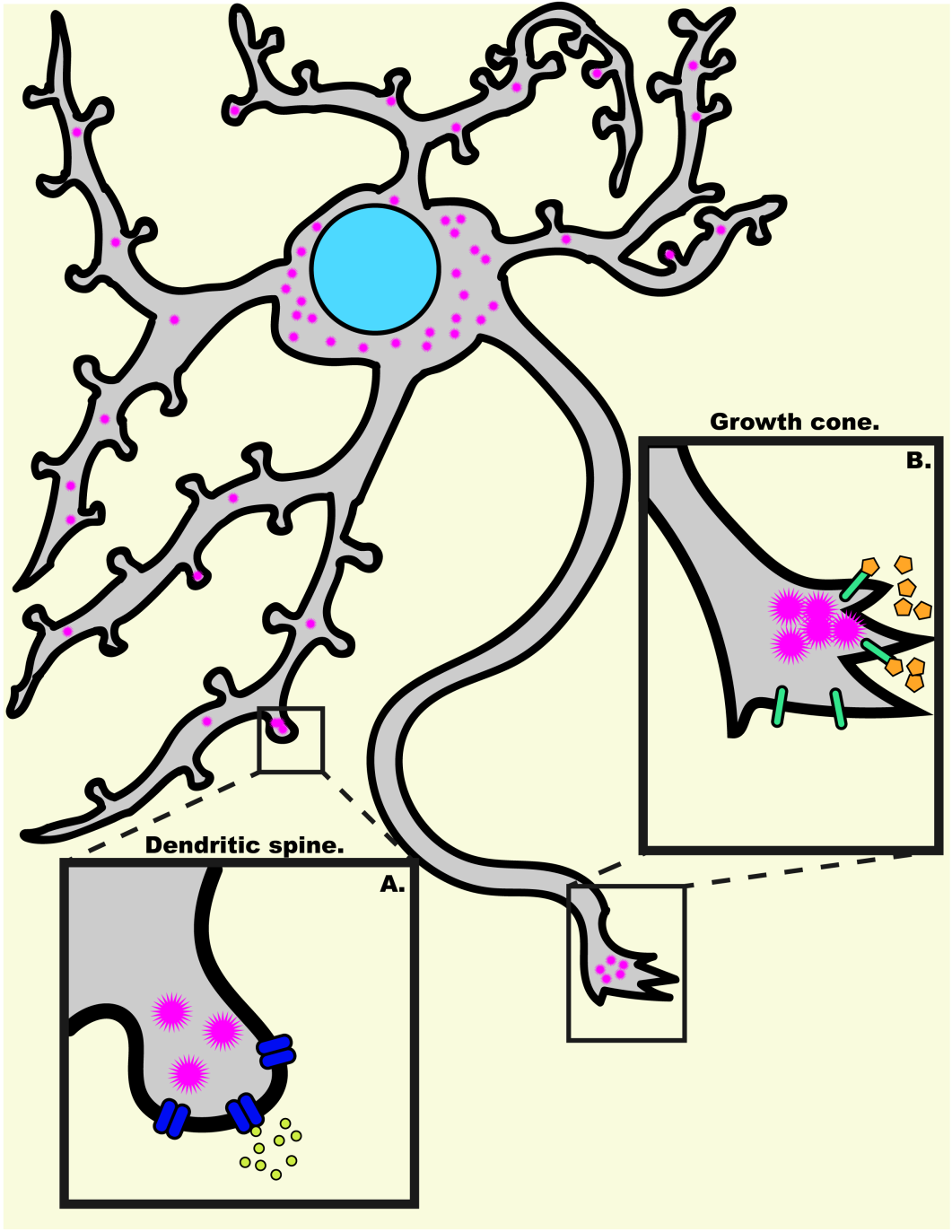


Fig. 3. Regulation of local translation in neuronal function.

Local translation is widespread in neurons, and contributes to neuronal function and growth. Local translation (pink stars), is regulated by synaptic activity in dendritic spines being induced by glutamate stimulation (yellow circles) of NMDAR (purple) activity, and is essential in LTP and long-term memory consolidation (A). Local translation is widespread in developing axons (B), contributing to axonal growth cone guidance and turning in response to growth cues such as BDNF and netrin-1 (gold pentagons).

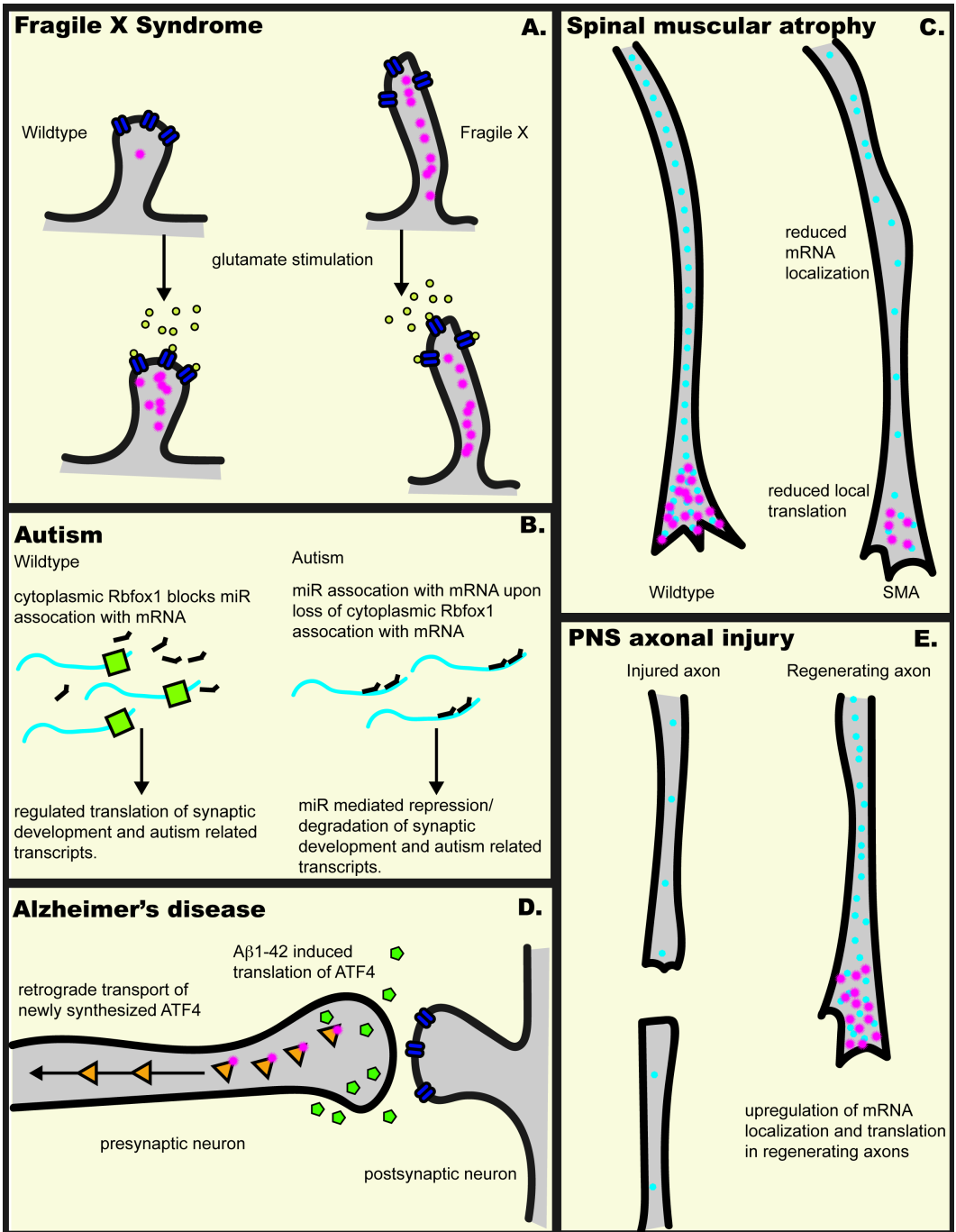


Fig. 4. Translation dysregulation in disease and regeneration.

Local translation (pink stars), is upregulated in fragile x syndrome (FXS) (A). FXS results from loss of the fragile x mental retardation protein (FMRP), which acts as a translational repressor. Upon loss of FMRP, baseline translation is enhanced in FXS relative to wildtype dendrites. This upregulated baseline translation leads to immature spines, which are insensitive to glutamate stimulated enhancement of local translation. Similar to FXS, autism is believed to result from dysregulated protein synthesis (B). Recent work has demonstrated cytoplasmic Rbfox1 binds to 3'UTRs of a number of synaptic and autism relevant transcripts. Loss of Rbfox1 opens up these 3'UTRs for miRNA association, and miRNA mediated repression and degradation of these transcripts. In addition to neurodevelopmental disorders, neurodegenerative disorders are characterized by widespread perturbations of local translation. Spinal muscular atrophy (SMA) (C) is a neurodegenerative disease of spinal motoneurons, characterized by widespread defects in RNP assembly. Evidence has demonstrated defects in localization of mRNA into the axons of SMA motoneurons relative to control neurons, and this reduced localization results in substantial defects in local translation in the axon. Recent evidences have also demonstrated local translation of specific transcripts, including ATF4, as contributing to neuronal death in Alzheimer's disease (AD) (D). A β 1-42 treatment of axonal terminals induces axonal synthesis of ATF4, a transcription factor involved in apoptotic response. Retrograde transport of ATF4 into the cell body results in eventual induction of apoptosis of the neurons. Upregulation of mRNA localization and local translation (E) is essential in axonal injury and regeneration, helping facilitate robust axonal growth.

Chapter 3

The survival of motor neuron protein acts as a molecular chaperone for mRNP assembly

Paul G. Donlin-Asp¹, Claudia Fallini¹, Jazmin Campos¹, Ching-Chieh Chou¹,
Megan E. Merritt^{1,3}, Han C. Phan^{4,5}, Gary J. Bassell^{1,2,3,5}, Wilfried Rossoll^{1,2,3,6*}.

¹Department of Cell Biology

²Center for Neurodegenerative Disease

³Laboratory of Translational Cell Biology

⁴Department of Pediatrics

⁵Department of Neurology

⁶Present address: Department of Neuroscience, Mayo Clinic, 4500 San Pablo
Road, Jacksonville, FL 32224, USA.

*Lead contact

Emory University School of Medicine,
Atlanta, GA 30322

Co-corresponding authors:

Wilfried Rossoll, Ph.D. and Gary J. Bassell, Ph.D.

Emory University School of Medicine

Whitehead Biomedical Research Building, Room 415

615 Michael St NE

Atlanta, GA. USA 30322

email: wrossol@emory.edu and gbassel@emory.edu

Tel: (404) 727-0668

FAX: (404) 727-0570

Summary

Spinal muscular atrophy (SMA) is a motor neuron disease caused by reduced levels of the survival of motor neuron (SMN) protein. SMN is part of a multiprotein complex that facilitates the assembly of spliceosomal small nuclear ribonucleoproteins (snRNPs). SMN has also been found to associate with mRNA binding proteins but the nature of this association was unknown. Here we have employed a combination of biochemical and advanced imaging methods to demonstrate that SMN promotes the molecular interaction between IMP1 protein and the 3' UTR zipcode region of *β-actin* mRNA, leading to assembly of messenger ribonucleoprotein complexes (mRNPs) that associate with the cytoskeleton to facilitate trafficking. We have identified defects in mRNP assembly in cells and tissues from SMA disease models and patients that depend on the SMN Tudor domain and explain the observed deficiency in mRNA localization and local translation, providing insight into SMA pathogenesis as an RNP-assembly disorder.

eTOC Blurb

Donlin-Asp et al. show that in both a murine model of spinal muscular atrophy and human patient samples the association of IMP1 protein with β -actin mRNA is impaired. These results support a role for the survival of motor neuron protein as a molecular chaperone for mRNP assembly.

Highlights

- SMN facilitates the association of IMP1 protein with the 3'UTR of *β-actin* mRNA.
- SMN-deficiency leads to reduced size of IMP1-containing mRNP granules.
- Rescue of mRNP assembly in SMA patient cells depends on the Tudor domain of SMN.
- Impairments of IMP1–mRNA assembly lead to decreased association with the cytoskeleton.

Introduction

Spinal muscular atrophy (SMA) is the leading genetic cause of infant mortality (Prior, 2010). SMA is characterized by synaptic defects in the motor circuitry, especially at the neuromuscular junction (NMJ), and a dying-back axonopathy. This is followed by a gradual loss of motor neurons in the spinal cord, and results in progressive muscle weakness and eventual death due to respiratory distress (Phan et al., 2015). SMA is caused by reduced survival of motor neuron (SMN) protein levels due to either a deletion or mutation in the *SMN1* gene. The ubiquitously expressed SMN protein is vital for normal cellular function, with complete loss of SMN in mice leading to early embryonic lethality (Schrank et al., 1997). In SMA patients, cells produce reduced levels of normal SMN protein from a duplication of the SMN encoding gene, *SMN2* (Lorson et al., 1999b). The mechanism underlying the higher sensitivity of motor neurons to reduced SMN protein levels remains unclear (Burghes and Beattie, 2009; Fallini et al., 2012b; Li et al., 2014a) (Donlin-Asp et al., 2016). SMN and its associated Gemin2-8 proteins function as a molecular chaperone, interacting with and assisting in the assembly of Sm proteins and snRNAs into spliceosomal snRNP complexes without being part of its final structure (Li et al., 2014a). Consistent with the role of SMN in snRNP assembly, splicing defects have been described in a number of SMA models (Baumer et al., 2009; Custer et al., 2016; Gabanella et al., 2007; Garcia et al., 2016; Praveen et al., 2012; See et al., 2014; Zhang et al., 2013). However, these defects are found ubiquitously throughout various tissues (Doktor et al., 2016; Shababi et al., 2014) suggesting additional pathways might contribute to the pathophysiology of SMA. We and others have previously shown SMA-specific defects in the axonal localization of polyA mRNA and

selected transcripts (*β-actin*, *Gap43*, *neuritin*) (Akten et al., 2011; Fallini et al., 2010; Fallini et al., 2016; Fallini et al., 2011; Rossoll et al., 2003) as well as mRNA-binding proteins (HuD, IMP1) (Akten et al., 2011; Fallini et al., 2014; Fallini et al., 2011; Hubers et al., 2011) in SMN-deficient motor neurons. We have also found that overexpression of both HuD and IMP1 can restore axon outgrowth and *Gap43* mRNA and protein localization in growth cones of SMA motor neurons (Fallini et al., 2016). Our findings led us to hypothesize that analogous to its role in snRNP assembly, SMN plays a critical role in the assembly of messenger ribonucleoproteins (mRNPs), and that the reported mRNA localization defects in SMA motor neurons may be caused by a failure to assemble RNA transport complexes (Donlin-Asp et al., 2016).

To test this hypothesis, we have employed a combination of genetic reporters, biochemical fractionations, pull-down assays, and superresolution microscopy methods to quantify the association of specific mRNAs and proteins in mRNP complexes. We consistently found defects in mRNP assembly in cells and tissues from SMA disease models and patients. SMN deficiency leads to reduced binding of mRBPs to their transcripts, the assembly of smaller mRNP granules, and their reduced association with microtubules and actin filaments. Taken together, our data demonstrate that SMN plays a role as a molecular chaperone for mRNPs, indicating that SMN-dependent mRNP-assembly defects cause axonal mRNA localization defects in SMA.

Results

Association of IMP1 protein with the 3'UTR of *β-actin* mRNA is impaired in cultured motor neurons from an SMA mouse model.

To establish a reporter assay for SMN-dependent assembly of mRNP

complexes, in which we could eliminate any direct effect from defects in splicing, we focused on the association of the β -actin 3' untranslated region (3'UTR) with its interacting protein, the *Igf2*-mRNA binding protein 1 or zipcode-binding protein 1 (IMP1/ZBP1) (Deshler et al., 1998; Ross et al., 1997). We have previously reported that IMP1 and SMN associate, and that reduced SMN levels cause impaired axonal localization of IMP1 in cultured primary motor neurons (Fallini et al., 2014). Importantly, the IMP1- β -actin interaction is well characterized, and known to be mediated through a sequence element in the 3'UTR of β -actin ("zipcode") and the mRNA-binding KH-domains of IMP1 (Chao et al., 2010; Farina et al., 2003; Patel et al., 2012).

To study the formation of IMP1- β -actin mRNP complexes, we employed Trimolecular Fluorescence Complementation (TriFC) (Milev et al., 2010; Rackham and Brown, 2004; Yin et al., 2013) as a direct *in situ* method to visualize their association in cells. This technique is a variation of bimolecular fluorescence complementation (BiFC) (Hu et al., 2006; Kerppola, 2013). TriFC measures the binding of an mRNA-binding protein to its target transcript. TriFC uses a set of three reporter constructs including two mRNA-binding proteins fused to split venus yellow fluorescent protein, which upon binding to the same engineered mRNA reporter construct restore the fluorescent venus signal. The mRNA reporter construct encodes cyan fluorescent protein (CFP) followed by a boxB stem loop sequence and the β -actin 3'UTR. The bacteriophage protein λ_{N22} fused to the N-terminal fragment of venus yellow fluorescent protein (YFP) is tethered to the reporter mRNA by binding the boxB motif. When IMP1 fused to the C-terminal fragment of YFP binds the β -actin 3-UTR, it can reconstitute a fluorescent YFP molecule together with the λ_{N22} fusion protein and thus the strength of the signal can be used to measure *in situ* RNA-protein interaction

(Figure 1A,B). Since the TriFC constructs are expressed as cDNAs, their maturation and translation in the cell will not be dependent on splicing, and therefore remain unaffected by SMN-dependent splicing defects. We found that the TriFC signal in primary cultured motor neurons was specific for the Full UTR construct and required both the BoxB motif and the full-length β -actin 3'UTR (Figure 1C-E). Importantly, we observe granular signal in the axon, which is reminiscent of fluorescent *in situ* hybridization signal for β -actin mRNA (Bassell et al., 1998; Fallini et al., 2016; Yao et al., 2006; Zhang et al., 1999). The weak signal for both the no UTR and the Δ BoxB control constructs illustrates the low background generated from IMP1 and λ_{N22} outside of binding to the same mRNA molecule, highlighting the specificity of the TriFC methodology. The Δ Zip construct shows more signal than the background levels in the Δ BoxB and no UTR constructs but less than the Full UTR construct. This is consistent with previous results demonstrating a homologous but less active secondary site downstream of the proximal zipcode motif that shows weak ability to localize β -actin (Kislauskis et al., 1994).

Utilizing TriFC, we next sought to address what was the spatiotemporal relationship of SMN to assembled IMP1- β -actin complexes. If SMN is indeed a chaperone for mRNP assembly, it will not remain part of the final assembled complex. To test this, we compared the co-localization of TriFC signal with SMN to that of TriFC signal with PABPC1, a poly(A) mRNA binding protein, which is a stable component of mRNP granules (Figure 1F-I). In primary motor neurons, PABPC1 shows strong co-localization with the TriFC signal in both the cell body and axon (Figure 1F-G). In comparison, SMN shows weaker co-localization with TriFC granules in the cell body (Figure 1F-G), where these complexes are initially assembled, but even lower levels of co-localization in the axon. In primary human

fibroblasts the same trend is observed (Figure 1H-I), with PABPC1 showing robust co-localization with the TriFC signal, unlike the signal for SMN. These data are consistent with a role for SMN as a molecular chaperone for IMP1- β -*actin* complex assembly.

To determine whether the IMP1- β -*actin* association is SMN-dependent, we employed this TriFC assay in motor neurons derived from a severe SMA mouse model (Monani et al., 2000). We observed a clear deficiency in the assembly of IMP1- β -*actin* complexes in SMA motor neurons (Figure 2A,B). Importantly, as the cellular production of the TriFC components does not directly depend on splicing, this defect in assembly of IMP1- β -*actin* complexes in SMA motor neurons is uncoupled from defective snRNP assembly. To provide biochemical evidence for impaired mRNP assembly, we performed RNA immunoprecipitation against IMP1 from embryonic brain lysates followed by qRT-PCR and found a similar reduction in the association of β -*actin* with IMP1 in SMA embryos (Figure 2C). Importantly, there is no change in steady state levels of either β -*actin* mRNA or IMP1 protein levels (Figure 2E,F), when SMN protein levels are reduced, suggesting a specific reduction in IMP1- β -*actin* association. Taken together, all of these data demonstrate an impairment of IMP1- β -*actin* association in SMA motor neurons and brain tissue, consistent with a role of SMN in the assembly of mRNP complexes.

IMP1 mRNP granules show assembly defects and reduced size in SMA patient fibroblasts.

We next sought to address if the IMP1- β -*actin* association defect is present in human SMA patient cells. We performed TriFC experiments in four SMA and four control primary fibroblast lines (Figure 3A,B) and found a clear

deficiency in the assembly of these IMP1– β -actin complexes in all SMA patient lines. These data confirm our results from murine SMA motor neurons, and demonstrate that the splicing-independent IMP1– β -actin assembly defect is conserved in human patient samples.

Similar to the SMA mouse model, IMP1 protein levels remain unchanged in SMA fibroblast lines relative to controls (Figure 4A,B), whereas SMN levels are reduced as expected. To determine if IMP1 association with mRNA is SMN-dependent, we employed an approach based on mRNA interactome capture (Castello et al., 2016b). Using UV-crosslinking, followed by affinity purification with oligo(dT) beads under stringent conditions, we were able to capture endogenous mRNA-protein association (Figure 4C). Our experiments revealed a reduced amount of IMP1 protein pulled down with mRNA in SMA patient fibroblasts (Figure 4D,E), confirming that the association of endogenous IMP1 with mRNA is defective under conditions of reduced SMN protein levels.

mRNP granules are thought to consist of one or multiple transcripts that are bound by a diverse set of mRBPs (Buxbaum et al., 2015; Castello et al., 2013; Holt and Schuman, 2013; Martin and Ephrussi, 2009). To determine the complexity of mRNP granules, we adapted a density centrifugation method that has been established for the size fractionation and isolation of mRNPs (Fritzsche et al., 2013). In SMA fibroblast lysates, IMP1 shows a leftward shift towards lighter fractions as compared to control lysates, with an almost complete depletion from the heaviest fraction, which is consistent with decreased granule size (Figure 5A,B). A similar SMA-specific defect is seen for the cytoplasmic polyA-binding protein PABPC1 (Figure S2A,B), which shows a similar shift towards lighter fractions in its distribution pattern. These data indicate that widespread reductions in mRNP granule size is present in SMA. Non-RNA

associated proteins, α -tubulin (Figure S1A,B) and β -actin (Figure S1C,D) do not show an altered gradient distribution.

IMP1 mRNP granules are reduced in volume in SMA patient fibroblasts.

We next undertook direct visualization of IMP1-containing granules in SMA and control fibroblasts to confirm this finding *in situ*. Employing superresolution structured illumination microscopy (SIM) (Gustafsson, 2000; Gustafsson et al., 2008), we compared the nanoscale structure of IMP1 granules in SMA and control fibroblasts (Figure 6A-D). In SMA fibroblasts, a clear reduction in granule volume is seen. This finding confirms our biochemical evidence of impaired IMP1 association with mRNA and decreased size in biochemical fractionation. As an additional confirmation, we sought to determine if reduction of the volume of IMP1 granules in SMA fibroblasts is SMN dependent. We found that exogenous expression of mCherry-SMN drastically increases IMP1 granule volume, thus corroborating our findings (Figure 6E,F). The restoration of granule volume is dependent on the Tudor domain of SMN. Previous results show that IMP1 and SMN associate in a Tudor domain dependent manner (Fallini et al., 2014), indicating that IMP1 granule assembly is dependent on a direct interaction with SMN. All of these data demonstrate that the assembly of IMP1-containing granules and probably other mRNPs is deficient in SMA.

IMP1 mRNP granules show decreased association with the cytoskeleton in SMA patient fibroblasts.

Previous work in primary motor neurons has demonstrated IMP1 mislocalization in both SMN-depleted and SMA motor neurons. Therefore, we

sought to assess if a similar localization defect occurs in SMA patient fibroblast lines (Figure 7A-C). Indeed, IMP1 shows altered distribution in SMA patient fibroblasts, with a specific reduction at the leading edge of the fibroblasts (Figure 7C), but no overall change in the actin rich lamellipodia. Interestingly, the distribution pattern of IMP1 signal in the lamellipodia is altered in the SMA patient fibroblasts (Figure 7A). Whereas in the control fibroblasts IMP1 aligns along linear structures in the lamellipodia (percent of cells showing linear IMP1 arrays; nDFb-1: 47.37%, nDFb-2: 56.86%, Ctrl78: 54.72%, Ctrl79: 51.85%) this ordered distribution pattern is reduced in SMA patient fibroblasts (percent of cells showing linear IMP1 arrays; SMApt1: 21.54%, SMApt2: 17.53%, SMA0232: 18.31%, SMA9677: 22.1%). Based on these results, we predicted that defects in mRNP assembly leads to a reduced formation of mature transport granules that are transported along cytoskeletal structures (Xing and Bassell, 2013).

Therefore, we sought to determine if as a consequence of reduced SMN levels, IMP1 shows altered association with the cytoskeleton. Utilizing SIM, we took advantage of the enhanced axial and lateral resolution to resolve IMP1 mRNP granule association with both microtubules and actin filaments (Figure 7D-G). Superresolution imaging and 3D reconstructions of all IMP1 signal falling in the volume of the cytoskeleton, allowed direct comparison of the total number of IMP1 granules associating with either actin or microtubules in control and SMA fibroblasts. This stringent analysis demonstrates a substantial reduction of IMP1 co-localization with both the actin and microtubule cytoskeleton in SMA fibroblasts relative to control lines (Figure 7A-D), consistent with the predicted mRNP assembly defect leading to a cytoskeleton association defect.

Furthermore, biochemical separation of proteins in the cytoskeleton-bound and free fractions, allowed direct assessment of the amount of IMP1 enriched on the

intact filamentous cytoskeleton (Wang et al., 2008a). This assay confirms reduced association of IMP1 with actin and tubulin in SMA patient vs. control fibroblasts (Figure 7E-F). Given that cytoskeletal protein levels were not affected (Figure S1), this reduced co-purification of IMP1 with the cytoskeleton likely reflects a specific defect in the assembly of transport-competent mRNP complexes. To test the effect of reduced association of IMP1 with the cytoskeleton and increased diffusion *in situ*, we performed fluorescence recovery after photobleaching (FRAP) to assess the dynamic behavior of IMP1 in control and SMA fibroblasts (Figure 7J-L). The maximal recovery of GFP-IMP1 in SMA patient fibroblasts is increased relative to the control lines, indicating a reduction in the immobile fraction (Figure 7K-L), which is consistent with a reduction in association and anchoring of IMP1 on the cytoskeleton. Taken together, these data provide a molecular mechanism how mRNAs and mRBPs fail to localize in SMA, with a reduction in functional SMN protein levels resulting in impaired association of mRBPs with mRNA, which leads to decreased assembly into mature transport complexes, causing mislocalization of mRNA and reduced local translation in SMA.

Discussion

The assembly of mRNA-binding proteins (mRBPs) with mRNAs into higher order mRNP granules regulates all stages of post-transcriptional regulation for mRNAs, including splicing, export, stability, subcellular localization, and translation of mRNAs. Misregulation of proper RNA-protein association via either excessive or reduced assembly of RNPs can lead to human diseases. Hyper-assembly into pathological mRNP aggregates is thought to contribute to a number of neurodegenerative disorders, including amyotrophic lateral sclerosis

(ALS) and multisystem proteinopathy (Shukla and Parker, 2016). Pathological RNP hyper-assembly has been well characterized, resulting in structures such as stress granules transitioning from a liquid droplet like state in normal stress granules to more persistent abnormal granules and finally detergent-insoluble pathological aggregates (Lin et al., 2015; Shukla and Parker, 2016). The mechanisms, and specifically the molecular machinery, which regulates proper mRNA-protein association remains to be fully elucidated (Li et al., 2013).

SMA is characterized by SMN-dependent defects in the formation of RNPs and therefore represents an RNP hypo-assembly disease. Previous work on SMN has conclusively identified it as a chaperone for the assembly of snRNPs (Burghes and Beattie, 2009; Li et al., 2014a), but it has been proposed to play additional roles, which would contribute to the neurodegeneration phenotype (Burghes and Beattie, 2009; Donlin-Asp et al., 2016; Li et al., 2014a). While indirect evidence has been collected for mRNA mislocalization for a number of transcripts including *β-actin*, *Gap43*, *neurtin* and polyA mRNA (Akten et al., 2011; Fallini et al., 2010; Fallini et al., 2016; Fallini et al., 2011; Rossoll et al., 2003), there has been a lack of thorough investigation into the SMN-dependent molecular mechanism that influence these processes. Recently, we and others have proposed that SMN may play a more general role as a chaperone for the assembly of not only heptameric Sm-protein and related LSm-protein complexes with a role in pre-mRNA splicing and histone mRNA 3'-processing, but potentially also for heterogeneous mRNP complexes that regulate mRNA localization and stability (Li 2014, Donlin-Asp 2016). However, until now direct evidence for a mechanistic role of SMN in mRNP complex assembly was missing.

Through this study we have for the directly addressed the functional role

of SMN in mRNA localization. Our results demonstrate that SMN, via a transient association, facilitates the assembly of IMP1 protein with β -actin mRNA independent of SMN's role in snRNP-assembly and splicing (Figure 1-3). This SMN-dependent defect in mRNP assembly leads to smaller IMP1 granules and proper assembly requires SMN's mRBP-binding Tudor domain (Figure 4-6, Figure S1-2). Assembly defects cause decreased association of IMP1 with the cytoskeleton and defective localization to the leading edge (Figure 7). Through employing a series of complementary biochemical and imaging methods across various *in vitro* and *in vivo* SMA disease models, we were able to demonstrate that SMN acts as a molecular chaperone for mRNP assembly, defined as a protein that interacts with and aids in the folding or assembly of other proteins without being part of their final structure (Kim et al., 2013). Our results suggest that beyond IMP1 granules there is a more general defect in bulk PABPC1 mRNP assembly that is likely to affect the localization of most transcripts (Figure S2A,B). This corroborates and further explains our previous finding that SMN-deficiency causes mislocalization of not only specific transcripts such as β -actin and *Gap43* (Fallini et al., 2016), but also bulk polyA mRNA in axons of motor neurons (Fallini et al., 2010; Fallini et al., 2016; Fallini et al., 2011) and a large assortment of specific mRNAs (Saal et al., 2014).

The complex network of SMN's protein interactions (Kroiss et al., 2008; Otter et al., 2007; Shafey et al., 2010), including Sm proteins (Buhler et al., 1999; Friesen et al., 2001), LSm proteins (Friesen and Dreyfuss, 2000; Pillai et al., 2003), and mRNA binding proteins (Akten et al., 2011; Fallini et al., 2014; Fallini et al., 2011; Hubers et al., 2011; Piazzon et al., 2008; Rossoll et al., 2002; Tadesse et al., 2008) highlights the variety of complex processes that are likely defective upon reduction of SMN protein levels. The mounting evidence that

SMN broadly functions as a chaperone for RNP assembly strongly suggests that defects in a broad spectrum of RNA processing, including splicing (Li et al., 2014a), stability, localization (Fallini et al., 2016; Rossoll et al., 2003), and translation (Fallini et al., 2016; Kye et al., 2014; Sanchez et al., 2013) contribute to SMA pathology. The contributions of each of these individual processes remain to be fully evaluated, however the dysregulation of all of these processes taken together likely explains the unique onset and presentation of the disease. For mRNP localization in particular, it remains to be seen how this manifests *in vivo*, and if local translation defects reported upon SMN deficiency (Fallini et al., 2016) stem from reductions in RNA delivery or from a direct role for SMN in axonal protein synthesis itself (Dombert et al., 2014; Kye et al., 2014; Prescott et al., 2014; Rage et al., 2013; Zhang et al., 2006). The observed defect in mRNP assembly in the cell body occurs upstream of the previously characterized localization defects, which then result in decreased local translation. Future studies will need to show how local dynamics of mRNP assembly and disassembly are affected in SMA, as mRNPs are well known to undergo dynamically regulated assembly and disassembly in distal regions of the axon, which may be a function of axonally localized SMN during development (Hao et al., 2015; Zhang et al., 2006; Zhang et al., 2003).

An important remaining question is the scope of RNP defects in SMA *in vivo*, and how these defects contribute to the disease phenotypes observed in SMA. Given the known functions of SMN, SMA likely is a disease of general RNP hypo-assembly, where one expects widespread effects on all stages of posttranscriptional regulation (Donlin-Asp et al., 2016; Shukla and Parker, 2016), which will lead to widespread alterations in splicing, stability, localization and translation of RNA transcripts. This raises an intriguing question if all of these

processes contribute to the manifestation of SMA pathology, or if specific defects in particular RNP classes result in certain phenotypes. Future work will need to address if rescuing the assembly of specific RNP classes, such as snRNPs or mRNPs, can mitigate some or all of the disease phenotypes.

Experimental Procedures

Cell culturing, transfections, and staining.

Primary motor neurons from wild type and SMA (*Smn*^{-/-}; *hSMN2*; Stock number: 005024, Jackson Laboratories) E13.5 mouse embryos were isolated, cultured, and transfected as previously described (Fallini et al., 2010). Primary fibroblast lines were acquired from Coriell (Ctrl: ND29178, ND29179, SMA: GM09677, GM00232), or derived from dermal skin biopsies obtained from Emory University Children's Healthcare of Atlanta (SMApt1 and SMApt2). Patients SMApt1 and SMApt2 presented with signs of muscle weakness by the age of 2 months and were diagnosed with SMA type I after evaluation by a neurologist followed by genetic testing. Quantitative dosage analysis of genomic DNA showed 0 copy of *SMN1* and 2 copies of *SMN2* for both patients, correlating with the clinical impression. Additionally, two neonatal dermal fibroblast lines from foreskin (nDF-1, nDF-2; Invitrogen) were used for experimental procedures. Fibroblasts were cultured as described previously (Vangipuram et al., 2013). Transfections were performed using Lipofectamine LTX (Invitrogen). Neuro2a cells were cultured as previously described. IF was performed against IMP1 (1:500, MBL) and alpha tubulin (1:250, Abcam) overnight at 4°C.

Image Acquisition and Analysis.

For fluorescence imaging, a 60x objective (1.4 NA) was used. Z-series (5 to 25 sections, 0.2µm thickness) were acquired with an epifluorescence microscope (Ti Eclipse, Nikon) equipped with a cooled CCD camera (HQ2, Photometrics). Z-stacks were deconvolved (Media Cybernetics) and analyzed using Imaris (Bitplane). For quantitative imaging experiments, image exposure settings were set at the beginning of the experiment and kept constant through all conditions

and investigators were kept blind to the genotypes of all samples at the time of imaging and throughout all subsequent image analysis. Images were prepared using the Fiji software package (ImageJ).

Steady state protein level assessment

E13.5 mouse brains were homogenized in lysis buffer (50mM Tris-HCl, 150mM NaCl, 2% Triton X-100, protease inhibitors) and sonicated on ice for 3x10 minutes. Primary human fibroblasts were trypsinized, washed in PBS and counted (BioRad), and cell number was normalized prior to lysis in RIPA buffer. Proteins were separated on a 10% polyacrylamide-SDS gel and hybridized with primary antibodies directed against SMN (BD Bioscience, 1:500), IMP1 (MBL, 1:1000), β -actin (Sigma, 1:1000), and tubulin (Sigma, 1:1000). The intensity of the protein bands was quantified using an Odyssey imaging system and LiCor Image Studio.

TriFC

TriFC constructs were cloned similarly to previous described (Rackham and Brown, 2004). For TriFC experiments, IMP1-VFP₁₋₁₅₄, λ N₂₂-VFP₁₅₅₋₂₃₉, and CFP-UTR's transfected into cells in a 1:1:1 ratio to limit oversaturation of TriFC signal. Expression of constructs was limited to 12-24 hours, and fixation was performed with 4% paraformaldehyde, followed by anti-GFP (Abcam) immunofluorescence with an Alexa647 secondary antibody. Exposure settings were held constant for all acquisitions for an experiment. Analysis was performed in Imaris (Bitplane). The total sum of pixel intensities was measured in a 3D volume for both the CFP and YFP channels, and the ratio of YFP/CFP was determined for the readout of TriFC signal.

RNA immunoprecipitation

RNA immunoprecipitation (RIP) experiments were performed following published protocols (Selth et al., 2009). For each RIP experiment, three SMA embryonic brain lysates were pooled as were three control littermate lysates.

Immunoprecipitations were carried out overnight at 4C using a polyclonal IMP1 antibody (MBL). Following washes, RNA was extracted using Trizol reagent (Invitrogen). qRT-PCR was performed on a LightCycler (Roche) using a previously described primer sets for *β-actin* (5'-TGTTACCAACTGGGACGACA-3' and 5'-GGGGTGTGGAAGGTCTCAA-3') and *Gapdh* (5'-GAGTCTACTGGTGTCTTCAC-3' and 5'-CCACAATGCCAAAGTTGTCAT-3') (Xing et al., 2012). Data was analyzed using the $2^{-\Delta\Delta Ct}$ method (Livak and Schmittgen, 2001).

mRNA interactome

The mRNA interactome capture approach (Castello et al., 2013) was adapted for use on smaller scale isolation. In short, fibroblasts grown to confluency in four 10cm tissue culture dishes per line, washed in cold PBS and UV-crosslinked at 400mJ. Cell pellets were lysed in 2ml of lysis buffer and split into two 1mL aliquots, one of which were treated with RNaseA/T1 mix for 10 mins at 37°C. 900µl of sample were then incubated with 250µL of oligo(dT) beads following the original protocol, with all subsequent washes being performed with 1mL of wash buffers. 60µL's of elution buffer was added to the beads along with RNaseA/T1 for 10 mins at 37°C. Samples were brought to 1X in SDS-PAGE buffer and run on 10% SDS-PAGE gels. Immunoblots against IMP1 were performed, and data was analyzed by quantifying IMP1 signal in both the Pulldown lane and the

Pulldown +RNaseA/T1 lane and dividing these values over the Input lane value to determine IMP1 enrichment.

RNP isolation

RNP isolation experiments were adapted for cells in culture from a published protocol (Fritzsche et al., 2013). The top eight 1 mL fractions were collected based on initial characterization of the gradient composition after a 2.5 hour centrifugation at 4°C at 40,000 RPM. Fractions were brought to 1X in SDS-PAGE lysis buffer and flash frozen in liquid nitrogen. Samples were run on 4-15% precast SDS-PAGE gels (Biorad) at 80V for 2 hours. Immunoblots against IMP1, α tubulin (Abcam), β -actin (Abcam) and PABPC1 (Abcam) were performed, and data was analyzed by quantifying the total sum of the signals in all fractions and dividing the total signal per individual fraction over this value to determine the total enrichment per individual fraction.

Structured Illumination Microscopy of IMP1 granules

Two-color 3D SIM was performed on a Nikon SIM microscope using a 100x (1.49 NA) object. 3D SIM images were analyzed in Imaris 8.1 software (Bitplane). For granule volume 3D surfaces were generated using a constant threshold for an experiment set and particle volume in nm^3 was recorded. Five individual fibroblasts were imaged per individual line and experiments were performed in triplicate for a total of 15 cells per line. For granule association with the cytoskeleton, either the actin or microtubule channel was used to generate a 3D surface. This surface was used to mask and duplicate the IMP1 channel into a new separate channel, representing the IMP1 signal that fell within the cytoskeleton volume, which was then subjected to particle counting, as was the

original IMP1 image. The total number of particles in the cytoskeleton associated channel over the total number of IMP1 particles represents the % cytoskeletal associated IMP1.

Cytoskeletal association of mRNPs

Quantification of cytoskeletal association of IMP1 was carried out as previously described for FMRP (Wang et al., 2008a). For RNase controls, RNaseA/T1 (Invitrogen) treatments were carried out at 37°C for 10 minutes. Lysate was spun down for 1 min at 700g to pellet nuclei, and the supernatant was spun down at 16,000g at room temp for 20 minutes. Both pellet and supernatant fractions were suspended to 1X SDS-PAGE buffer and then run on 10% polyacrylamide gels. Western blots were performed for IMP1 to assess enrichment in the cytoskeletal pellet. Blots were quantified by assessing IMP1 in the pellet over IMP1 in the supernatant.

Fluorescence Recovery After Photobleaching

Primary human fibroblasts expressing GFP-IMP1 were grown in glass bottom dishes (MatTek). Imaging was performed on a Nikon A1R laser-scanning confocal microscope (equipped with a 60×/1.40 NA oil immersion objective and a temperature-regulated enclosure at 37°C. FRAP sequences consisted of two prebleach images, photobleaching of a section the cell at 100% laser intensity for 1 second pulses for a total of 10 bleach pulses, followed by acquisition of postbleach images every 1s for 5 min. Fluorescence recovery was calculated as the ratio of the background-subtracted fluorescence intensities within the bleach area to an unbleached region of the cell. Normalized value curves and exponential curves were generated in Graphpad Prism (GraphPad Software).

Statistical methods

Statistical analyses were performed by tests appropriate for experimental design.

For single comparisons either the Student T-test or Kolmogrov-Smirnov test was used and for multiple comparisons Tukey's multiple comparisons were used.

Analysis was performed in GraphPad Prism (GraphPad Software). SEM is represented as error bars in the graphs

Author Contributions:

Conceptualization, P.G.D.A, C.F, G.J.B, and W.R; Methodology, P.G.D.A, C.F, and W.R.; Investigation, P.G.D.A; Formal Analysis, P.G.D.A, and J.C; Writing--- Original Draft, P.G.D.A, and W.R; Writing--- Reviewing and Editing, P.G.D.A, C.F, G.J.B, and W.R; Funding Acquisition, G.J.B, and W.R; Resources, P.G.D.A, C.F, C.C.C., H.C.P, and M.E.M; Supervision, G.J.B, and W.R.

Acknowledgments:

The authors thank Lian Li and Shirley Huang for excellent technical support. This work was supported by the Muscular Dystrophy Association (MDA) and Weissman Family Foundation to GJB; the US National Institute of Health (NIH) Grant NS091749 to WR; the National Research Service Award (NRSA) training award F31NS084730-01 and ARCS Fellowship Roche Foundation award to PGDA. This research project was supported in part by the Emory University Integrated Cellular Imaging Microscopy Core of the Emory Neuroscience NINDS Core Facilities grant, P30NS055077. This study used samples from the NINDS Cell Line Repository (<http://ccr.coriell.org/ninds>), as well as clinical data. NINDS and NIGMS Repository sample numbers corresponding to the samples used are: ND29178, ND29179, GM09677, and GM00232.

Figures:

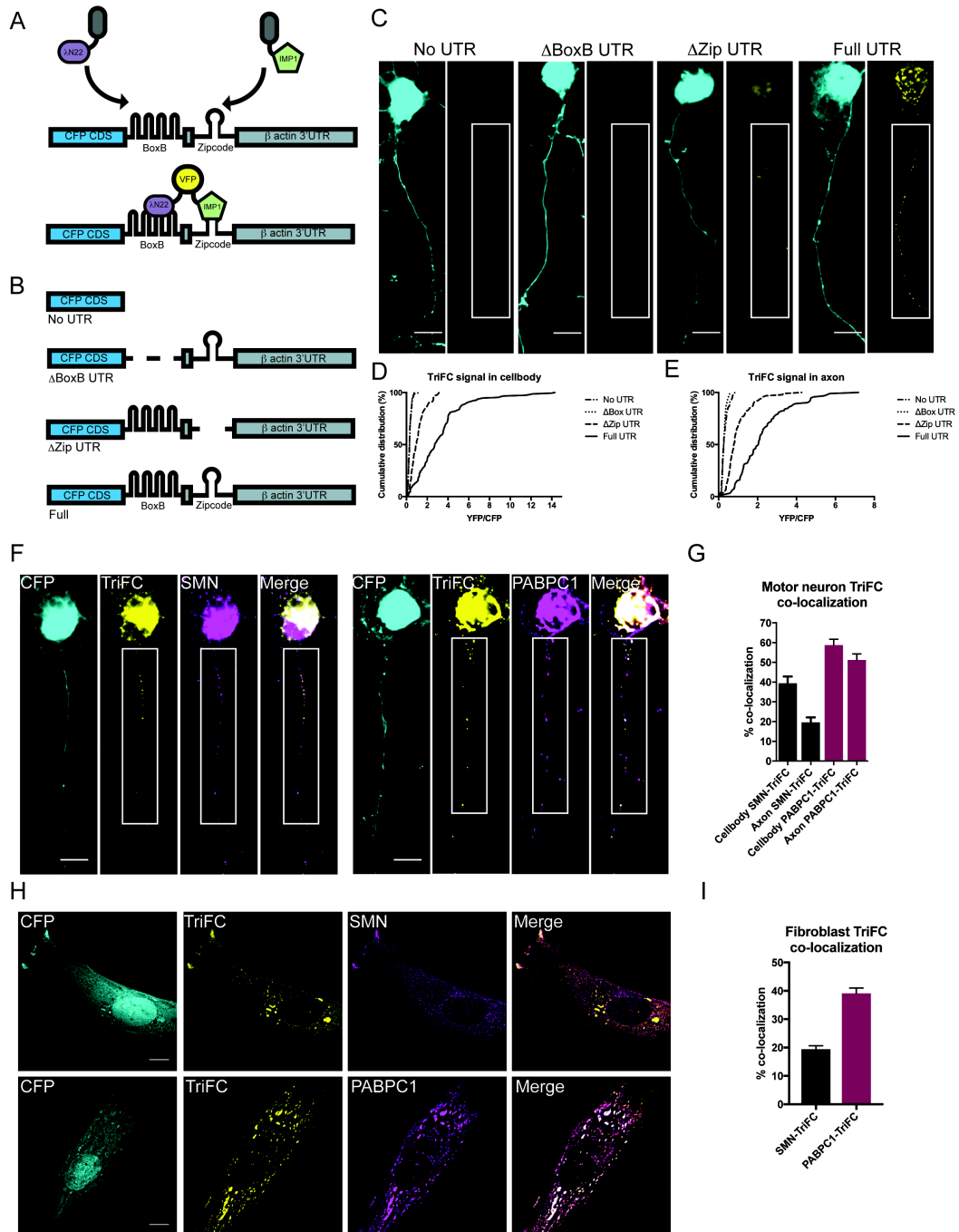


Figure 1:

Trimolecular Fluorescence Complementation (TriFC) allows visualization of RNA and protein association *in situ*. **A.** Schematic of TriFC methodology. Upon expression of IMP1 and λN_{22} fused to complimentary fragments of venus yellow fluorescent protein, only binding of both fusion proteins to the same mRNA reporter will lead to reconstitution of the fluorescent protein. **B.** Reporter constructs include the entire β -actin 3' untranslated region (**Full UTR**), a negative control lacking the 3'UTR (**no UTR**), a control lacking the binding site for the bacteriophage RNA-binding protein λN_{22} binding site (**Δ BoxB UTR**), and one lacking the main IMP1-binding "zipcode" region (**Δ Zip UTR**). **C.** Example images of TriFC controls in primary murine motor neurons. YFP intensities were normalized in all examples. For axonal segments in white boxes brightness and contrast were enhanced to highlight axonal granule signal (insets). Scale bar = 10 μ m. **D.** Quantification of YFP/CFP signals for the cell body. Analyzed by Tukey's multiple comparisons, for breakdown of statistical comparisons see Table S1. N=5, >50 cells/condition. Mean \pm SEM; No UTR: .319 \pm .0190, Δ Box UTR: .314 \pm .015, Δ Zip UTR: 1.10 \pm .076, Full UTR: 3.22 \pm .209. **E.** Quantification of YFP/CFP signals for the axon. Analyzed by Tukey's multiple comparisons, for breakdown of statistical comparisons see Table S2. N=5, >50 cells/condition. Mean \pm SEM; No UTR: .311 \pm .018, Δ Box UTR: .277 \pm .011, Δ Zip UTR: .990 \pm .073, Full UTR: 2.24 \pm .141. **F.** Example images of TriFC signal

localization relative to SMN (left) or PABPC1 (right) in primary murine motor neurons. For enlarged axonal segments in white boxes, brightness and contrast were enhanced to highlight axonal granule signal (insets). Scale bar = 10 μ m. **G.** Quantification of co-localization of TriFC signal with SMN and PABPC1 for the axon and cell body. N=4, >40 cells/condition. Mean \pm SEM; Cell body SMN-TriFC: 39.39% \pm 3.454%, Axon SMN-TriFC: 19.6% \pm 2.531%, Cell body PABPC1-TriFC: 58.77% \pm 2.944%, Axon PABPC1-TriFC: 51.26% \pm 3.012%. **H.** Example images of TriFC signal localization relative to SMN (top) or PABPC1 (bottom) in primary human fibroblasts. Scale bar = 10 μ m. **I.** Quantification of co-localization of TriFC signal with SMN and PABPC1. N=3, 50 cells/condition. Mean \pm SEM; SMN-TriFC: 19.44% \pm 1.221%, PABPC1-TriFC: 39.09% \pm 1.892%.

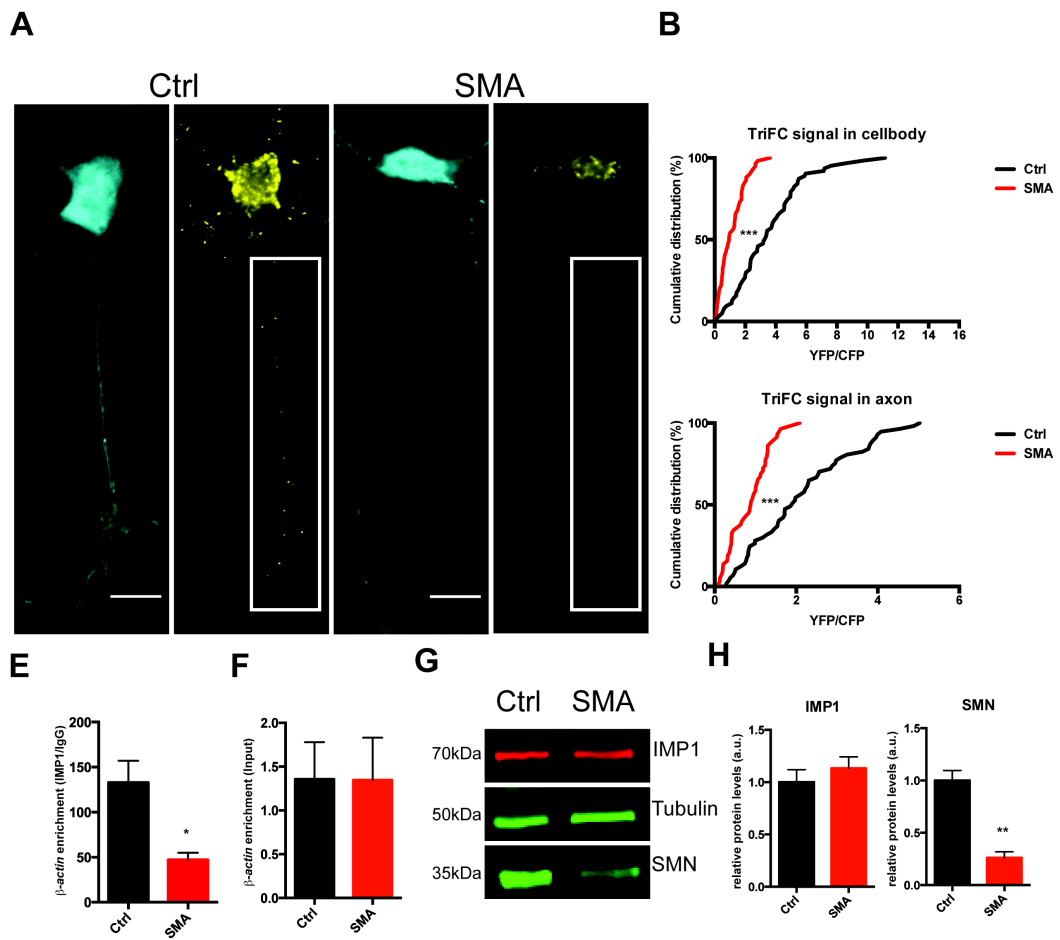


Figure 2:

IMP1 and *β-actin* association is reduced in an SMA mouse model. **A.** TriFC in SMA motor neurons show reduced IMP1–*β-actin* granule assembly relative to wild type littermate controls. Scale bar =10μm. **B.** Quantification of cell body and axonal TriFC signal. n=3, >50 cells/condition. Analyzed by Kolmogorov-Smirnov test, p<.0001. Cell body values mean ± SEM; Ctrl: 3.555 ± .288, SMA: 1.130 ± .108; axon values for mean ± SEM; Ctrl: 2.098 ± .169, SMA: .851 ± .065. **C.** RNA-immunoprecipitation with anti-IMP1 antibodies from embryonic brain lysate shows reduced association with *β-actin* mRNA in SMA brain lysate versus littermate controls. n=3, analyzed by Student T-test, p<0.05. Error bars +/- SEM. Mean ± SEM; Ctrl: 132.9 ± 24.12, SMA: 47.22 ± 7.74. **D.** Input levels of *β-actin* mRNA are unchanged. Error bars +/- SEM. Mean ± SEM; Ctrl: 1.357 ± .423, SMA: 1.343 ± .483; p= .989. **E.** IMP1 protein levels also remain unchanged, whereas SMN levels are significantly reduced. **F.** Quantification of E, n=3, analyzed by Student T-test, p<.01. Error bars +/- SEM. IMP1 protein levels mean ± SEM; Ctrl: 1.00 ± .120, SMA: 1.134 ± .108; p= .454; SMN protein levels mean ± SEM; Ctrl: 1.00 ± .096, SMA: .262 ± .0561; p= .003.

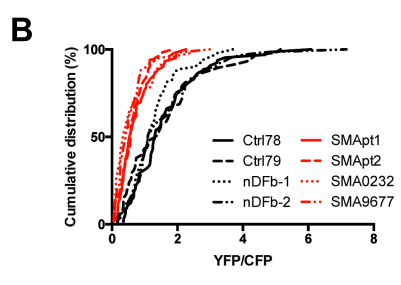
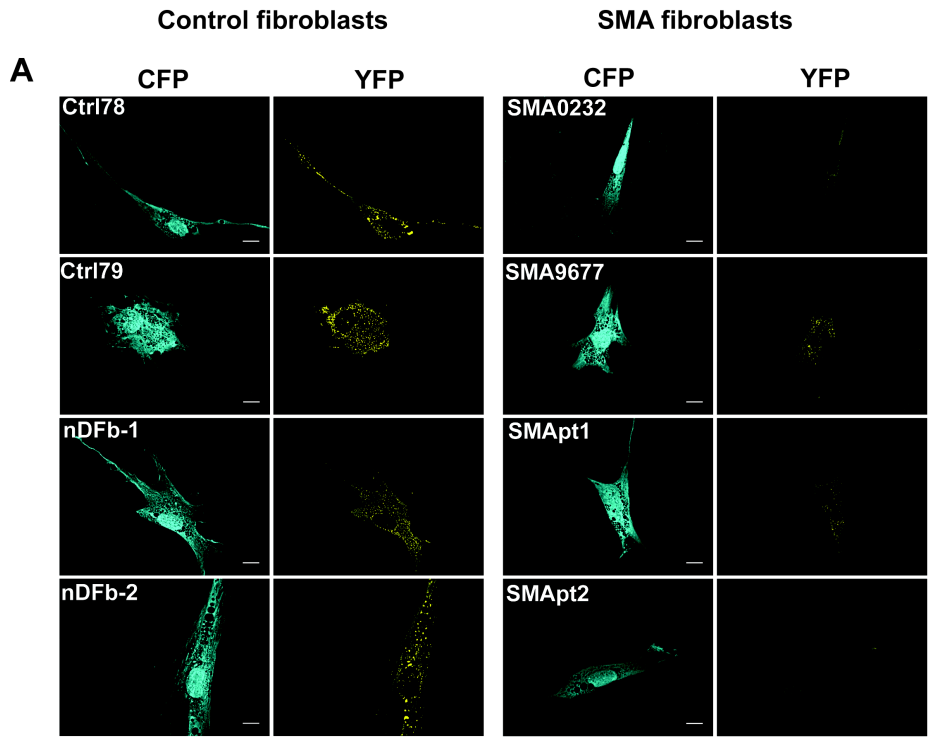


Figure 3:

IMP1 and β -actin association is reduced in SMA patient fibroblasts. **A.** TriFC in SMA primary fibroblasts show reduced IMP1- β -actin granule assembly relative to control fibroblast lines (Ctrl78,79 and nDFb1,2). Scale bar = 10 μ m. **B.** Quantification A. n=3, >50 cells/condition. Mean \pm SEM; Ctrl78: 1.620 \pm .147, Ctrl79: 1.743 \pm .179 nDFb-1: 1.456 \pm .124, nDFb-2: 1.737 \pm .185, SMApt1: .774 \pm .0791, SMApt2: .634 \pm .0626, SMA0232: .610 \pm .089, SMA9677: .559 \pm .075. Analyzed by Tukey's multiple comparisons. For a detailed breakdown of statistical comparisons see Table S3.

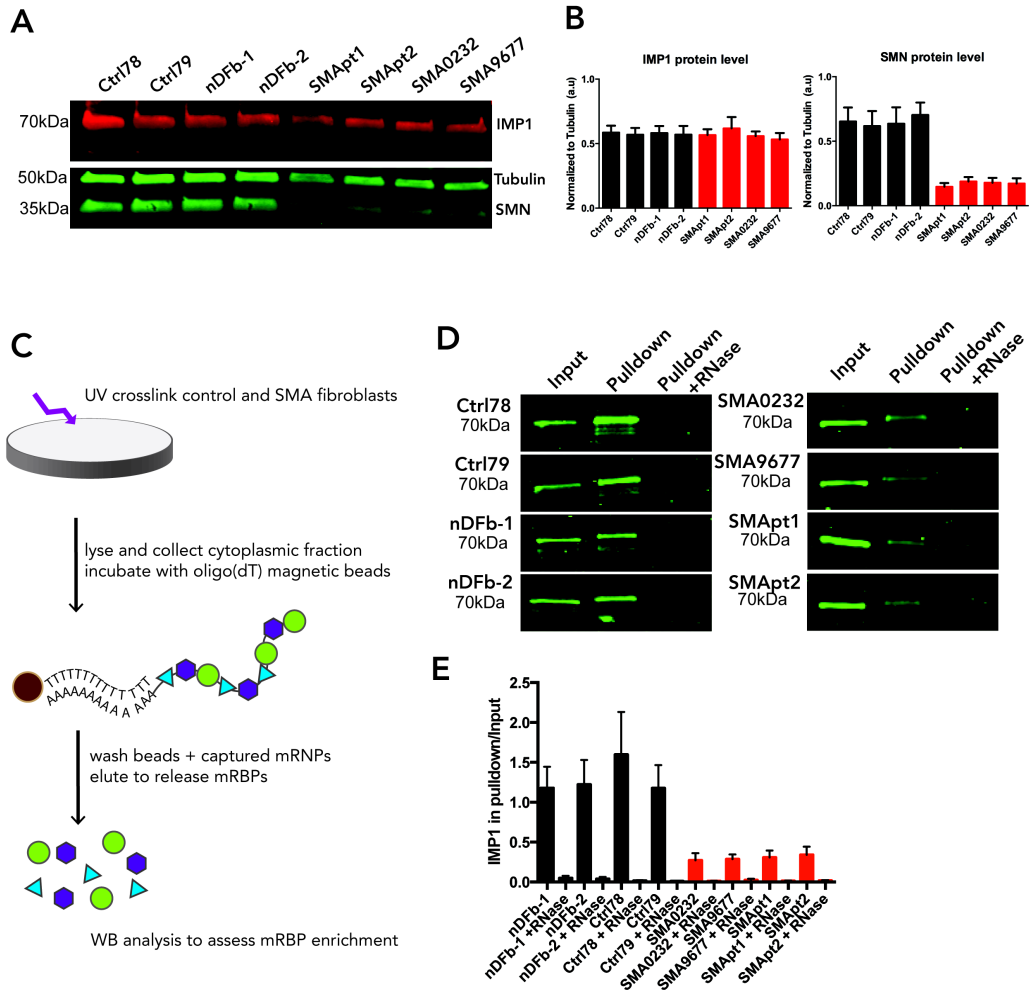


Figure 4:

IMP1 association with mRNA is impaired in SMA patient fibroblasts. **A.** IMP1 protein levels in SMA patient fibroblasts remain unchanged relative to controls, whereas SMN levels are significantly reduced. **B.**

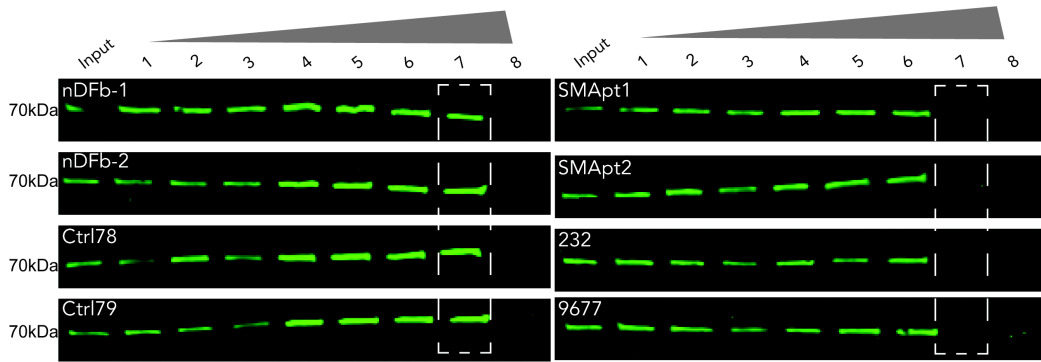
Quantification of A. n=3, for statistical comparisons see Table S4 for IMP1 values and Table S5 for SMN values. Error bars +/- SEM. SMN protein levels mean \pm SEM; Ctrl 78: $.652 \pm .109$, Ctrl 79: $.617 \pm .117$, nDFb-1: $.636 \pm .128$, nDFb-2: $.703 \pm .097$, SMApt1: $.147 \pm .0279$, SMApt2: $.188 \pm .034$, SMA0232: $.178 \pm .038$, SMA9677: $.172 \pm .040$. **C.** Schematic

representation of the mRNA interactome assay. Control or SMA patient fibroblasts are subjected to UV-crosslinking and cytoplasmic lysates are incubated with oligo(dT) beads. Isolates are then used for western blot analysis for assessment of IMP1 association with mRNA. **D.** Quantification of mRNA-binding proteins demonstrates a significant decrease in the amount of IMP1 protein pulled down from SMA patient fibroblasts. **E.**

Quantification of D. n=6, for statistical comparisons see Table S6. Error bars +/- SEM. Mean \pm SEM; nDFb-1: 1.179 ± 0.265 , nDFb-1 +RNase: 0.049 ± 0.029 , nDFb-2: 1.222 ± 0.309 , nDFb-2 + RNase: 0.036 ± 0.026 , Ctrl78: 1.596 ± 0.536 , Ctrl78 + RNase: 0.016 ± 0.008 , Ctrl79: 1.176 ± 0.289 , Ctrl79 + RNase: 0.009 ± 0.003 , SMA0232: 0.272 ± 0.09 , SMA0232 + RNase: 0.012 ± 0.004 , SMA9677: 0.287 ± 0.058 , SMA9677 + RNase: 0.024 ± 0.016 , SMApt1: 0.308 ± 0.087 , SMApt1 + RNase: 0.013 ± 0.005 ,

SM Apt2: 0.341 ± 0.102 , SM Apt2 + RNase: 0.017 ± 0.007 .

A



B

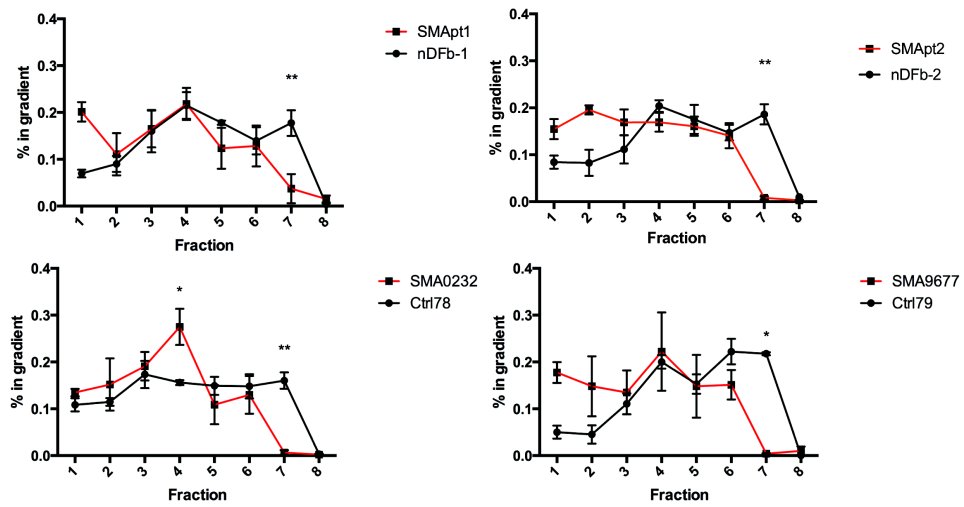


Figure 5:

IMP1 granules show reduced complexity in SMA patient samples. **A.** Cytoplasmic RNP isolates from fibroblasts were subjected to Optiprep gradient centrifugation and fractions were analyzed for the presence of IMP1. SMA lysates show altered distribution of IMP1 complexes relative to control fractions. **B.** Distributions plotted as enrichment in % of the total signal in all fractions found in one particular fraction. n=3, analyzed by Sidak's multiple comparisons test, *p<.05, **p<.01. Error bars +/- SEM.

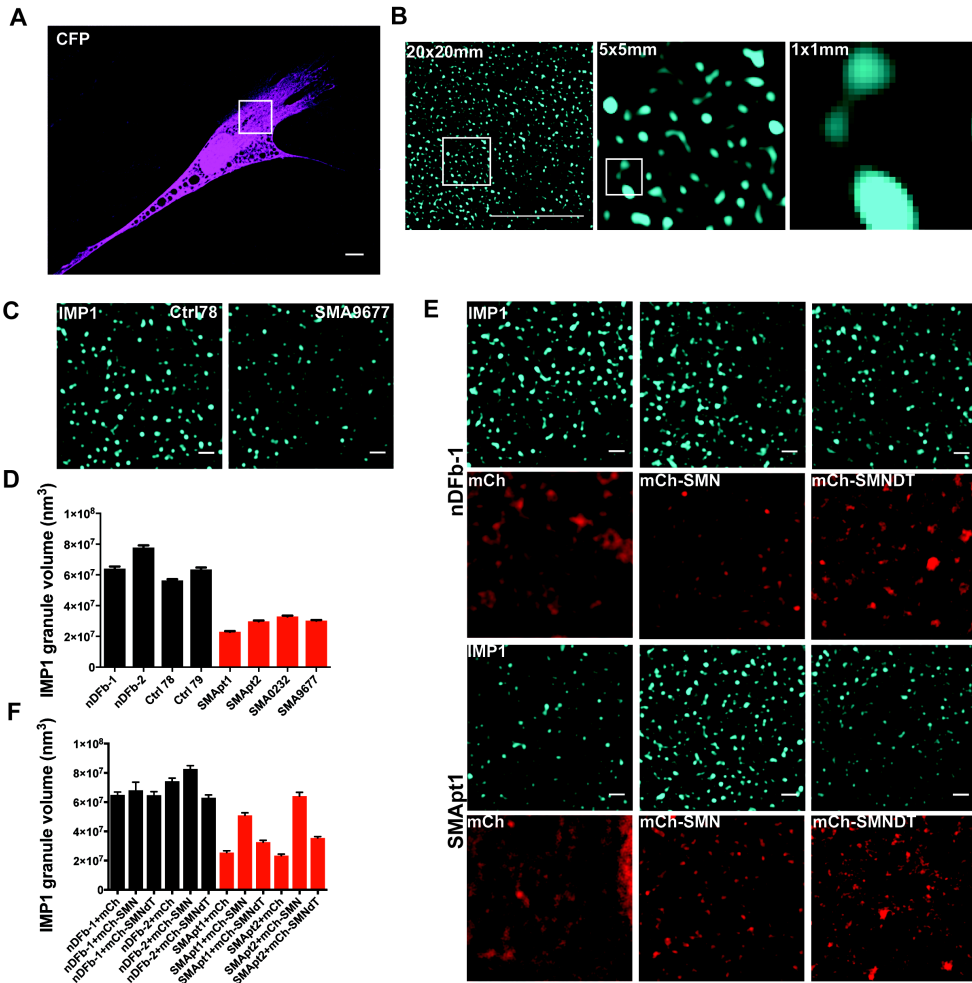


Figure 6:

IMP1 granules are reduced in size in SMA patient samples and can be rescued by restoring expression of SMN. **A.** A CFP expressing control fibroblast pseudo-colored in magenta to highlight cell morphology and size. The inset highlights a 20 μ m x 20 μ m window to illustrate the regions of cells imaged in B. Scale bar =10 μ m. **B.** 20 μ m x 20 μ m view of IMP1 granules in a Ctrl and SMA fibroblast line, with inset region being a 5 μ m x 5 μ m region. An enlargement of inset from 5 μ m x 5 μ m region is shown, with an additional inset highlighting a 1 μ m x 1 μ m region. Enlargement of the 1 μ m x 1 μ m region highlighting the size of IMP1 granules. Scale bar =10 μ m. **C.** Superresolution Structured Illumination Microscopy (SIM) fluorescence imaging reveals that IMP1-containing granules have decreased volume in SMA fibroblasts. Scale bar = 1 μ m. **D.** Quantification of C. n=3, 15 cells/condition. Analyzed by Tukey's multiple comparisons test. For breakdown of statistical comparisons see Table S7. Error bars +/- SEM. Mean \pm SEM; Ctrl78: 5.64E+07 \pm 812009, Ctrl79: 6.35E+07 \pm 1.27E+06, nDFb-1: 6.42E+07 \pm 1.33E+06, nDFb-2: 7.78E+07 \pm 1.40E+06, SMApt1: 2.31E+07 \pm 390215, SMApt2: 2.99E+07 \pm 494158, SMA0232: 3.31E+07 \pm 492832, SMA9677: 3.03E+07 \pm 431995. **E.** Expression of mCherry-tagged full-length SMN but not the SMN Δ Tudor deletion mutant rescues IMP1 granule volume in 2 SMA lines. Scale bar = 1 μ m. **F.**

Quantification of E. n=3, 15 cells/condition, for statistical comparisons see Table S8. Scale bar = 1 μ m. Error bars +/- SEM. Mean \pm SEM; nDFb-1 mCherry: 6.49E+07 \pm 1.97E+06, nDFb-1 mCherry-SMN: 6.81E+07 \pm 5.55E+06, nDFb-1 mCherry-SMN Δ Tudor: 6.47E+07 \pm 2.40E+06, nDFb-2 mCherry: 7.42E+07 \pm 2.18E+06, nDFb-2 mCherry-SMN: 8.26E+07 \pm 2.36E+06, nDFb-2 mCherry-SMN Δ Tudor: 6.30E+07 \pm 1.90E+06, SMApt1 mCherry: 2.56E+07 \pm 1.15E+06, SMApt1 mCherry-SMN: 5.10E+07 \pm 1.68E+06, SMApt1 mCherry-SMN Δ Tudor: 3.26E+07 \pm 1.23E+06, SMApt2 mCherry: 2.34E+07 \pm 9.68E+05, SMApt2 mCherry-SMN: 6.41E+07 \pm 2.57E+06, SMApt2 mCherry-SMN Δ Tudor: 3.55E+07 \pm 918038.

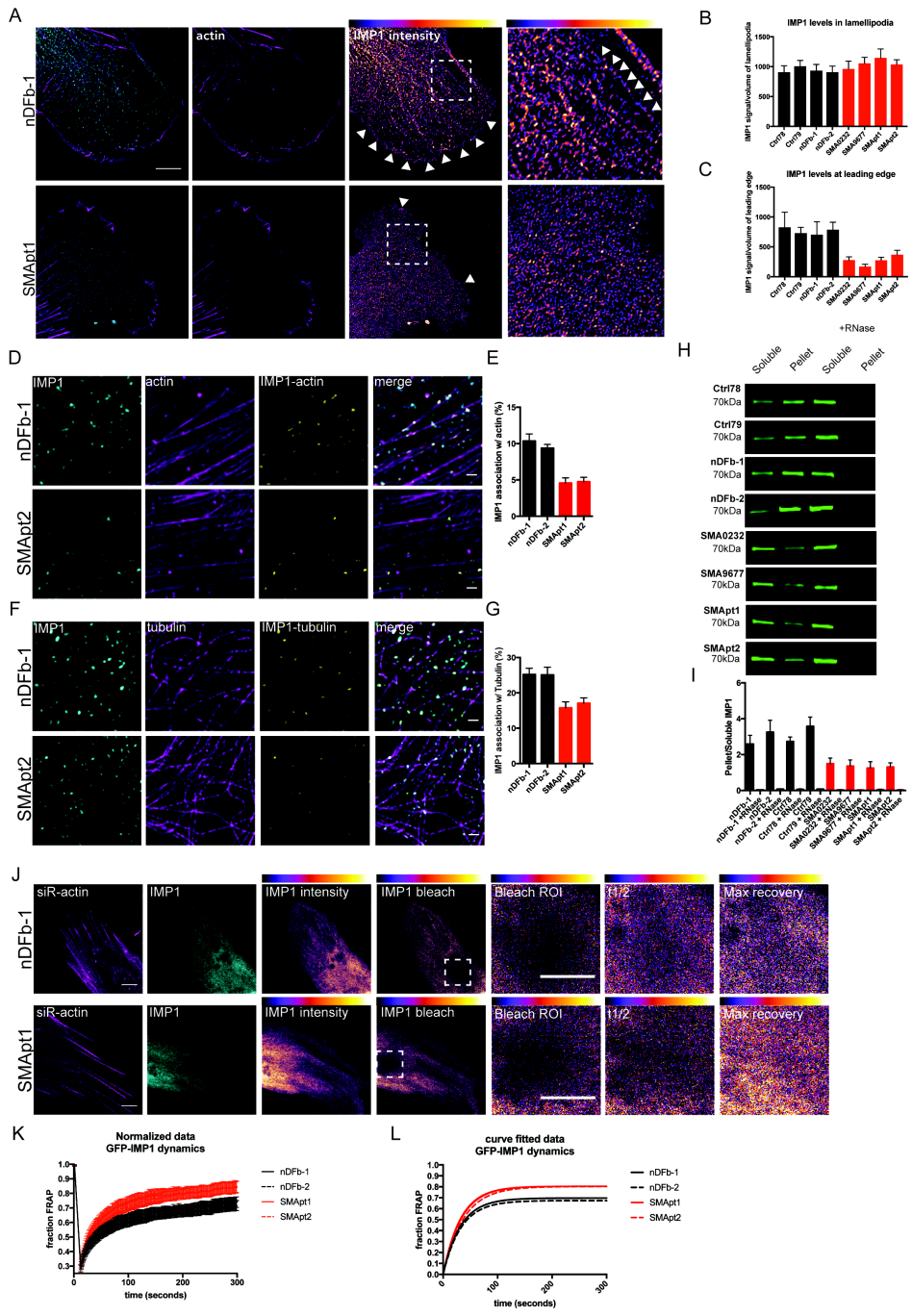


Figure 7:

IMP1 complexes show reduced association with the cytoskeleton in SMA

fibroblasts. **A.** IMP1 protein within the lamellipodia of SMA fibroblasts fails

to properly localize to the leading edge. Arrowheads indicate the leading

edge and highlight assembly of IMP1 along linear structures in control

fibroblasts (insets). **B.** Quantification of IMP1 levels in the lamellipodia.

n=3, >40 cells per condition, analyzed by Tukey's multiple comparisons.

For breakdown of statistical comparisons see Table S9. Error bars +/-

SEM. Mean \pm SEM; Ctrl78: 906.3 ± 109.6 , Ctrl79: 1007 ± 97.18 , nDFb-1:

932.5 ± 104.2 , nDFb-2: 908.3 ± 101.2 , SMA0232: 963.2 ± 130.8 ,

SMA9677: 1057 ± 98.44 , SMApt1: 1148 ± 147.4 , SMApt2: 1038 ± 78.02 .

C. Quantification of IMP1 levels in the leading edge. n=3, >40 cells per

condition, analyzed by Tukey's multiple comparisons. For breakdown of

statistical comparisons see Table S10. Error bars +/- SEM. Mean \pm SEM;

Ctrl78: 827.7 ± 253.8 , Ctrl79: 731 ± 96.75 , nDFb-1: 704.2 ± 216 , nDFb-2:

787 ± 126 , SMA0232: 278.8 ± 55.85 , SMA9677: 172.4 ± 35.46 , SMApt1:

277.2 ± 49.13 , SMApt2: 369.9 ± 72.14 . **D.** SIM imaging reveals decreased

association of IMP1 granules with actin filaments. Scale bar = $1\mu\text{m}$. **E.**

Quantification of D. n=3, 15/cells per condition, analyzed by Tukey's

multiple comparisons. For breakdown of statistical comparisons see Table

S11. Error bars +/- SEM. Mean \pm SEM; nDFb-1: 25.2 ± 1.767 , nDFb-2:

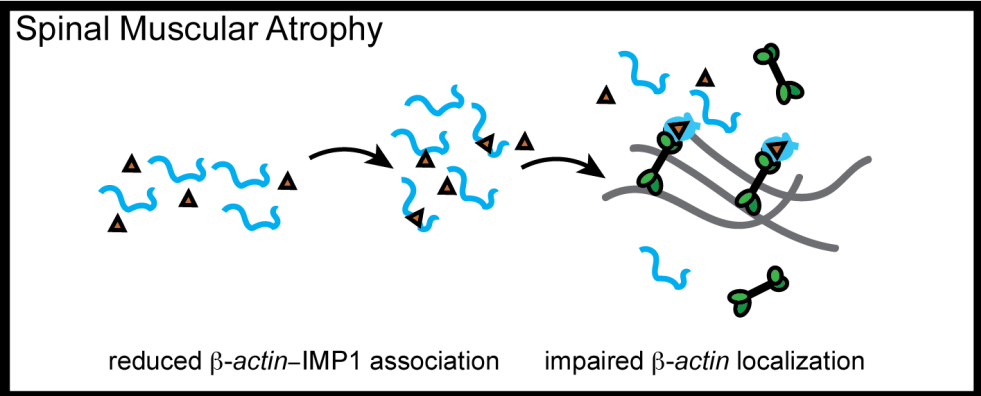
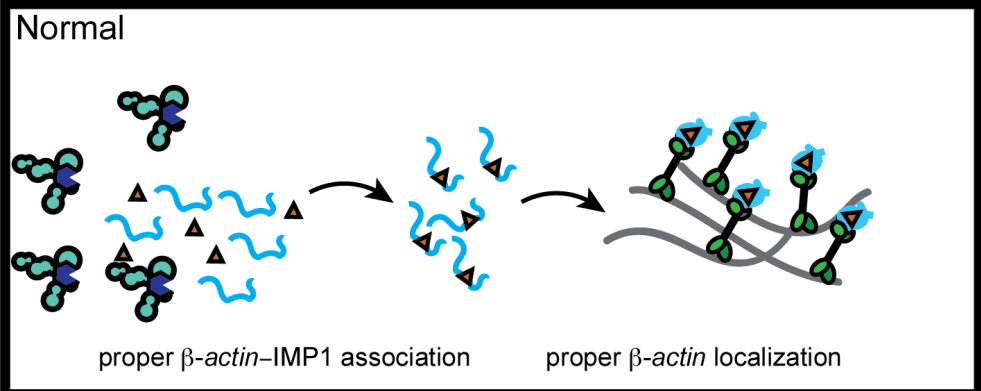
25.06 ± 2.181 , SMApt1: 15.9 ± 1.809 , SMApt2: 17.09 ± 1.507 . **F.** SIM

imaging demonstrates reduced association of IMP1 granules with

microtubules. Scale bar = $1\mu\text{m}$. **G.** Quantification of F. n=3, 15/cells per

condition, analyzed by Tukey's multiple comparisons. For breakdown of statistical comparisons see Table S12. Error bars +/- SEM. Mean \pm SEM; nDFb-1: 25.2 ± 1.767 , nDFb-2: 25.06 ± 2.181 , SMApt1: 15.9 ± 1.809 , SMApt2: 17.09 ± 1.507 . **H.** Cytoskeleton pelleting shows a reduction in the amount of IMP1 pelleted in SMA fibroblasts relative to the controls, demonstrating an impairment in association with the cytoskeleton. RNaseA/T1 treatment fully releases IMP1 from the cytoskeletal pellet. **I.** Quantification of H. n=5, analyzed by Tukey's multiple comparisons. For breakdown of statistical comparisons see Table S13. Error bars +/- SEM. Mean \pm SEM; nDFb-1: 2.586 ± 0.491 , nDFb-1 +RNase: 0.039 ± 0.015 , nDFb-2: 3.251 ± 0.660 , nDFb-2 + RNase: 0.075 ± 0.023 , Ctrl78: 2.732 ± 0.243 , Ctrl78 + RNase: 0.058 ± 0.028 , Ctrl79: 3.577 ± 0.509 , Ctrl79 + RNase: 0.069 ± 0.017 , SMA0232: 1.497 ± 0.312 , SMA0232 + RNase: 0.037 ± 0.014 , SMA9677: 1.362 ± 0.342 , SMA9677 + RNase: 0.026 ± 0.009 , SMApt1: 1.251 ± 0.350 , SMApt1 + RNase: 0.052 ± 0.018 , SMApt2: 1.311 ± 0.226 , SMApt2 + RNase: 0.033 ± 0.010 . **J.** FRAP analysis of GFP-IMP1 dynamics reveals a decrease in the immobile fraction in SMA patient fibroblasts. Representative images of GFP-IMP1 in control and SMA fibroblasts pre and post bleaching. $t_{1/2}$ values: nDFb-1: 40.56s, nDFb-2: 44.64s, SMApt1: 32.05s, SMApt2: 35.61s. Immobile fraction values: nFb-1: .314, nDFb-2: .336, SMApt1: .206, SMApt2: .208. **K.** Normalized GFP-IMP1 FRAP recovery curves for control and SMA fibroblasts. **L.** Curve fitted GFP-IMP1 FRAP recovery curves for control

and SMA fibroblasts.







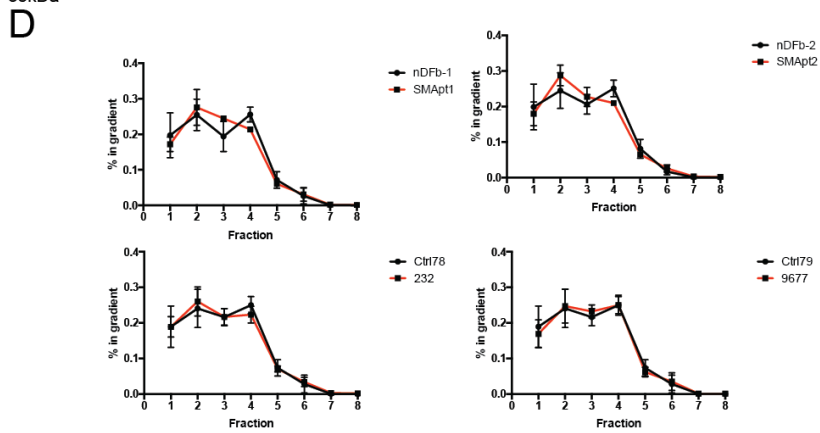
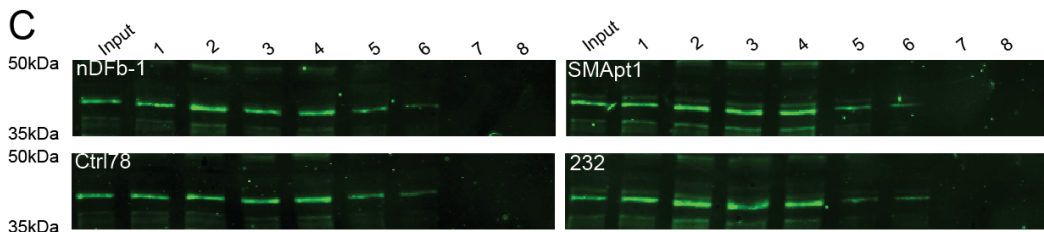
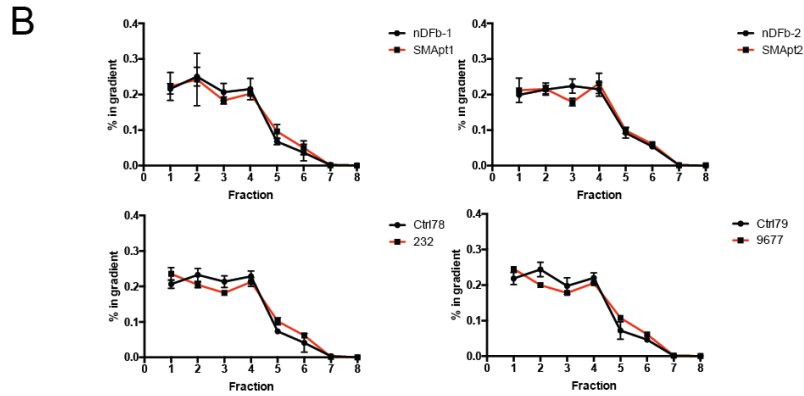
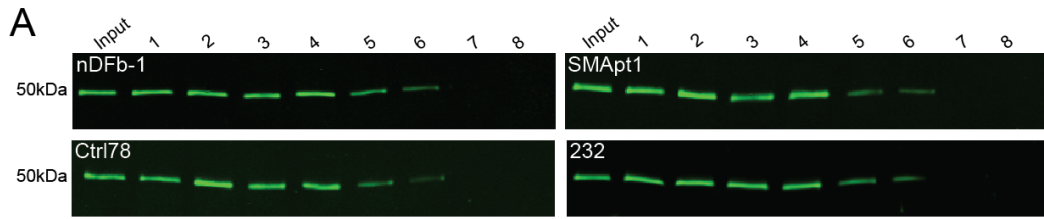
 SMN complex
  β -actin mRNA
  IMP1
  motor protein

Figure 8:

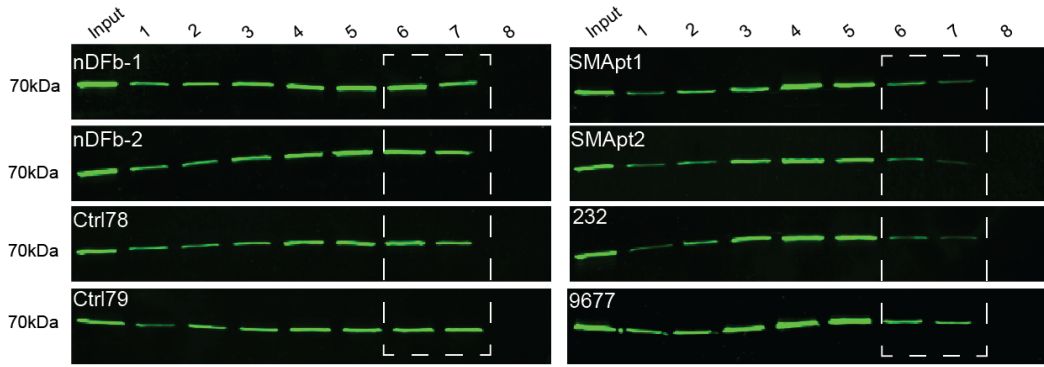
SMN functions as a chaperone of IMP1- β -actin granule assembly, and is defective in SMA. Under normal conditions, proper assembly of IMP1- β -actin granules facilitates their association with motor proteins and allows proper cytoskeletal association and subcellular localization within the cell. In SMA, the reduction of SMN protein levels and subsequently reduction in function SMN complexes, results in reduced IMP1- β -actin granules being assembled. This leads to fewer granules being able to associate with motor proteins which directly results in the reported subcellular mislocalization defect.



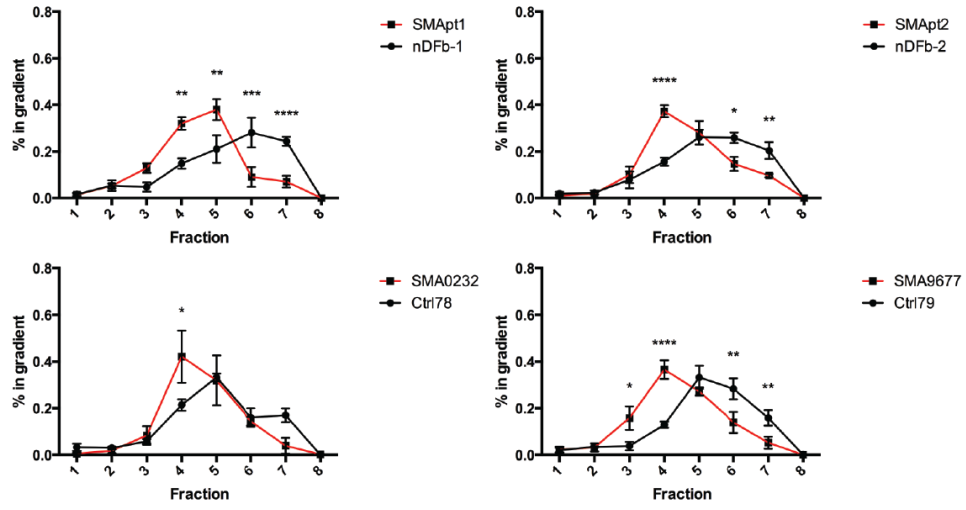
Supplemental Figure 1:

Cytoskeletal proteins show unaltered distributions in SMA fibroblasts relative to controls. **A.** Cytoplasmic lysates from fibroblasts were fractionated via Optiprep gradient centrifugation and fractions were analyzed for the presence of tubulin by western blot analysis. SMA lysates shows unaltered distribution of tubulin relative to control fractions. **B.** Distributions plotted as enrichment in % of the total signal in all fractions found in one particular fraction. n=3, analyzed by Sidak's multiple comparisons test. Error bars +/- SEM. **C.** Cytoplasmic lysates from fibroblasts were fractionated via Optiprep gradient centrifugation and fractions were analyzed for the presence of actin. SMA lysates shows unaltered distribution of actin relative to control fractions. **D.** Distributions plotted as enrichment in % of the total signal in all fractions found in one particular fraction. n=3, analyzed by Sidak's multiple comparisons test. Error bars +/- SEM.

A



B



Supplemental Figure 2:

PABPC1 granules show reduced complexity in SMA patient samples. **A.** Cytoplasmic lysates from fibroblasts were subjected to Optiprep gradient centrifugation and fractions were analyzed for the presence of PABPC1. SMA lysates shows altered distribution of PABPC1 complexes relative to control fractions. **B.** Distributions are plotted as enrichment in % of the total signal in all fractions found in one particular fraction. n=3, analyzed by Sidak's multiple comparisons test, *p<.05, **p<.01., ***p<.001, ****p<.0001. Error bars +/- SEM.

Number of families	1
Number of comparisons per family	6
Alpha	0.05

Tukey's multiple comparisons test	Mean Diff.	95% CI of diff.	Significant?	Summary
No UTR vs. ΔBox UTR	0.0044 53	-0.5897 to 0.5986	No	ns
No UTR vs. ΔZip UTR	-0.7825	-1.377 to -0.1883	Yes	**
No UTR vs. Full UTR	-2.899	-3.432 to -2.366	Yes	****
ΔBox UTR vs. ΔZip UTR	-0.787	-1.381 to -0.1928	Yes	**
ΔBox UTR vs. Full UTR	-2.904	-3.437 to -2.370	Yes	****
ΔZip UTR vs. Full UTR	-2.117	-2.650 to -1.583	Yes	****

Supplemental Table 1: Statistical comparisons for figure 1D. Cell body TriFC values were assessed using a one way ANOVA and Tukey's multiple comparisons test. Test was conducted with 1 family, 6 comparisons per family and an alpha of .05. ns: not significant, *: $p < .05$, **: $p < .01$, ***: $p < .001$, ****: $p < .0001$.

Number of families	1
Number of comparisons per family	6
Alpha	0.05

Tukey's multiple comparisons test	Mean Diff.	95% CI of diff.	Significant?	Summary
No UTR vs. 5Box UTR	0.0345	-0.2570 to 0.3260	No	ns
No UTR vs. 5Zip UTR	-0.6792	-0.9707 to -0.3877	Yes	****
No UTR vs. Full UTR	-1.928	-2.219 to -1.636	Yes	****
5Box UTR vs. 5Zip UTR	-0.7137	-1.005 to -0.4222	Yes	****
5Box UTR vs. Full UTR	-1.962	-2.254 to -1.671	Yes	****
5Zip UTR vs. Full UTR	-1.249	-1.540 to -0.9571	Yes	****

Supplemental Table 2: Statistical comparisons for figure 1E. Axon TriFC values were assessed using a one way ANOVA and Tukey's multiple comparisons test. Test was conducted with 1 family, 6 comparisons per family and an alpha of .05. ns: not significant, *: $p < .05$, **: $p < .01$, ***: $p < .001$, ****: $p < .0001$.

Compare column means (main column effect)

Tukey's multiple comparisons test	Mean Diff.	95% CI of diff.	Significant?	Summary
Number of families	1			
Number of comparisons per family	28			
Alpha	0.05			
Ctrl78 vs. Ctrl79	-0.1228	-0.6174 to 0.3718	No	ns
Ctrl78 vs. nDFb-1	0.1645	-0.3301 to 0.6590	No	ns
Ctrl78 vs. nDFb-2	-0.1168	-0.6113 to 0.3778	No	ns
Ctrl78 vs. SMApt1	0.8463	0.3517 to 1.341	Yes	****
Ctrl78 vs. SMApt2	0.9857	0.4911 to 1.480	Yes	****
Ctrl78 vs. SMA0232	1.01	0.5150 to 1.504	Yes	****
Ctrl78 vs. SMA9677	1.061	0.5660 to 1.555	Yes	****
Ctrl79 vs. nDFb-1	0.2873	-0.2073 to 0.7818	No	ns
Ctrl79 vs. nDFb-2	0.006054	-0.4885 to 0.5006	No	ns
Ctrl79 vs. SMApt1	0.9691	0.4745 to 1.464	Yes	****
Ctrl79 vs. SMApt2	1.108	0.6139 to 1.603	Yes	****
Ctrl79 vs. SMA0232	1.132	0.6378 to 1.627	Yes	****
Ctrl79 vs. SMA9677	1.183	0.6889 to 1.678	Yes	****
nDFb-1 vs. nDFb-2	-0.2812	-0.7758 to 0.2133	No	ns
nDFb-1 vs. SMApt1	0.6818	0.1872 to 1.176	Yes	***
nDFb-1 vs. SMApt2	0.8212	0.3266 to 1.316	Yes	****
nDFb-1 vs. SMA0232	0.8451	0.3506 to 1.340	Yes	****

nDFb-1 vs. SMA9677	0.8962	0.4016 to 1.391	Yes	****
nDFb-2 vs. SMApt1	0.963	0.4685 to 1.458	Yes	****
nDFb-2 vs. SMApt2	1.102	0.6079 to 1.597	Yes	****
nDFb-2 vs. SMA0232	1.126	0.6318 to 1.621	Yes	****
nDFb-2 vs. SMA9677	1.177	0.6828 to 1.672	Yes	****
SMApt1 vs. SMApt2	0.1394	-0.3552 to 0.6340	No	ns
SMApt1 vs. SMA0232	0.1633	-0.3313 to 0.6579	No	ns
SMApt1 vs. SMA9677	0.2143	-0.2802 to 0.7089	No	ns
SMApt2 vs. SMA0232	0.0239 2	-0.4706 to 0.5185	No	ns
SMApt2 vs. SMA9677	0.0749 5	-0.4196 to 0.5695	No	ns
SMA0232 vs. SMA9677	0.0510 2	-0.4435 to 0.5456	No	ns

Supplemental Table 3: Statistical comparisons for figure 3B. Fibroblast TriFC values were assessed using a two way ANOVA and Tukey's multiple comparisons test. Test was conducted with 1 family, 28 comparisons per family and an alpha of .05. ns: not significant, *: $p < .05$, **: $p < .01$, ***: $p < .001$, ****: $p < .0001$.

Compare column means (main column effect)

Number of families 1
 Number of comparisons per family 28
 Alpha 0.05

Tukey's multiple comparisons test	Mean Diff.	95% CI of diff.	Significant?	Summary
Ctrl78 vs. Ctrl79	0.01659	-0.1318 to 0.1649	No	ns
Ctrl78 vs. nDFb-1	0.00452	-0.1438 to 0.1529	No	ns
Ctrl78 vs. nDFb-2	0.01596	-0.1324 to 0.1643	No	ns
Ctrl78 vs. SMApt1	0.01914	-0.1292 to 0.1675	No	ns
Ctrl78 vs. SMApt2	-0.032	-0.1804 to 0.1164	No	ns
Ctrl78 vs. SMA0232	0.02831	-0.1200 to 0.1767	No	ns
Ctrl78 vs. SMA9677	0.08215	-0.06621 to 0.2305	No	ns
Ctrl79 vs. nDFb-1	0.01207	-0.1604 to 0.1363	No	ns
Ctrl79 vs. nDFb-2	0.00062	-0.1490 to 0.1477	No	ns
Ctrl79 vs. SMApt1	0.00255	-0.1458 to 0.1509	No	ns
Ctrl79 vs. SMApt2	0.04859	-0.1969 to 0.09978	No	ns
Ctrl79 vs. SMA0232	0.01173	-0.1366 to 0.1601	No	ns
Ctrl79 vs. SMA9677	0.06556	-0.08280 to 0.2139	No	ns
nDFb-1 vs. nDFb-2	0.01144	-0.1369 to 0.1598	No	ns
nDFb-1 vs. SMApt1	0.01462	-0.1337 to 0.1630	No	ns
nDFb-1 vs. SMApt2	0.03652	-0.1849 to 0.1118	No	ns
nDFb-1 vs. SMA0232	0.02379	-0.1246 to 0.1118	No	ns

		0.1722		
		-0.07074 to		
nDFb-1 vs. SMA9677	0.07763	0.2260	No	ns
	0.00317	-0.1452 to		
nDFb-2 vs. SMApt1	8	0.1515	No	ns
	-	-0.1963 to		
nDFb-2 vs. SMApt2	0.04796	0.1004	No	ns
		-0.1360 to		
nDFb-2 vs. SMA0232	0.01235	0.1607	No	ns
		-0.08218 to		
nDFb-2 vs. SMA9677	0.06619	0.2145	No	ns
	-	-0.1995 to		
SMApt1 vs. SMApt2	0.05114	0.09722	No	ns
	0.00917	-0.1392 to		
SMApt1 vs. SMA0232	3	0.1575	No	ns
		-0.08535 to		
SMApt1 vs. SMA9677	0.06301	0.2114	No	ns
		-0.08805 to		
SMApt2 vs. SMA0232	0.06031	0.2087	No	ns
		-0.03422 to		
SMApt2 vs. SMA9677	0.1141	0.2625	No	ns
		-0.09453 to		
SMA0232 vs. SMA9677	0.05383	0.2022	No	ns

Supplemental Table 4: Statistical comparisons for IMP1 protein levels for figure 4B. Steady state IMP1 values were assessed using a two way ANOVA and Tukey's multiple comparisons test. Test was conducted with 1 family, 28 comparisons per family and an alpha of .05. ns: not significant.

Compare column means (main column effect)

Number of families 1
 Number of comparisons per family 28
 Alpha 0.05

Tukey's multiple comparisons test	Mean Diff.	95% CI of diff.	Significant?	Summary
Ctrl78 vs. Ctrl79	0.03468	-0.1714 to 0.2408	No	ns
Ctrl78 vs. nDFb-1	0.01609	-0.1900 to 0.2222	No	ns
Ctrl78 vs. nDFb-2	0.05117	-0.2573 to 0.1549	No	ns
Ctrl78 vs. SMApt1	0.5046	0.2985 to 0.7107	Yes	****
Ctrl78 vs. SMApt2	0.4638	0.2577 to 0.6699	Yes	****
Ctrl78 vs. SMA0232	0.4742	0.2681 to 0.6803	Yes	****
Ctrl78 vs. SMA9677	0.4794	0.2733 to 0.6855	Yes	****
Ctrl79 vs. nDFb-1	0.01859	-0.2247 to 0.1875	No	ns
Ctrl79 vs. nDFb-2	0.08585	-0.2920 to 0.1203	No	ns
Ctrl79 vs. SMApt1	0.4699	0.2638 to 0.6761	Yes	****
Ctrl79 vs. SMApt2	0.4291	0.2230 to 0.6353	Yes	****
Ctrl79 vs. SMA0232	0.4395	0.2334 to 0.6456	Yes	****
Ctrl79 vs. SMA9677	0.4447	0.2386 to 0.6508	Yes	****
nDFb-1 vs. nDFb-2	0.06727	-0.2734 to 0.1389	No	ns
nDFb-1 vs. SMApt1	0.4885	0.2824 to 0.6947	Yes	****
nDFb-1 vs. SMApt2	0.4477	0.2416 to 0.6538	Yes	****

nDFb-1 vs. SMA0232	0.4581	0.2520 to 0.6642	Yes	****
nDFb-1 vs. SMA9677	0.4633	0.2572 to 0.6694	Yes	****
nDFb-2 vs. SMApt1	0.5558	0.3497 to 0.7619	Yes	****
nDFb-2 vs. SMApt2	0.515	0.3089 to 0.7211	Yes	****
nDFb-2 vs. SMA0232	0.5254	0.3193 to 0.7315	Yes	****
nDFb-2 vs. SMA9677	0.5306	0.3244 to 0.7367	Yes	****
	-			
SMApt1 vs. SMApt2	0.0408	-0.2469 to 0.1653	No	ns
	-			
SMApt1 vs. SMA0232	0.0304	-0.2365 to 0.1757	No	ns
	-			
SMApt1 vs. SMA9677	0.0252	-0.2314 to 0.1809	No	ns
	0.0103	-0.1957 to		
SMApt2 vs. SMA0232	9	0.2165	No	ns
	0.0155	-0.1906 to		
SMApt2 vs. SMA9677	7	0.2217	No	ns
	0.0051	-0.2009 to		
SMA0232 vs. SMA9677	78	0.2113	No	ns

Supplemental Table 5: Statistical comparisons for SMN protein levels for figure 4B. Steady state SMN values were assessed using a two way ANOVA and Tukey's multiple comparisons test. Test was conducted with 1 family, 28 comparisons per family and an alpha of .05. ns: not significant. *: $p < .05$, **: $p < .01$, ***: $p < .001$, ****: $p < .0001$.

Compare column means (main column effect)

Number of families	1			
Number of comparisons per family	120			
Alpha	0.05			
Tukey's multiple comparisons test	Mean Diff.	95% CI of diff.	Significant?	Summary
nDFb-1 vs. nDFb-1 +RNase	1.13	0.3104 to 1.949	Yes	***
nDFb-1 vs. nDFb-2	0.0431	-0.8623 to 0.7760	No	ns
nDFb-1 vs. nDFb-2 + RNase	1.142	0.3229 to 1.961	Yes	***
nDFb-1 vs. Ctrl78	-0.4179	-1.237 to 0.4013	No	ns
nDFb-1 vs. Ctrl78 + RNase	1.162	0.3431 to 1.981	Yes	***
nDFb-1 vs. Ctrl79	0.0024	-0.8167 to 0.8216	No	ns
nDFb-1 vs. Ctrl79 + RNase	58	0.3508 to 1.989	Yes	***
nDFb-1 vs. SMA0232	0.9067	0.08754 to 1.726	Yes	*
nDFb-1 vs. SMA0232 + RNase	1.167	0.3475 to 1.986	Yes	***
nDFb-1 vs. SMA9677	0.8919	0.07276 to 1.711	Yes	*
nDFb-1 vs. SMA9677 + RNase	1.154	0.3349 to 1.973	Yes	***
nDFb-1 vs. SMApt1	0.8705	0.05133 to 1.690	Yes	*
nDFb-1 vs. SMApt1 + RNase	1.165	0.3461 to 1.984	Yes	***
nDFb-1 vs. SMApt2	0.8374	0.01820 to 1.657	Yes	*
nDFb-1 vs. SMApt2 + RNase	1.162	0.3425 to 1.981	Yes	***
nDFb-1 +RNase vs. nDFb-2	-1.173	-1.992 to -0.3535	Yes	***
nDFb-1 +RNase vs. nDFb-2 +	0.0125	-0.8067 to	No	ns

RNase		0.8317		
		-2.367 to -		
nDFb-1 +RNase vs. Ctrl78	-1.547	0.7283	Yes	****
nDFb-1 +RNase vs. Ctrl78 + RNase	0.0327	-0.7865 to		
	1	0.8519	No	ns
		-1.946 to -		
nDFb-1 +RNase vs. Ctrl79	-1.127	0.3079	Yes	***
nDFb-1 +RNase vs. Ctrl79 + RNase	0.0404	-0.7788 to		
		0.8596	No	ns
nDFb-1 +RNase vs. SMA0232	-0.2229	-1.042 to		
		0.5963	No	ns
nDFb-1 +RNase vs. SMA0232 + RNase	0.0370	-0.7821 to		
	7	0.8562	No	ns
nDFb-1 +RNase vs. SMA9677	-0.2376	-1.057 to		
		0.5815	No	ns
nDFb-1 +RNase vs. SMA9677 + RNase	0.0244	-0.7947 to		
	7	0.8436	No	ns
		-1.078 to		
nDFb-1 +RNase vs. SMApt1	-0.2591	0.5601	No	ns
nDFb-1 +RNase vs. SMApt1 + RNase	0.0357	-0.7834 to		
	3	0.8549	No	ns
		-1.111 to		
nDFb-1 +RNase vs. SMApt2	-0.2922	0.5270	No	ns
nDFb-1 +RNase vs. SMApt2 + RNase	0.0320	-0.7871 to		
	9	0.8513	No	ns
		0.3660 to		
nDFb-2 vs. nDFb-2 + RNase	1.185	2.004	Yes	***
		-1.194 to		
nDFb-2 vs. Ctrl78	-0.3748	0.4444	No	ns
		0.3863 to		
nDFb-2 vs. Ctrl78 + RNase	1.205	2.025	Yes	***
		-0.7736 to		
nDFb-2 vs. Ctrl79	0.0456	0.8648	No	ns
		0.3939 to		
nDFb-2 vs. Ctrl79 + RNase	1.213	2.032	Yes	***
		0.1307 to		
nDFb-2 vs. SMA0232	0.9499	1.769	Yes	**
nDFb-2 vs. SMA0232 + RNase		0.3906 to		
	1.21	2.029	Yes	***
		0.1159 to		
nDFb-2 vs. SMA9677	0.9351	1.754	Yes	*
nDFb-2 vs. SMA9677 + RNase		0.3780 to		
	1.197	2.016	Yes	***
		0.09447 to		
nDFb-2 vs. SMApt1	0.9136	1.733	Yes	*
nDFb-2 vs. SMApt1 + RNase	1.208	0.3893 to	Yes	***

		2.028		
nDFb-2 vs. SMApt2	0.8805	0.06134 to 1.700	Yes	*
nDFb-2 vs. SMApt2 + RNase	1.205	0.3856 to 2.024	Yes	***
nDFb-2 + RNase vs. Ctrl78	-1.56	-2.379 to 0.7408	Yes	****
nDFb-2 + RNase vs. Ctrl78 + RNase	0.0202	-0.7990 to 0.8394	No	ns
nDFb-2 + RNase vs. Ctrl79	-1.14	-1.959 to 0.3204	Yes	***
nDFb-2 + RNase vs. Ctrl79 + RNase	0.0278	-0.7913 to 0.8471	No	ns
nDFb-2 + RNase vs. SMA0232	-0.2354	-1.055 to 0.5838	No	ns
nDFb-2 + RNase vs. SMA0232 + RNase	0.0245	-0.7946 to 0.8437	No	ns
nDFb-2 + RNase vs. SMA9677	-0.2501	-1.069 to 0.5690	No	ns
nDFb-2 + RNase vs. SMA9677 + RNase	0.0119	-0.8072 to 0.8311	No	ns
nDFb-2 + RNase vs. SMApt1	-0.2716	-1.091 to 0.5476	No	ns
nDFb-2 + RNase vs. SMApt1 + RNase	0.0232	-0.7959 to 0.8424	No	ns
nDFb-2 + RNase vs. SMApt2	-0.3047	-1.124 to 0.5145	No	ns
nDFb-2 + RNase vs. SMApt2 + RNase	0.0195	-0.7996 to 0.8388	No	ns
Ctrl78 vs. Ctrl78 + RNase	1.58	0.7610 to 2.399	Yes	****
Ctrl78 vs. Ctrl79	0.4204	-0.3988 to 1.240	No	ns
Ctrl78 vs. Ctrl79 + RNase	1.588	0.7687 to 2.407	Yes	****
Ctrl78 vs. SMA0232	1.325	0.5055 to 2.144	Yes	****
Ctrl78 vs. SMA0232 + RNase	1.585	0.7654 to 2.404	Yes	****
Ctrl78 vs. SMA9677	1.31	0.4907 to 2.129	Yes	****
Ctrl78 vs. SMA9677 + RNase	1.572	0.7528 to 2.391	Yes	****
Ctrl78 vs. SMApt1	1.288	0.4692 to 2.108	Yes	****
Ctrl78 vs. SMApt1 + RNase	1.583	0.7640 to 2.402	Yes	****

		2.402		
		0.4361 to		
Ctrl78 vs. SMApt2	1.255	2.074	Yes	****
		0.7604 to		
Ctrl78 vs. SMApt2 + RNase	1.58	2.399	Yes	****
		-1.979 to -		
Ctrl78 + RNase vs. Ctrl79	-1.16	0.3407	Yes	***
Ctrl78 + RNase vs. Ctrl79 + RNase	0.0076	-0.8115 to		
	89	0.8269	No	ns
		-1.075 to		
Ctrl78 + RNase vs. SMA0232	-0.2556	0.5636	No	ns
Ctrl78 + RNase vs. SMA0232 + RNase	0.0043	-0.8148 to		
	63	0.8235	No	ns
		-1.090 to		
Ctrl78 + RNase vs. SMA9677	-0.2704	0.5488	No	ns
	-			
Ctrl78 + RNase vs. SMA9677 + RNase	0.0082	-0.8274 to		
	37	0.8109	No	ns
		-1.111 to		
Ctrl78 + RNase vs. SMApt1	-0.2918	0.5274	No	ns
Ctrl78 + RNase vs. SMApt1 + RNase	0.0030	-0.8162 to		
	22	0.8222	No	ns
		-1.144 to		
Ctrl78 + RNase vs. SMApt2	-0.3249	0.4943	No	ns
	-			
Ctrl78 + RNase vs. SMApt2 + RNase	0.0006	-0.8198 to		
	161	0.8186	No	ns
		0.3483 to		
Ctrl79 vs. Ctrl79 + RNase	1.168	1.987	Yes	***
		0.08508 to		
Ctrl79 vs. SMA0232	0.9043	1.723	Yes	*
		0.3450 to		
Ctrl79 vs. SMA0232 + RNase	1.164	1.983	Yes	***
		0.07030 to		
Ctrl79 vs. SMA9677	0.8895	1.709	Yes	*
		0.3324 to		
Ctrl79 vs. SMA9677 + RNase	1.152	1.971	Yes	***
		0.04888 to		
Ctrl79 vs. SMApt1	0.868	1.687	Yes	*
		0.3437 to		
Ctrl79 vs. SMApt1 + RNase	1.163	1.982	Yes	***
		0.01574 to		
Ctrl79 vs. SMApt2	0.8349	1.654	Yes	*
		0.3400 to		
Ctrl79 vs. SMApt2 + RNase	1.159	1.978	Yes	***
Ctrl79 + RNase vs. SMA0232	-0.2633	-1.082 to	No	ns

		0.5559		
	-			
Ctrl79 + RNase vs. SMA0232 + RNase	0.0033 26	-0.8225 to 0.8158	No	ns
		-1.097 to		
Ctrl79 + RNase vs. SMA9677	-0.278	0.5411	No	ns
	-			
Ctrl79 + RNase vs. SMA9677 + RNase	0.0159 3	-0.8351 to 0.8032	No	ns
		-1.119 to		
Ctrl79 + RNase vs. SMApt1	-0.2995	0.5197	No	ns
	-			
Ctrl79 + RNase vs. SMApt1 + RNase	0.0046 67	-0.8238 to 0.8145	No	ns
		-1.152 to		
Ctrl79 + RNase vs. SMApt2	-0.3326	0.4866	No	ns
	-			
Ctrl79 + RNase vs. SMApt2 + RNase	0.0083 05	-0.8275 to 0.8109	No	ns
SMA0232 vs. SMA0232 + RNase	0.2599	-0.5592 to 1.079	No	ns
	-			
SMA0232 vs. SMA9677	0.0147 8	-0.8340 to 0.8044	No	ns
SMA0232 vs. SMA9677 + RNase	0.2473	-0.5718 to 1.067	No	ns
	-			
SMA0232 vs. SMApt1	0.0362 1	-0.8554 to 0.7830	No	ns
SMA0232 vs. SMApt1 + RNase	0.2586	-0.5606 to 1.078	No	ns
	-			
SMA0232 vs. SMApt2	0.0693 4	-0.8885 to 0.7498	No	ns
SMA0232 vs. SMApt2 + RNase	0.255	-0.5642 to 1.074	No	ns
SMA0232 + RNase vs. SMA9677	-0.2747	-1.094 to 0.5445	No	ns
SMA0232 + RNase vs. SMA9677 + RNase	-0.0126	-0.8318 to 0.8066	No	ns
SMA0232 + RNase vs. SMApt1	-0.2961	-1.115 to 0.5230	No	ns
	-			
SMA0232 + RNase vs. SMApt1 + RNase	0.0013 41	-0.8205 to 0.8178	No	ns
SMA0232 + RNase vs.	-0.3293	-1.148 to	No	ns

SMApt2		0.4899		
	-			
SMA0232 + RNase vs. SMApt2 + RNase	0.0049	-0.8242 to 0.8142	No	ns
	79			
SMA9677 vs. SMA9677 + RNase	0.2621	-0.5571 to 1.081	No	ns
	-			
	0.0214	-0.8406 to 0.7978	No	ns
SMA9677 vs. SMApt1	2			
SMA9677 vs. SMApt1 + RNase	0.2734	-0.5458 to 1.093	No	ns
	-			
	0.0545	-0.8737 to 0.7646	No	ns
SMA9677 vs. SMApt2	5			
SMA9677 vs. SMApt2 + RNase	0.2697	-0.5494 to 1.089	No	ns
SMA9677 + RNase vs. SMApt1	-0.2835	-1.103 to 0.5356	No	ns
SMA9677 + RNase vs. SMApt1 + RNase	0.0112	-0.8079 to 0.8304	No	ns
	6			
SMA9677 + RNase vs. SMApt2	-0.3167	-1.136 to 0.5025	No	ns
SMA9677 + RNase vs. SMApt2 + RNase	0.0076	-0.8116 to 0.8268	No	ns
	21			
SMApt1 vs. SMApt1 + RNase	0.2948	-0.5244 to 1.114	No	ns
	-			
	0.0331	-0.8523 to 0.7860	No	ns
SMApt1 vs. SMApt2	3			
SMApt1 vs. SMApt2 + RNase	0.2912	-0.5280 to 1.110	No	ns
SMApt1 + RNase vs. SMApt2	-0.3279	-1.147 to 0.4912	No	ns
	-			
SMApt1 + RNase vs. SMApt2 + RNase	0.0036	-0.8228 to 0.8155	No	ns
	38			
SMApt2 vs. SMApt2 + RNase	0.3243	-0.4949 to 1.143	No	ns

Supplemental Table 6: Statistical comparisons for IMP1 association with mRNA levels for figure 4E. IMP1 pulldown/IMP1 input values were assessed using a two way ANOVA and Tukey's multiple comparisons test. Test was conducted with 1 family, 120 comparisons per family and an alpha of .05. ns: not significant. *: $p < .05$, **: $p < .01$, ***: $p < .001$, ****: $p < .0001$.

Number of families 1
 Number of comparisons per family 28
 Alpha 0.05

Tukey's multiple comparisons test	Mean Diff.	95% CI of diff.	Significant?	Summary
Ctrl 78 vs. Ctrl 79	155700	-2.687e+006 to 5.800e+006	No	ns
Ctrl 78 vs. nDFb-1	599700	-1.024e+007 to -1.754e+006	Yes	***
Ctrl 78 vs. nDFb-2	1773000	-2.197e+007 to -1.348e+007	Yes	****
Ctrl 78 vs. SMApt1	3793000	3.368e+007 to 4.217e+007	Yes	****
Ctrl 78 vs. SMApt2	3198000	2.774e+007 to 3.622e+007	Yes	****
Ctrl 78 vs. SMA0232	2915000	2.491e+007 to 3.340e+007	Yes	****
Ctrl 78 vs. SMA9677	2915000	2.491e+007 to 3.340e+007	Yes	****
Ctrl 79 vs. nDFb-1	7554000	-1.180e+007 to -3.311e+006	Yes	****
Ctrl 79 vs. nDFb-2	1928000	-2.353e+007 to -1.504e+007	Yes	****
Ctrl 79 vs. SMApt1	3637000	3.213e+007 to 4.061e+007	Yes	****
Ctrl 79 vs. SMApt2	3042000	2.618e+007 to 3.467e+007	Yes	****
Ctrl 79 vs. SMA0232	2760000	2.335e+007 to 3.184e+007	Yes	****
Ctrl 79 vs. SMA9677	2760000	2.335e+007 to 3.184e+007	Yes	****
nDFb-1 vs. nDFb-2	1173000	-1.597e+007 to -7.485e+006	Yes	****
nDFb-1 vs. SMApt1	4392000	3.968e+007 to 4.817e+007	Yes	****
nDFb-1 vs. SMApt2	3798000	3.373e+007 to 4.222e+007	Yes	****
nDFb-1 vs. SMA0232	3515000	3.091e+007 to	Yes	****

	000	3.939e+007		
nDFb-1 vs. SMA9677	35150	3.091e+007 to		
	000	3.939e+007	Yes	****
nDFb-2 vs. SMApt1	55650	5.141e+007 to		
	000	5.990e+007	Yes	****
nDFb-2 vs. SMApt2	49710	4.546e+007 to		
	000	5.395e+007	Yes	****
nDFb-2 vs. SMA0232	46880	4.264e+007 to		
	000	5.112e+007	Yes	****
nDFb-2 vs. SMA9677	46880	4.264e+007 to		
	000	5.112e+007	Yes	****
	-			
SMApt1 vs. SMApt2	59480	-1.019e+007 to -		
	00	1.704e+006	Yes	***
	-			
SMApt1 vs. SMA0232	87730	-1.302e+007 to -		
	00	4.530e+006	Yes	****
	-			
SMApt1 vs. SMA9677	87730	-1.302e+007 to -		
	00	4.530e+006	Yes	****
	-			
SMApt2 vs. SMA0232	28250	-7.069e+006 to		
	00	1.418e+006	No	ns
	-			
SMApt2 vs. SMA9677	28250	-7.069e+006 to		
	00	1.418e+006	No	ns
SMA0232 vs.		-4.243e+006 to		
SMA9677	0	4.243e+006	No	ns

Supplemental Table 7: Statistical comparisons for figure 6D. IMP1 granule volume values were assessed using a one way ANOVA and Tukey's multiple comparisons test. Test was conducted with 1 family, 28 comparisons per family and an alpha of .05. ns: not significant, *: $p < .05$, **: $p < .01$, ***: $p < .001$, ****: $p < .0001$

Number of families	1
Number of comparisons per family	66
Alpha	0.05

Tukey's multiple comparisons test	Mean Diff.	95% CI of diff.	Significant?	Summary
nDFb-2+mCh vs. nDFb-1+mCh	93250	-1.381e+006 to 2.003e+007	No	ns
nDFb-2+mCh vs. SMApt1+mCh	48690	3.798e+007 to 5.939e+007	Yes	****
nDFb-2+mCh vs. SMApt2+mCh	50820	4.011e+007 to 6.153e+007	Yes	****
nDFb-2+mCh vs. nDFb-1+mCh-SMNdT	95100	-1.275e+006 to 2.030e+007	No	ns
nDFb-2+mCh vs. nDFb-2+mCh-SMNdT	11280	571336 to 2.198e+007	Yes	*
nDFb-2+mCh vs. SMApt1+mCh-SMN	23250	1.420e+007 to 3.231e+007	Yes	****
nDFb-2+mCh vs. SMApt2+mCh-SMN	10100	-524343 to 2.072e+007	No	ns
-	-	-	-	-
nDFb-2+mCh vs. nDFb-2+mCh-SMN	83510	-1.764e+007 to 937582	No	ns
nDFb-2+mCh vs. nDFb-1+mCh-SMN	61570	-4.955e+006 to 1.727e+007	No	ns
nDFb-2+mCh vs. SMApt1+mCh-SMNdT	41620	3.144e+007 to 5.179e+007	Yes	****
nDFb-2+mCh vs. SMApt2+mCh-SMNdT	38750	2.803e+007 to 4.946e+007	Yes	****
nDFb-1+mCh vs. SMApt1+mCh	39360	2.798e+007 to 5.075e+007	Yes	****
nDFb-1+mCh vs. SMApt2+mCh	41500	3.011e+007 to 5.288e+007	Yes	****
nDFb-1+mCh vs. nDFb-1+mCh-SMNdT	18591	-1.127e+007 to 1.165e+007	No	ns
nDFb-1+mCh vs. nDFb-2+mCh-SMNdT	19520	-9.433e+006 to 1.334e+007	No	ns
nDFb-1+mCh vs. SMApt1+mCh-SMN	13930	4.079e+006 to 2.378e+007	Yes	***
nDFb-1+mCh vs. SMApt2+mCh-SMN	77394	-1.053e+007 to 1.208e+007	No	ns
nDFb-1+mCh vs. nDFb-	-	-2.774e+007 to -	Yes	****

2+mCh-SMN	17680	7.611e+006		
	000			
	-			
nDFb-1+mCh vs. nDFb-1+mCh-SMN	31670	-1.494e+007 to 8.601e+006	No	ns
nDFb-1+mCh vs. SMApt1+mCh-SMNdT	32290	2.140e+007 to 4.318e+007	Yes	****
nDFb-1+mCh vs. SMApt2+mCh-SMNdT	29420	1.803e+007 to 4.082e+007	Yes	****
SMApt1+mCh vs. SMApt2+mCh	21330	-9.252e+006 to 1.352e+007	No	ns
	00			
	-			
SMApt1+mCh vs. nDFb-1+mCh-SMNdT	39180	-5.064e+007 to 2.772e+007	Yes	****
	000			
	-			
SMApt1+mCh vs. nDFb-2+mCh-SMNdT	37410	-4.880e+007 to 2.603e+007	Yes	****
	000			
	-			
SMApt1+mCh vs. SMApt1+mCh-SMN	25440	-3.528e+007 to 1.559e+007	Yes	****
	000			
	-			
SMApt1+mCh vs. SMApt2+mCh-SMN	38590	-4.990e+007 to 2.728e+007	Yes	****
	000			
	-			
SMApt1+mCh vs. nDFb-2+mCh-SMN	57040	-6.710e+007 to 4.697e+007	Yes	****
	000			
	-			
SMApt1+mCh vs. nDFb-1+mCh-SMN	42530	-5.430e+007 to 3.076e+007	Yes	****
	000			
	-			
SMApt1+mCh vs. SMApt1+mCh-SMNdT	70720	-1.796e+007 to 3.815e+006	No	ns
	00			
	-			
SMApt1+mCh vs. SMApt2+mCh-SMNdT	99410	-2.134e+007 to 1.454e+006	No	ns
	00			
	-			
SMApt2+mCh vs. nDFb-1+mCh-SMNdT	41310	-5.277e+007 to 2.985e+007	Yes	****
	000			
	-			
SMApt2+mCh vs. nDFb-2+mCh-SMNdT	39540	-5.093e+007 to 2.816e+007	Yes	****
	000			
	-			
SMApt2+mCh vs. SMApt1+mCh-SMN	27570	-3.742e+007 to 1.772e+007	Yes	****
	000			
SMApt2+mCh vs. SMApt2+mCh-SMN	40720	-5.203e+007 to 2.941e+007	Yes	****
	-			

	000			
	-			
SMApt2+mCh vs. nDFb-2+mCh-SMN	5917000	-6.924e+007 to -4.911e+007	Yes	****
	-			
SMApt2+mCh vs. nDFb-1+mCh-SMN	4466000	-5.643e+007 to -3.290e+007	Yes	****
	-			
SMApt2+mCh vs. SMApt1+mCh-SMNdT	920500	-2.009e+007 to 1.682e+006	No	ns
	-			
SMApt2+mCh vs. SMApt2+mCh-SMNdT	1207000	-2.347e+007 to 679286	Yes	*
nDFb-1+mCh-SMNdT vs. nDFb-2+mCh-SMNdT	176600	-9.695e+006 to 1.323e+007	No	ns
nDFb-1+mCh-SMNdT vs. SMApt1+mCh-SMN	1374000	3.806e+006 to 2.368e+007	Yes	***
nDFb-1+mCh-SMNdT vs. SMApt2+mCh-SMN	588030	-1.080e+007 to 1.197e+007	No	ns
	-			
nDFb-1+mCh-SMNdT vs. nDFb-2+mCh-SMN	1786000	-2.801e+007 to 7.711e+006	Yes	****
	-			
nDFb-1+mCh-SMNdT vs. nDFb-1+mCh-SMN	335300	-1.519e+007 to 8.488e+006	No	ns
nDFb-1+mCh-SMNdT vs. SMApt1+mCh-SMNdT	3211000	2.114e+007 to 4.307e+007	Yes	****
nDFb-1+mCh-SMNdT vs. SMApt2+mCh-SMNdT	2924000	1.777e+007 to 4.071e+007	Yes	****
nDFb-2+mCh-SMNdT vs. SMApt1+mCh-SMN	1198000	2.127e+006 to 2.182e+007	Yes	**
	-			
nDFb-2+mCh-SMNdT vs. SMApt2+mCh-SMN	117800	-1.249e+007 to 1.013e+007	No	ns
	-			
nDFb-2+mCh-SMNdT vs. nDFb-2+mCh-SMN	1963000	-2.969e+007 to 9.563e+006	Yes	****
	-			
nDFb-2+mCh-SMNdT vs. nDFb-1+mCh-SMN	512000	-1.689e+007 to 6.648e+006	No	ns
nDFb-2+mCh-SMNdT vs. SMApt1+mCh-SMNdT	3034000	1.945e+007 to 4.123e+007	Yes	****
nDFb-2+mCh-SMNdT vs. SMApt2+mCh-SMNdT	2747000	1.608e+007 to 3.886e+007	Yes	****
SMApt1+mCh-SMN vs. SMApt2+mCh-SMN	-13150	-2.291e+007 to 3.395e+006	Yes	***

	000			
	-			
SMApt1+mCh-SMN vs. nDFb-2+mCh-SMN	31600 000	-3.989e+007 to - 2.332e+007	Yes	****
	-			
SMApt1+mCh-SMN vs. nDFb-1+mCh-SMN	17100 000	-2.738e+007 to - 6.806e+006	Yes	****
SMApt1+mCh-SMN vs. SMApt1+mCh-SMNdT	18360 000	9.096e+006 to 2.763e+007	Yes	****
SMApt1+mCh-SMN vs. SMApt2+mCh-SMNdT	15490 000	5.635e+006 to 2.535e+007	Yes	****
	-			
SMApt2+mCh-SMN vs. nDFb-2+mCh-SMN	18450 000	-2.843e+007 to - 8.473e+006	Yes	****
	-			
SMApt2+mCh-SMN vs. nDFb-1+mCh-SMN	39410 00	-1.563e+007 to 7.752e+006	No	ns
SMApt2+mCh-SMN vs. SMApt1+mCh-SMNdT	31520 000	2.071e+007 to 4.232e+007	Yes	****
SMApt2+mCh-SMN vs. SMApt2+mCh-SMNdT	28650 000	1.733e+007 to 3.997e+007	Yes	****
nDFb-2+mCh-SMN vs. nDFb-1+mCh-SMN	14510 000	4.012e+006 to 2.500e+007	Yes	***
nDFb-2+mCh-SMN vs. SMApt1+mCh-SMNdT	49970 000	4.047e+007 to 5.946e+007	Yes	****
nDFb-2+mCh-SMN vs. SMApt2+mCh-SMNdT	47100 000	3.702e+007 to 5.717e+007	Yes	****
nDFb-1+mCh-SMN vs. SMApt1+mCh-SMNdT	35460 000	2.417e+007 to 4.674e+007	Yes	****
nDFb-1+mCh-SMN vs. SMApt2+mCh-SMNdT	32590 000	2.081e+007 to 4.437e+007	Yes	****
	-			
SMApt1+mCh-SMNdT vs. SMApt2+mCh-SMNdT	28690 00	-1.377e+007 to 8.027e+006	No	ns

Supplemental Table 8: Statistical comparisons for figure 6F. IMP1 granule volume with either mCherry, SMN-mCherry or SMN Δ tudor-mCherry values were assessed using one way ANOVA and Tukey's multiple comparisons test. Test was conducted with 1 family, 66 comparisons per family and an alpha of .05. ns: not significant, *: p<.05, **, p<.01, ***: p<.001, ****: p<.0001.

Compare column means (main column effect)

Number of families 1
 Number of comparisons per family 28
 Alpha 0.05

Tukey's multiple comparisons test	Mean Diff.	95.00% CI of diff.	Significant?	Summary	Adjusted P Value
Ctrl78 vs. Ctrl79	116	-319.6 to 551.6	No	ns	0.9923
Ctrl78 vs. nDFb-1	1.446	-434.2 to 437.1	No	ns	>0.9999
Ctrl78 vs. nDFb-2	52.8	-382.8 to 488.4	No	ns	>0.9999
Ctrl78 vs. SMA0232	44.04	-479.7 to 391.6	No	ns	>0.9999
Ctrl78 vs. SMA9677	110.3	-546 to 325.3	No	ns	0.9943
Ctrl78 vs. SMApt1	252.6	-688.2 to 183.1	No	ns	0.6402
Ctrl78 vs. SMApt2	104.2	-539.9 to 331.4	No	ns	0.996
Ctrl79 vs. nDFb-1	114.6	-550.2 to 321.1	No	ns	0.9928
Ctrl79 vs. nDFb-2	-63.2	-498.8 to 372.4	No	ns	0.9998
Ctrl79 vs. SMA0232	-160	-595.7 to 275.6	No	ns	0.9516
Ctrl79 vs. SMA9677	226.3	-662 to 209.3	No	ns	0.7578
Ctrl79 vs. SMApt1	368.6	-804.2 to 67.06	No	ns	0.1661
Ctrl79 vs. SMApt2	220.2	-655.9 to 215.4	No	ns	0.7826
nDFb-1 vs. nDFb-2	51.35	-384.3 to 487	No	ns	>0.9999
nDFb-1 vs. SMA0232	45.49	-481.1 to 390.2	No	ns	>0.9999
nDFb-1 vs. SMA9677	111.8	-547.4 to 323.9	No	ns	0.9938
nDFb-1 vs. SMApt1	-254	-689.7 to 181.6	No	ns	0.6334

		-	-541.3 to			
nDFb-1 vs. SMApt2	105.7	330		No	ns	0.9956
nDFb-2 vs.			-532.5 to			
SMA0232	96.84	338.8		No	ns	0.9975
nDFb-2 vs.			-598.8 to			
SMA9677	163.1	272.5		No	ns	0.9464
			-741 to			
nDFb-2 vs. SMApt1	305.4	130.3		No	ns	0.3912
			-592.7 to			
nDFb-2 vs. SMApt2	-157	278.6		No	ns	0.9562
SMA0232 vs.			-501.9 to			
SMA9677	66.29	369.3		No	ns	0.9998
SMA0232 vs.			-644.2 to			
SMApt1	208.5	227.1		No	ns	0.8267
SMA0232 vs.			-495.8 to			
SMApt2	-60.2	375.4		No	ns	0.9999
SMA9677 vs.			-577.9 to			
SMApt1	142.3	293.4		No	ns	0.9745
SMA9677 vs.			-429.5 to			
SMApt2	6.095	441.7		No	ns	>0.9999
			-287.3 to			
SMApt1 vs. SMApt2	148.3	584		No	ns	0.9678

Supplemental Table 9: Statistical comparisons for figure 7B. IMP1 levels in the lamellipodia was assessed using two way ANOVA and Tukey's multiple comparisons test. Test was conducted with 1 family, 6 comparisons per family and an alpha of .05. ns: not significant, *: $p < .05$, **: $p < .01$, ***: $p < .001$, ****: $p < .0001$.

Compare column means (main column effect)

Number of families	1					
Number of comparisons per family	28					
Alpha	0.05					
Tukey's multiple comparisons test	Mean Diff.	95.00% CI of diff.	Significant?	Summary	Adjusted P Value	
Ctrl78 vs. Ctrl79	96.75	-485.4 to 678.9	No	ns	0.9996	
Ctrl78 vs. nDFb-1	123.6	-458.5 to 705.7	No	ns	0.9981	
Ctrl78 vs. nDFb-2	40.76	-541.4 to 622.9	No	ns	>0.9999	
Ctrl78 vs. SMA0232	549	-33.17 to 1131	No	ns	0.0806	
Ctrl78 vs. SMA9677	655.3	73.19 to 1237	Yes	*	0.0154	
Ctrl78 vs. SMApt1	550.5	-31.6 to 1133	No	ns	0.0789	
Ctrl78 vs. SMApt2	457.9	-124.3 to 1040	No	ns	0.2443	
Ctrl79 vs. nDFb-1	26.83	-555.3 to 609	No	ns	>0.9999	
Ctrl79 vs. nDFb-2	-56	-638.1 to 526.1	No	ns	>0.9999	
Ctrl79 vs. SMA0232	452.2	-129.9 to 1034	No	ns	0.259	
Ctrl79 vs. SMA9677	558.6	-23.56 to 1141	No	ns	0.0705	
Ctrl79 vs. SMApt1	453.8	-128.4 to 1036	No	ns	0.2549	
Ctrl79 vs. SMApt2	361.1	-221 to 943.3	No	ns	0.5556	

nDFb-1 vs. nDFb-2	-82.83	-665 to 499.3	No	ns	0.9999
nDFb-1 vs. SMA0232	425.4	-156.8 to 1008	No	ns	0.336
nDFb-1 vs. SMA9677	531.7	-50.39 to 1114	No	ns	0.1017
nDFb-1 vs. SMApt1	426.9	-155.2 to 1009	No	ns	0.3311
nDFb-1 vs. SMApt2	334.3	-247.8 to 916.4	No	ns	0.6516
nDFb-2 vs. SMA0232	508.2	-73.93 to 1090	No	ns	0.1375
nDFb-2 vs. SMA9677	614.6	32.43 to 1197	Yes	*	0.0303
nDFb-2 vs. SMApt1	509.8	-72.36 to 1092	No	ns	0.1348
nDFb-2 vs. SMApt2	417.1	-165 to 999.2	No	ns	0.3618
SMA0232 vs. SMA9677	106.4	-475.8 to 688.5	No	ns	0.9993
SMA0232 vs. SMApt1	1.571	-580.6 to 583.7	No	ns	>0.9999
SMA0232 vs. SMApt2	-91.08	-673.2 to 491	No	ns	0.9997
SMA9677 vs. SMApt1	-104.8	-686.9 to 477.3	No	ns	0.9994
SMA9677 vs. SMApt2	-197.4	-779.6 to 384.7	No	ns	0.9685
SMApt1 vs. SMApt2	-92.65	-674.8 to 489.5	No	ns	0.9997

Supplemental Table 10: Statistical comparisons for figure 7C. IMP1 levels in the leading edge were assessed using two way ANOVA and Tukey's multiple comparisons test. Test was conducted with 1 family, 6 comparisons per family and an alpha of .05. ns: not significant, *: $p < .05$, **: $p < .01$, ***: $p < .001$, ****: $p < .0001$.

Number of families	1
Number of comparisons per family	6
Alpha	0.05

Tukey's multiple comparisons test	Mean Diff.	95% CI of diff.	Significant?	Summary
nDFb-1 vs. nDFb-2	0.9786	-1.717 to 3.674	No	ns
nDFb-1 vs. SMApt1	5.77	3.075 to 8.465	Yes	****
nDFb-1 vs. SMApt2	5.597	2.902 to 8.292	Yes	****
nDFb-2 vs. SMApt1	4.791	2.096 to 7.486	Yes	****
nDFb-2 vs. SMApt2	4.619	1.923 to 7.314	Yes	***
SMApt1 vs. SMApt2	-0.1727	-2.868 to 2.523	No	ns

Supplemental Table 11: Statistical comparisons for figure 7E. IMP1 granule association with the actin cytoskeleton values were assessed using two way ANOVA and Tukey's multiple comparisons test. Test was conducted with 1 family, 6 comparisons per family and an alpha of .05. ns: not significant, *: $p < .05$, **: $p < .01$, ***: $p < .001$, ****: $p < .0001$.

Number of families	1
Number of comparisons per family	6
Alpha	0.05

Tukey's multiple comparisons test	Mean Diff.	95% CI of diff.	Significant?	Summary
nDFb-1 vs. nDFb-2	0.1362	-6.724 to 6.996	No	ns
nDFb-1 vs. SMApt1	9.296	2.437 to 16.16	Yes	**
nDFb-1 vs. SMApt2	8.106	1.246 to 14.97	Yes	*
nDFb-2 vs. SMApt1	9.16	2.300 to 16.02	Yes	**
nDFb-2 vs. SMApt2	7.969	1.110 to 14.83	Yes	*
SMApt1 vs. SMApt2	-1.191	-8.051 to 5.669	No	ns

Supplemental Table 12: Statistical comparisons for figure 7G. IMP1 granule association with the microtubule cytoskeleton values were assessed using two way ANOVA and Tukey's multiple comparisons test. Test was conducted with 1 family, 6 comparisons per family and an alpha of .05. ns: not significant, *: $p < .05$, **, $p < .01$.

Compare column means (main column effect)

Number of families	1
Number of comparisons per family	120
Alpha	0.05

Tukey's multiple comparisons test	Mean Diff.	95% CI of diff.	Significant?	Summary
nDFb-1 vs. nDFb-1 +RNase	2.547	1.217 to 3.877	Yes	****
nDFb-1 vs. nDFb-2	0.6659	-1.996 to 0.6638	No	ns
nDFb-1 vs. nDFb-2 + RNase	2.511	1.181 to 3.841	Yes	****
nDFb-1 vs. Ctrl78	0.1469	-1.477 to 1.183	No	ns
nDFb-1 vs. Ctrl78 + RNase	2.528	1.198 to 3.857	Yes	****
nDFb-1 vs. Ctrl79	0.9914	-2.321 to 0.3383	No	ns
nDFb-1 vs. Ctrl79 + RNase	2.517	1.187 to 3.847	Yes	****
nDFb-1 vs. SMA0232	1.089	-0.2409 to 2.418	No	ns
nDFb-1 vs. SMA0232 + RNase	2.548	1.219 to 3.878	Yes	****
nDFb-1 vs. SMA9677	1.224	0.004430 to 2.554	No	ns
nDFb-1 vs. SMA9677 + RNase	2.56	1.230 to 3.889	Yes	****
nDFb-1 vs. SMApt1	1.334	1.204 to 2.664	Yes	*
nDFb-1 vs. SMApt1 + RNase	2.533	1.204 to 3.863	Yes	****
nDFb-1 vs. SMApt2	1.274	-0.05527 to 2.604	No	ns
nDFb-1 vs. SMApt2 + RNase	2.553	1.223 to 3.882	Yes	****
nDFb-1 +RNase vs. nDFb-2	-3.213	-4.542 to -1.883	Yes	****
nDFb-1 +RNase vs. nDFb-2 + RNase	0.0360	-1.366 to 1.294	No	ns

	1			
nDFb-1 +RNase vs. Ctrl78	-2.694	-4.023 to -1.364	Yes	****
nDFb-1 +RNase vs. Ctrl78 + RNase	0.0192	-1.349 to 1.310	No	ns
nDFb-1 +RNase vs. Ctrl79	-3.538	-4.868 to 2.209	Yes	****
nDFb-1 +RNase vs. Ctrl79 + RNase	0.0299	-1.360 to 1.300	No	ns
nDFb-1 +RNase vs. SMA0232	-1.458	-2.788 to 0.1285	Yes	*
nDFb-1 +RNase vs. SMA0232 + RNase	0.0014	-1.328 to 1.331	No	ns
nDFb-1 +RNase vs. SMA9677	-1.323	-2.653 to 0.006717	No	ns
nDFb-1 +RNase vs. SMA9677 + RNase	0.0126	-1.317 to 1.342	No	ns
nDFb-1 +RNase vs. SMApt1	-1.213	-2.542 to 0.1169	No	ns
nDFb-1 +RNase vs. SMApt1 + RNase	0.0135	-1.343 to 1.316	No	ns
nDFb-1 +RNase vs. SMApt2	-1.273	-2.602 to 0.05718	No	ns
nDFb-1 +RNase vs. SMApt2 + RNase	0.0057	-1.324 to 1.335	No	ns
nDFb-2 vs. nDFb-2 + RNase	3.177	1.847 to 4.506	Yes	****
nDFb-2 vs. Ctrl78	0.519	-0.8107 to 1.849	No	ns
nDFb-2 vs. Ctrl78 + RNase	3.194	1.864 to 4.523	Yes	****
nDFb-2 vs. Ctrl79	0.3255	-1.655 to 1.004	No	ns
nDFb-2 vs. Ctrl79 + RNase	3.183	1.853 to 4.513	Yes	****
nDFb-2 vs. SMA0232	1.755	0.4249 to 3.084	Yes	**
nDFb-2 vs. SMA0232 + RNase	3.214	1.884 to 4.544	Yes	****
nDFb-2 vs. SMA9677	1.89	0.5601 to 3.219	Yes	***
nDFb-2 vs. SMA9677 + RNase	3.225	1.896 to 4.555	Yes	****
nDFb-2 vs. SMApt1	2	0.6703 to	Yes	***

		3.330		
nDFb-2 vs. SMApt1 + RNase	3.199	1.870 to 4.529	Yes	****
nDFb-2 vs. SMApt2	1.94	0.6106 to 3.270	Yes	***
nDFb-2 vs. SMApt2 + RNase	3.218	1.889 to 4.548	Yes	****
nDFb-2 + RNase vs. Ctrl78	-2.658	-3.987 to - 1.328	Yes	****
nDFb-2 + RNase vs. Ctrl78 + RNase	0.0167 6	-1.313 to 1.346	No	ns
nDFb-2 + RNase vs. Ctrl79	-3.502	-4.832 to - 2.173	Yes	****
nDFb-2 + RNase vs. Ctrl79 + RNase	0.0061 03	-1.324 to 1.336	No	ns
nDFb-2 + RNase vs. SMA0232	-1.422	-2.752 to - 0.09246	Yes	*
nDFb-2 + RNase vs. SMA0232 + RNase	0.0374 2	-1.292 to 1.367	No	ns
nDFb-2 + RNase vs. SMA9677	-1.287	-2.617 to 0.04272	No	ns
nDFb-2 + RNase vs. SMA9677 + RNase	0.0486 6	-1.281 to 1.378	No	ns
nDFb-2 + RNase vs. SMApt1	-1.177	-2.506 to 0.1529	No	ns
nDFb-2 + RNase vs. SMApt1 + RNase	0.0224 3	-1.307 to 1.352	No	ns
nDFb-2 + RNase vs. SMApt2	-1.236	-2.566 to 0.09319	No	ns
nDFb-2 + RNase vs. SMApt2 + RNase	0.0417 3	-1.288 to 1.371	No	ns
Ctrl78 vs. Ctrl78 + RNase	2.675	1.345 to 4.004	Yes	****
Ctrl78 vs. Ctrl79	0.8445	-2.174 to 0.4852	No	ns
Ctrl78 vs. Ctrl79 + RNase	2.664	1.334 to 3.994	Yes	****
Ctrl78 vs. SMA0232	1.236	-0.09405 to 2.565	No	ns
Ctrl78 vs. SMA0232 + RNase	2.695	1.366 to 4.025	Yes	****
Ctrl78 vs. SMA9677	1.371	0.04113 to 2.700	Yes	*
Ctrl78 vs. SMA9677 + RNase	2.706	1.377 to 4.036	Yes	****
Ctrl78 vs. SMApt1	1.481	0.1513 to	Yes	*

		2.811		
		1.351 to		
Ctrl78 vs. SMApt1 + RNase	2.68	4.010	Yes	****
		0.09159 to		
Ctrl78 vs. SMApt2	1.421	2.751	Yes	*
		1.370 to		
Ctrl78 vs. SMApt2 + RNase	2.699	4.029	Yes	****
		-4.849 to -		
Ctrl78 + RNase vs. Ctrl79	-3.519	2.189	Yes	****
		-		
Ctrl78 + RNase vs. Ctrl79 + RNase	0.0106	-1.340 to		
	6	1.319	No	ns
		-2.769 to -		
Ctrl78 + RNase vs. SMA0232	-1.439	0.1092	Yes	*
Ctrl78 + RNase vs. SMA0232 + RNase	0.0206	-1.309 to		
	5	1.350	No	ns
		-2.633 to		
Ctrl78 + RNase vs. SMA9677	-1.304	0.02596	No	ns
Ctrl78 + RNase vs. SMA9677 + RNase	0.0319	-1.298 to	No	ns
		1.362		
		-2.523 to		
Ctrl78 + RNase vs. SMApt1	-1.194	0.1361	No	ns
Ctrl78 + RNase vs. SMApt1 + RNase	0.0056	-1.324 to		
	63	1.335	No	ns
		-2.583 to		
Ctrl78 + RNase vs. SMApt2	-1.253	0.07642	No	ns
Ctrl78 + RNase vs. SMApt2 + RNase	0.0249	-1.305 to		
	6	1.355	No	ns
		2.179 to		
Ctrl79 vs. Ctrl79 + RNase	3.508	4.838	Yes	****
		0.7505 to		
Ctrl79 vs. SMA0232	2.08	3.410	Yes	****
		2.210 to		
Ctrl79 vs. SMA0232 + RNase	3.54	4.869	Yes	****
		0.8856 to		
Ctrl79 vs. SMA9677	2.215	3.545	Yes	****
		2.221 to		
Ctrl79 vs. SMA9677 + RNase	3.551	4.881	Yes	****
		0.9958 to		
Ctrl79 vs. SMApt1	2.325	3.655	Yes	****
		2.195 to		
Ctrl79 vs. SMApt1 + RNase	3.525	4.854	Yes	****
		0.9361 to		
Ctrl79 vs. SMApt2	2.266	3.595	Yes	****
		2.214 to		
Ctrl79 vs. SMApt2 + RNase	3.544	4.874	Yes	****

Ctrl79 + RNase vs. SMA0232	-1.428	-2.758 to -0.09856	Yes	*
Ctrl79 + RNase vs. SMA0232 + RNase	0.0313	1	No	ns
Ctrl79 + RNase vs. SMA9677	-1.293	-2.623 to 0.03662	No	ns
Ctrl79 + RNase vs. SMA9677 + RNase	0.0425	6	No	ns
Ctrl79 + RNase vs. SMApt1	-1.183	-2.513 to 0.1468	No	ns
Ctrl79 + RNase vs. SMApt1 + RNase	0.0163	2	No	ns
Ctrl79 + RNase vs. SMApt2	-1.243	-2.572 to 0.08708	No	ns
Ctrl79 + RNase vs. SMApt2 + RNase	0.0356	2	No	ns
SMA0232 vs. SMA0232 + RNase	1.46	0.1299 to 2.789	Yes	*
SMA0232 vs. SMA9677	0.1352	-1.195 to 1.465	No	ns
SMA0232 vs. SMA9677 + RNase	1.471	0.1411 to 2.800	Yes	*
SMA0232 vs. SMApt1	0.2453	-1.084 to 1.575	No	ns
SMA0232 vs. SMApt1 + RNase	1.445	0.1149 to 2.774	Yes	*
SMA0232 vs. SMApt2	0.1856	-1.144 to 1.515	No	ns
SMA0232 vs. SMApt2 + RNase	1.464	0.1342 to 2.794	Yes	*
SMA0232 + RNase vs. SMA9677	-1.324	-2.654 to 0.005306	No	ns
SMA0232 + RNase vs. SMA9677 + RNase	0.0112	4	No	ns
SMA0232 + RNase vs. SMApt1	-1.214	-2.544 to 0.1155	No	ns
SMA0232 + RNase vs. SMApt1 + RNase	0.0149	-	No	ns
SMA0232 + RNase vs. SMApt2	-1.274	-2.604 to 0.05577	No	ns
SMA0232 + RNase vs. SMApt2 + RNase	0.0043	11	No	ns
SMA9677 vs. SMA9677 + RNase	1.336	0.005936 to 2.665	Yes	*
SMA9677 vs. SMApt1	0.1102	-1.220 to	No	ns

		1.440		
SMA9677 vs. SMApt1 + RNase	1.309	-0.02030 to 2.639	No	ns
	0.0504	-1.279 to		
SMA9677 vs. SMApt2	6	1.380	No	ns
SMA9677 vs. SMApt2 + RNase	1.329	-0.0009950 to 2.658	No	ns
SMA9677 + RNase vs. SMApt1	-1.225	-2.555 to 0.1042	No	ns
	-			
SMA9677 + RNase vs. SMApt1 + RNase	0.0262	-1.356 to 1.303	No	ns
	3			
SMA9677 + RNase vs. SMApt2	-1.285	-2.615 to 0.04453	No	ns
	-			
SMA9677 + RNase vs. SMApt2 + RNase	0.0069	-1.337 to 1.323	No	ns
	31			
SMApt1 vs. SMApt1 + RNase	1.199	-0.1305 to 2.529	No	ns
	-	-1.389 to		
SMApt1 vs. SMApt2	0.0597	1.270	No	ns
SMApt1 vs. SMApt2 + RNase	1.219	-0.1112 to 2.548	No	ns
SMApt1 + RNase vs. SMApt2	-1.259	-2.589 to 0.07076	No	ns
SMApt1 + RNase vs. SMApt2 + RNase	0.0193	-1.310 to 1.349	No	ns
SMApt2 vs. SMApt2 + RNase	1.278	-0.05146 to 2.608	No	ns

Supplemental Table 13: Statistical comparisons for figure 7I. IMP1 pellet/IMP1 soluble values were assessed using a two way ANOVA and Tukey's multiple comparisons test. Test was conducted with 1 family, 120 comparisons per family and an alpha of .05. ns: not significant, *: $p < .05$, **: $p < .01$, ***: $p < .001$, ****: $p < .0001$.

Chapter 4: Conclusions and future directions.

Overview:

Despite considerable progress in understanding the processes of mRNA localization and local translation in axons, the molecular mechanisms that govern the assembly of mRNAs and mRBPs into mRNP transport granules are poorly understood. A recent study on the interactome of two distinct neuronal RNA-binding proteins shows that they share only a third of the identified proteins, suggesting that specific mRBP-associated transport granules are much more heterogeneous than previously anticipated (Fritzsche et al., 2013). The molecular machinery that assembles transcripts with a specific set of proteins that regulate their translocation process along microtubules, their stability, and their dissociation from the mRNPs, resulting in the mRNA being translated by ribosomes, remains unknown. The work presented in this dissertation furthers our understanding of mRNA and protein association. In my dissertation I hypothesized *that the survival of motor neuron (SMN) protein functions as a chaperone for mRNA and protein complex (mRNP) assembly*. The primary findings that provide support for this hypothesis are as follows:

1. mRNAs and mRNA-binding proteins are mislocalized in motor neurons derived from an SMA mouse model.

2. Overexpression of mRNA binding proteins regulating the localization and translation of the mislocalized mRNAs can rescue axonal defects in SMA motor neurons, including mRNA mislocalization.
3. Association of IMP1 protein with β -actin mRNA is impaired in SMA mouse motor neurons and SMA patient fibroblasts.
4. Binding of IMP1 protein with poly(A)-mRNA is reduced in SMA patient fibroblasts.
5. Association of IMP1 with the actin and tubulin cytoskeleton is reduced in SMA patient fibroblasts.

In this final chapter, I will discuss the future directions raised by the data and analysis discussed in this work. Additionally, I will discuss the further implications of SMA as a disease of broad RNP hypo-assembly (Donlin-Asp et al., 2016; Shukla and Parker, 2016), with a wide range of RNP types likely to be regulated by SMN (Li et al., 2014b).

SMN as a chaperone for RNP assembly

Evidence for SMN as a broad chaperone for RNP assembly comes from its complex network of protein interactions (Shafey et al., 2010; Terns

and Terns, 2001), including Sm proteins (Buhler et al., 1999; Friesen et al., 2001), LSm proteins (Friesen and Dreyfuss, 2000; Pillai et al., 2003), and mRNA binding proteins (Akten et al., 2011; Fallini et al., 2014; Fallini et al., 2011; Hubers et al., 2011; Piazzon et al., 2008; Rossoll et al., 2002; Tadesse et al., 2008) highlights the complex processes that are likely defective upon reduction of SMN protein levels (Figure 1). Increasing evidence for SMN functioning as a chaperone for RNP assembly suggests that defects in a broad spectrum of RNA processing functions, including splicing (Li et al., 2014a), stability, localization (Donlin-Asp et al., 2016; Fallini et al., 2016), and translation (Fallini et al., 2016; Kye et al., 2014; Sanchez et al., 2013) all contribute to SMA pathology.

For the field at large a remaining question is the scope of RNP assembly defects in SMA *in vivo*, and how these defects contribute to the disease phenotypes observed in SMA patients. Given the known functions of SMN, SMA likely is a disease of general RNP hypo-assembly, where one expects widespread effects on all stages of posttranscriptional regulation (Fallini et al., 2016; Shukla and Parker, 2016), which will lead to widespread alterations in the splicing, stability, localization and translation of RNA transcripts. This raises an intriguing experimental question to address, specifically characterizing the full extent of RNA binding proteins altered in their association with target transcripts in SMA.

As discussed at the end of Chapter 1 of this dissertation, novel technologies that have been developed in the past number of years will

allow testing the full extent of RNP complexes hypo-assembled in SMA, and to what extent they contribute to pathology *in vivo*.

What mRNA binding proteins are regulated in their association with mRNA by SMN?

Of the known mRNA binding proteins associated with SMN, the majority have come from candidate based screens based on known mislocalized mRNAs such as *β-actin* (Fallini et al., 2016; Rossoll et al., 2003), *Gap43* (Fallini et al., 2016) and *neurtin* (Akten et al., 2011). During my thesis studies, I focused on the association of IMP1 with *β-actin* mRNA (Chapter 3 Figure 1-3) but we also detected changes in the association with IMP1 with bulk mRNA (Chapter 3 Figure 4). This in particular raises an important question as to how widespread perturbations in mRNA-protein association occur in SMA, specifically whether defects are limited to a subset of specialized mRNA binding proteins or whether the defect is much more general (Figure 2). Testing this question has become possible with RNA interactome capture (Castello et al., 2013, 2016b) (Figure 3). Utilizing the same amount of starting cells from control and SMA fibroblasts, performing the poly(A)-RNA interactome capture followed by mass spec analysis would allow capturing all mRNA-protein associations occurring in both control and SMA fibroblasts to allow side by side comparisons and quantitative analysis. This will allow sensitive analysis to determine if 1) *SMN regulates the association of only a subset of mRNA*

binding proteins with mRNA, 2) if SMN broadly regulates the association of mRNA binding proteins with mRNA, leading to global mRNP assembly defects in SMA samples, and 3) if SMN broadly regulates the association of mRNA binding proteins with mRNA, leading to global alterations, both decreases and increases, in mRNP assembly in SMA samples.

What RNP complexes show alterations in their assembly in SMA?

Currently, while a number of RNP classes have been linked to SMN (Li et al., 2014b), only snRNPs and, in this present work mRNPs, have been rigorously tested in SMA samples to demonstrate assembly defects, raising the important question as to what other complexes are altered in their assembly upon reduced SMN levels. In this work we presented data from RNP fractionation over an optiprep gradient (Fritzsche et al., 2013) (Chapter 3 Figure 5, Supplemental Figure 2 & 3), which is an ideal assay for answering this question (Figure 4). Experiments using antibodies against the poly(A)-binding protein PABP1 suggest that not only IMP1-containing complexes but a broad range of mRNPs may be defective in their assembly in SMA. By performing quantitative mass spectrometry and transcriptomics analysis on the fractions, it would be possible to determine the RNA and protein compositions of a number of cellular complexes of different sizes, both RNP and non-RNP related, to get a snapshot at the extent of assembly defects in SMA samples. This will allow determination if *1) only a subset of RNP complexes, including snRNPs and mRNPs are*

regulated by SMN, 2) if RNP complexes of a wide variety are regulated by SMN, and show global decreases in their size and decreased migration through the fractions in SMA samples, and 3) if RNP complexes of a wide variety are regulated by SMN, and show global alterations, both decreases and increases, in their size and decreased migration through the fractions in SMA samples.

To what extent do non-splicing related RNP changes contribute to pathology in SMA *in vivo*?

The majority of work on the function of SMN, and the defects in motor neurons in SMA by extension, have been carried out in cultured cell lines and primary neurons *in vitro*, raising the question about the extent of defects that occur *in vivo* in SMA mouse models. Pioneering work in the zebrafish model of SMA have given critical insight into the existence of axonal defects (McWhorter et al., 2003) and axonal localization of SMN during early development (Hao le et al., 2015), and suggested that non-snRNP rescue of SMN activity can relieve axonal defects (Carrel et al., 2006). These findings highlight the need to apply novel techniques in SMA mouse models to compare results from the *in vitro* and zebrafish datasets.

Two key questions that remain to be explored *in vivo*, are 1) is mRNA in axons of motor neurons mislocalized and 2), does this lead to decreased local translation at the presynaptic side of the neuromuscular junction? To study the SMA phenotype develop over a longer period of

time after birth, a new SMA intermediate severity mouse model has been generated (Bowerman et al., 2012), the SMA (2B/-) mouse.. The mouse model allows for longer sampling of time points *in vivo*, including points prior to onset of symptoms and during the course of symptom manifestation.

To address if mRNAs are mislocalized in mature axons (Shigeoka et al., 2016), highly sensitive approaches may be needed, since RNA levels are expected to be lower relative to dendrites and developing axons. Therefore, multiple novel strategies likely will have to be employed, encompassing both sequencing and imaging approaches. Previous studies have already successfully been able to sequence RNA from sciatic nerve preparations (Yi et al., 2015). Therefore, using this as starting material for sequencing and comparing these samples from both control and SMA animals, it will be possible to get a snapshot of the axonal population of mRNA at multiple time points. The SMA2B mouse can be crossed with the RiboTag mouse, which allows for cre-dependent cell type specific labeling of ribosomes with an HA-tagged ribosomal protein. Similar to the landmark study demonstrating mature axonal translation (Shigeoka et al., 2016), using a motor neuron specific cre-driver, this will allow for the unbiased isolation of mRNAs associated with ribosomes (translatome) from the sciatic nerve and neuromuscular junctions from various muscle groups in both SMA and control animals. RNA sequencing will allow identification of mRNAs associated with ribosome in both conditions.

Utilizing the information gleaned from such analysis it will be possible to determine if 1) *bulk mRNA is mislocalized in axons in SMA animals in vivo*, 2) *specific mRNAs are mislocalized in axons in SMA animals in vivo*, 3) *mRNAs show various patterns of change in axons in SMA animals, with some decreased and others showing enhanced localization, in vivo*, and 4) *ribosome-associated mRNAs are not mislocalized in mature axons in vivo*. With these results, utilizing novel advances in fluorescent *in situ* hybridization (FISH) it will then be possible to visualize the localization patterns for specific transcripts and their encoded proteins at the axon terminals at the neuromuscular junction.

Are defects seen in SMA mouse motor neurons also present in human patient derived samples?

Another unresolved question in the field is how many of the defects characterized in various SMA models, such as mouse models, are actually recapitulated in patient samples. In Chapter 4 for a number of studies we utilized both SMA mouse motor neurons and SMA patient fibroblasts for experiments, however it remains to be seen if similar defects are seen in SMA patient motor neurons. Induced pluripotent stem cell (iPSC) technology has been successfully used with SMA (Ebert et al., 2009; Faravelli et al., 2015; Nizzardo et al., 2015), and SMA iPSC motor neurons did present with a phenotype in culture. Initial studies in our hands (Figure 4) demonstrate that SMA iPSC motor neuron cultures

present with both an axonal length defect (Figure 5A,B) and show reduced TriFC signal, indicating mRNP assembly defects (Figure 5C,D). These studies while preliminary, highlight the need to further explore the iPSC motor neuron phenotypes from SMA patients, specifically to determine whether mRNAs are mislocalized from the axons of human motor neurons just like in SMA mouse motor neuron preparations.

Future directions for SMA therapy

Perhaps the most pressing issue within the SMA field is the development of effective therapeutic strategies for the disease. The main strategic aim for therapeutic strategies have been to raise SMN protein levels. Early clinical attempts using histone deacetylase inhibitors (HDAC inhibitors), in an attempt to boost the transcription of *SMN2* and thus raise SMN protein levels (Avila et al., 2007; Dayangac-Erden et al., 2009; Evans et al., 2011; Hauke et al., 2009; Kernochan et al., 2005; Kwon et al., 2011; Liu et al., 2014; Riessland et al., 2010). As these failed to demonstrate any clinical benefit, newer strategies were pursued. Anti-sense oligonucleotide (ASOs) targeting *SMN2* to block the splicing out of Exon 7 have shown promise in various models of SMA (Keil et al., 2014; Nizzardo et al., 2014; Osman et al., 2014; Porensky et al., 2012; Singh et al., 2015; Staropoli et al., 2015) and recently have made it to phase 3 clinical trials. Perhaps the most promising development, however has been a recent clinical trials using adeno associated viruses (AAV) rescue

of SMN levels in newly diagnosed patients, as this strategy has the possibility of rescuing SMN levels in a critical developmental window and has the best chance to rescue SMA pathophysiology. While these clinical breakthroughs have offered renewed hope at the round of successful SMA therapies, these strategies have been designed for the rescue of SMN levels in newly diagnosed patients or younger patients, and it remains to be seen if they will work well for post symptomatic patients or if additional therapeutic strategies or combination of therapies will need to be pursued. From this work (Appendix, Figure 3) an intriguing possibility for manipulating RNP assembly through regulation of the steady state levels of various RNA binding proteins may offer some therapeutic benefit. The rationale here (Figure 6) is best summarized in regards to a standard chemical equation with RNAs and RNA binding proteins on one side of the equation, and RNP complexes on the other. Since SMA is likely a hypo-assembly disease where this balance is tipped towards the “reactants”, manipulation of this side may help push the formation of more fully assembled RNP complexes. Interestingly, early drug screens for SMA therapeutic compounds picked up an inhibitor of the scavenger decapping enzyme (DcpS) (Gogliotti et al., 2013). While the first thought was that this compounds rescue of SMA pathology was due to increasing SMN levels, likely through stabilizing the mRNA, further work failed to show this was the case. Interestingly, this compound still improved survival, motor

function, and motor unit pathology in two SMA mouse models (Gogliotti et al., 2013; Van Meerbeke et al., 2013).

Given that DcpS does participate in mRNA turnover, it may be that its beneficial effects in SMA are mediated through stabilization of mRNA, and in turn enhancing formation of mRNP complexes. To test this possibility, HEK cells were treated for 1-3 days at varying concentrations with the DcpS inhibitor RG3039, and 12 hours prior to fixation were transfected with the TriFC constructs (Figure 7). Consistently, longer and higher treatments of RG3039 promoted enhanced mRNP complex formation, consistent with our hypothesis. To address if this was due to enhancement of mRNA levels, we performed poly(A) FISH in HEK cells treated with RG3039 (Figure 8). Again, longer and higher treatments resulted in increased poly(A) FISH signal- suggestive that mRNA levels may be enhanced via stabilization with the RG3039 treatment. Taken together with our previous demonstration of mRBP overexpression rescue of SMA phenotypes (Appendix, Figure 3) these data strongly suggest that modulation of mRNP complex assembly either through enhancing mRBP levels or stabilization of mRNA may provide therapeutic benefit in SMA patients.

Insight into if modulation of mRNP assembly can rescue SMA pathology will provide critical insight into the extent to which mRNP assembly defects themselves contribute to SMA pathology. Additionally, if SMN indeed broadly acts as an RNP chaperone, it remains a critical

question to address if broad defects in RNP assembly contribute to the specific manifestation of SMA pathology, or if specific defects in particular RNP classes result in specific phenotypes. Future work will need to address if rescuing the assembly of specific RNP classes, such as snRNPs or mRNPs, can mitigate some or all of the disease phenotypes.

Why are motor neurons affected in SMA?

Perhaps in the field the most pertinent scientific question is why the disease manifests primarily in motor neurons, despite the fact that SMN is ubiquitously expressed. This outstanding question is highly complex, as multiple explanations are possible, including motor neuron specific splicing events or a role for SMN in highly polarized motor neurons. However with increasing evidence that there are widespread splicing defects *in vivo* (Doktor et al., 2016), and while motor neuron rescue of SMN has benefit for motility and survival, it is only to a point, as full systemic rescue of SMN is required for maximal survival benefit (Hao et al., 2013; Hua et al., 2011; Lutz et al., 2011). These data suggest SMA is characterized by motor neuron pathology because they are the first cell population to fail *in vivo* and cause death in affected patients before other defects may become manifest. This will only be resolved by more *in vivo* studies, focusing on assessing additional tissues with increasing scrutiny.

Material and methods-

Cell culturing, transfections, staining and RG3039 treatment.

HEK cells were cultured as previously described (Williams et al., 2016), and transfected using Turbofect (Thermo). RG3039 was applied to cells at working concentrations of 20, 40 or 60 μM , for 24/48/72 hours. Media was changed and fresh drug was added every 24 hours until the end of the experiment.

TriFC

TriFC constructs were cloned similarly to previous described (Rackham and Brown, 2004). For the ECFP 3'UTR constructs, both the BoxB sequence repeats inserted along with the 3'UTR of *β -actin* and deletion constructs were generated using splicing by overlapping extension. IMP1-GFP and λN_{22} -GFP were subcloned by replacing VFP_{1-154} and $\text{VFP}_{155-239}$ with GFP. For TriFC experiments in HEK cells, IMP1- VFP_{1-154} , λN_{22} - $\text{VFP}_{155-239}$, CFP-UTR's and the empty pcDNA3 plasmid were transfected into cells in a 1:1:1:3 ratio to limit oversaturation of TriFC signal. For motor neuron cultures, pcDNA3 was omitted from the transfection and all constructs were transfected in a 1:1:1 ratio. Expression of constructs was limited to 12-24 hours, and fixation was performed with 4% paraformaldehyde, followed by anti-GFP (Abcam) immunofluorescence with an Alexa647 secondary antibody for identification of transfected cells in a blinded fashion. Exposure settings were held constant for all

acquisitions for an experiment. Analysis was performed in Imaris (Bitplane). 3D masks were generated for both the cell body and axonal fractions for motor neurons, and cell bodies for fibroblasts and Neuro2a cells. The total sum of pixel intensities was measured in a 3D volume for both the CFP and YFP channels, and the ratio of YFP/CFP was determined for the readout of TriFC signal. Cumulative distribution plots were generated from the sum of all experiments in Prism (GraphPad).

Fluorescence in situ Hybridization and Immunofluorescence.

HEK cells were fixed for 15 minutes with 4% paraformaldehyde in PBS. Fluorescence in situ hybridization (FISH) was performed as described previously (Fallini et al., 2011) with some modifications. Briefly, fixed HEK cells were rinsed in PBS containing 5 mM MgCl₂ and equilibrated in 1x SSC buffer for 10'. Cells were then washed in 10% formamide (Sigma) for 10' before preincubation in hybridization buffer (20% dextran sulfate, 4x SSC, 4 mg/ml BSA, 20 mM ribonucleoside vanadyl complex, and 10 mM sodium phosphate buffer, pH 7.0) at 37°C for 1.5 h. Probes (1µl) were resuspended with 10 µg each of E. coli tRNA and salmon sperm DNA in 50 µl hybridization buffer and incubated with the coverslips at 37°C overnight. A cy5-labeled oligo dT probe (Biosearch Technologies) was used to detect poly(A)-positive mRNAs.

Image Acquisition and Analysis.

For high resolution imaging, a 60x objective (1.4 NA) was used. Z-series (5 to 10 sections, 0.2 μm thickness) were acquired with an epifluorescence microscope (Ti, Nikon) equipped with a cooled CCD camera (HQ2, Photometrics). For low magnification imaging, a 10x or 20x phase objective was used and single optical slices were acquired. Z-stacks were deconvolved (AutoquantX2, Media Cybernetics) and analyzed using the Imaris software (Bitplane). Axon length measurements were performed as described (Fallini et al., 2012a).

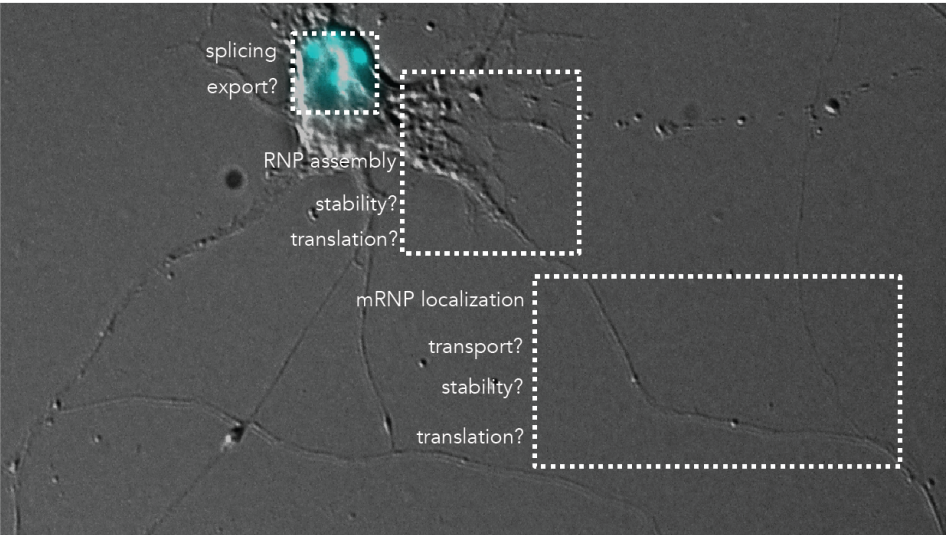


Figure 1: Widespread disruptions in a number of RNP mediated processes contribute to SMA pathology.

RNA-protein interactions regulate all classes of RNAs and the processes they control throughout the cell. Given that increasing evidence points to multiple classes of RNPs regulated by SMN, its increasingly clear that a number of RNA regulated processes are also likely altered in SMA. This figure displays an overly simplistic view of some of the processes that could be disrupted in SMA.

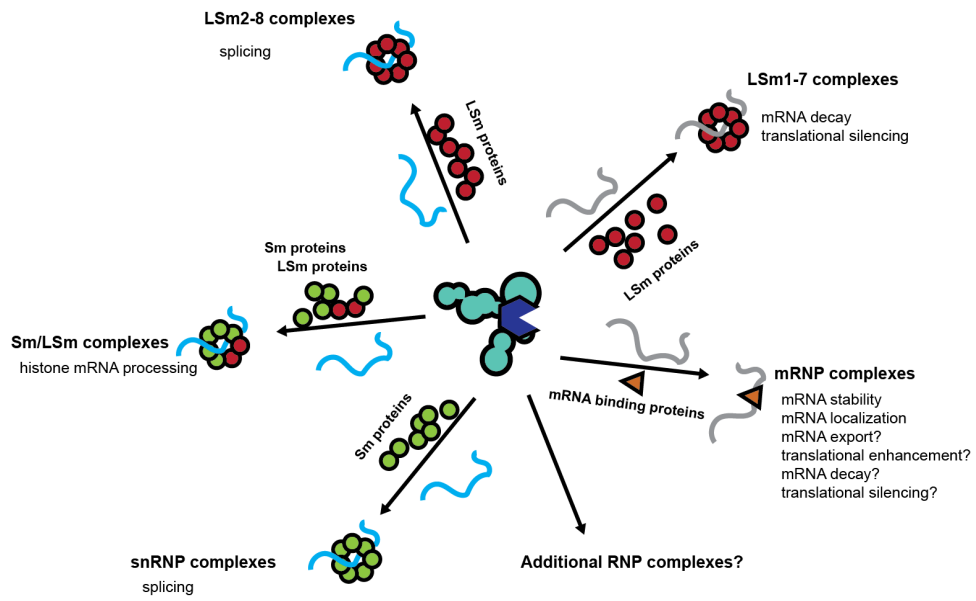


Figure 2: SMN in RNP assembly

Increasing evidence points to multiple classes of RNPs regulated by SMN, including those of Sm protein containing snRNPs, LSm containing complexes involved in both splicing and RNA decay, and mRNPs regulating localization, transport and stability of mRNA. It remains likely that SMN assembles other classes of RNPs as well.

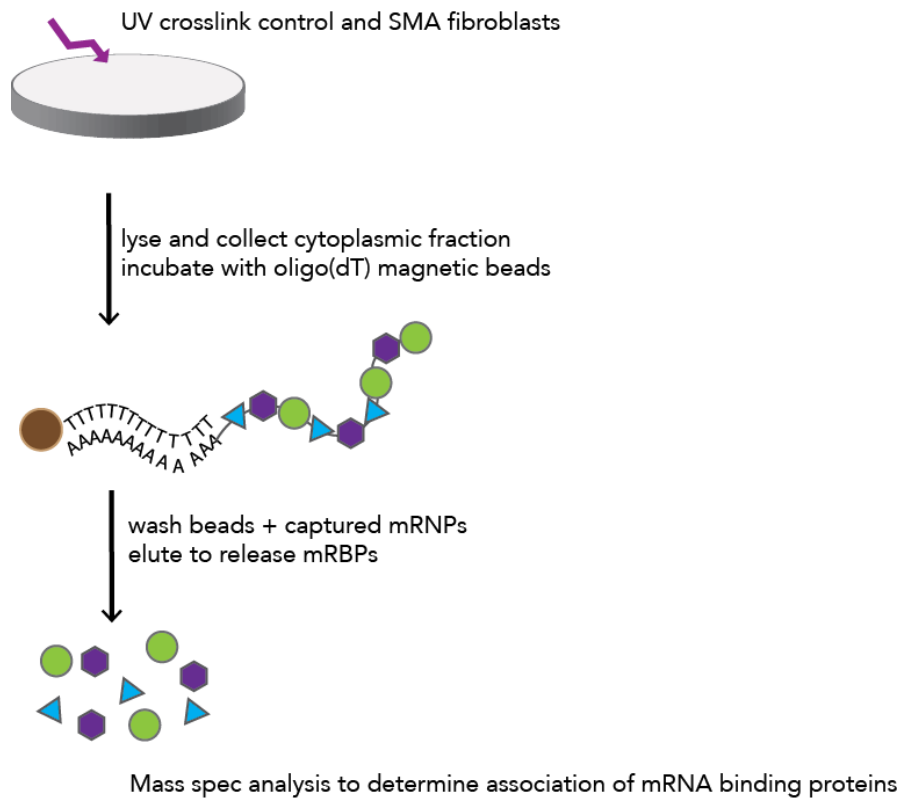
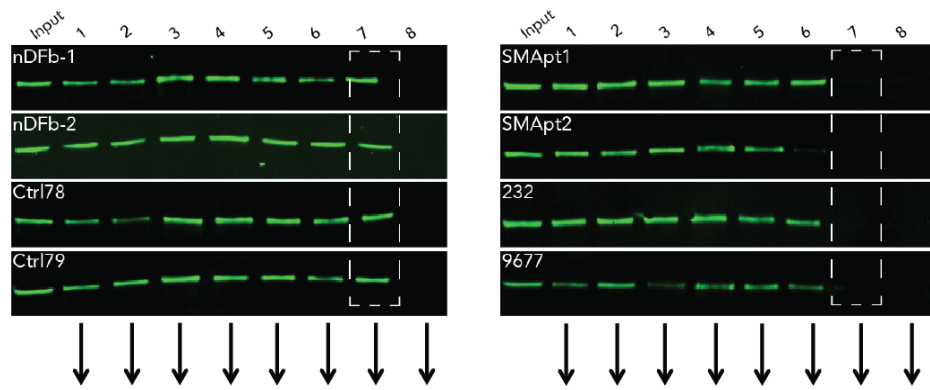


Figure 3: RNA interactome capture for identification of altered mRNA-protein associations globally in SMA.

Schematic representation of the mRNA interactome assay. Control or SMA patient fibroblasts are subjected to UV-crosslinking and cytoplasmic lysates are incubated with oligo(dT) beads. Isolates could then be subjected to mass spec analysis for assessment of mRNA binding proteins in SMA samples relative to controls.

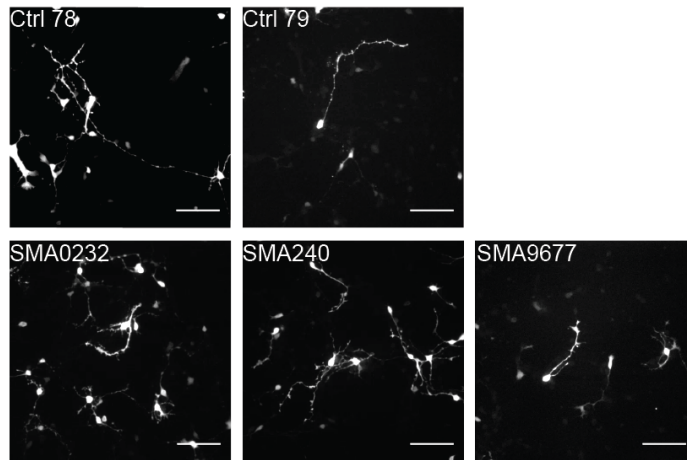


Mass spec, assess relative fraction composition, compare between controls and SMA patient lines

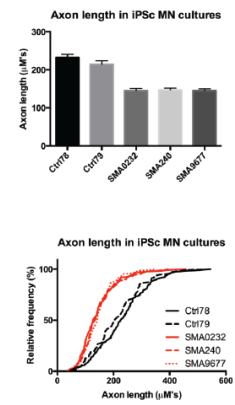
Figure 4. RNP gradient isolation to assess widespread changes in RNP granule size and complexity in SMA patient samples

As previously shown (Chapter 4 Figure 5) MP1 granules show reduced complexity in SMA patient samples in Cytoplasmic RNP isolates from fibroblasts were subjected to Optiprep gradient centrifugation and fractionation. Rather than performing western blot analysis, performing mass spec on each of the fractions from both SMA and control samples would allow their compositions to be compared between SMA and controls. This will allow characterization of differences in the size and distribution of various classes of RNP complexes in the samples.

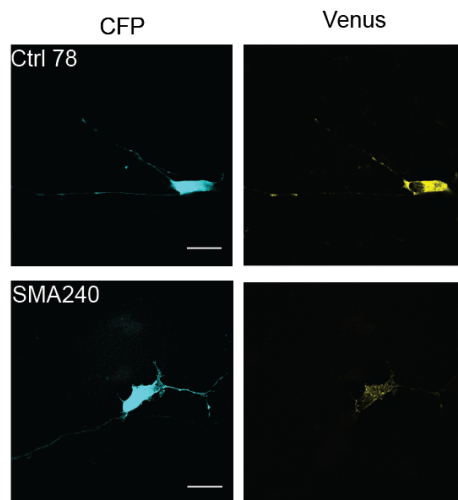
A.



B.



C.



D.

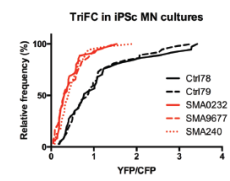


Figure 5. SMA iPSC motor neurons display similar defects to SMA mouse motor neurons

A. EGFP was transfected into the iPSC motor neuron cultures from 2 control lines and 3 SMA lines. SMA iPSC motor neurons display shorter axons relative to control motor neurons. B. Quantification of A. C. SMA iPSC motor neurons display impaired IMP1- β -actin association, as shown by impaired TriFC signal. D. Quantification of C.

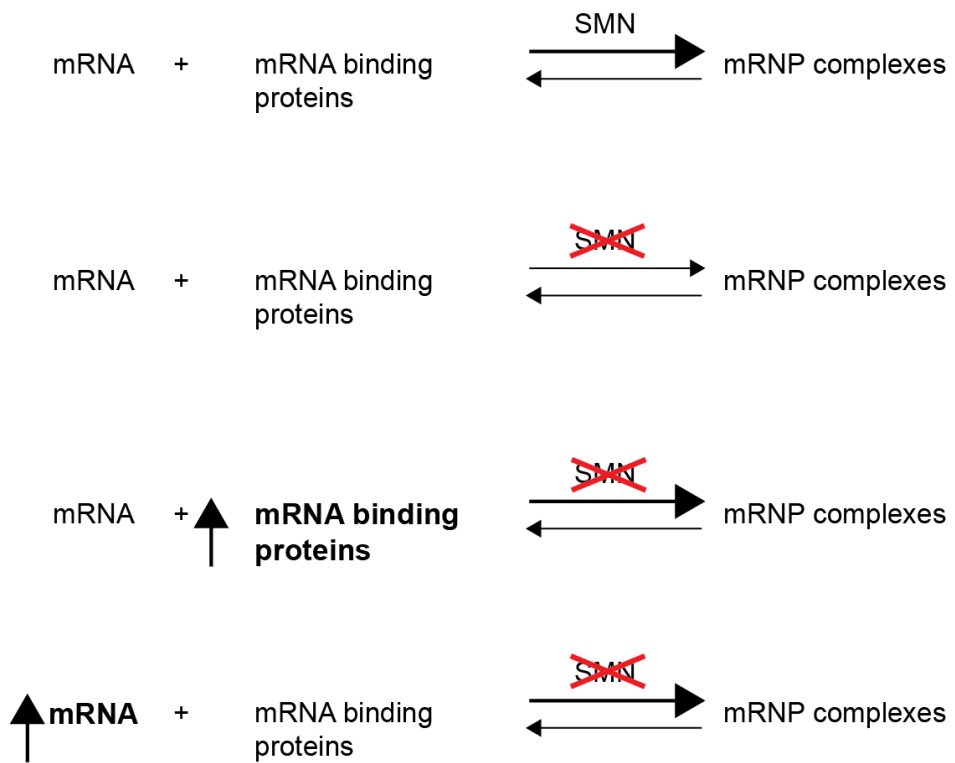


Figure 6. Manipulating mRNA levels as a therapy in SMA

Work presented in this dissertation supports the model of SMN as a chaperone for mRNP assembly. Reduction in SMN levels results in a less function mRNP complexes. Previous work has shown SMA defects are rescued by overexpression of mRNA binding proteins, resulting in rescue of mRNA and protein localization defects in SMA motor neurons, likely due to enhanced mRNP complex assembly. Theoretically, increasing mRNA levels in the cell through increased transcription or stabilization of the mRNA would likely also increase mRNP complex assembly and rescue axonal defects in SMA motor neurons.

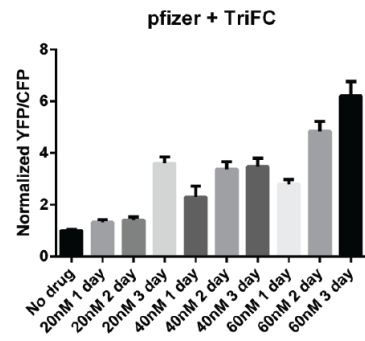
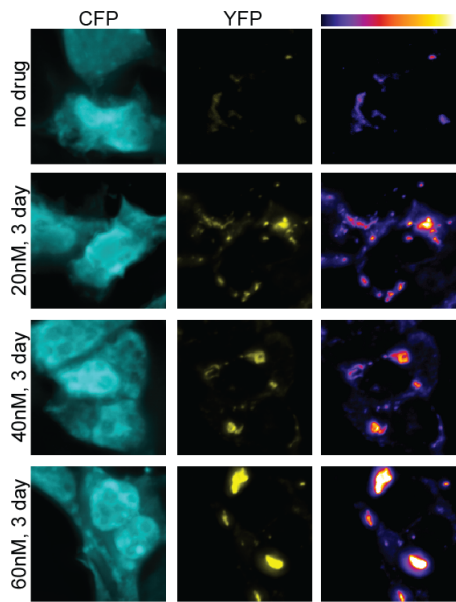


Figure 7. RG3039 treatment increases mRNP assembly of β actin mRNA and IMP1

Cells were transfected with full length TriFC reporter plasmid containing the entire β -*actin* 3' untranslated region and the phage RNA-binding protein λ N₂₂ binding site. Normalized ratios of YFP (TriFC signal) / CFP (transfection control) indicate a time and dose-dependent increase in mRNP assembly upon RG3039 treatment. One way ANOVA multiple comparisons (to mean of 0nM), all except 20nM 1&2 days significant. In HEK293 cells, n= 3

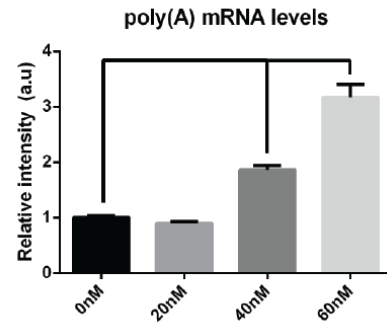
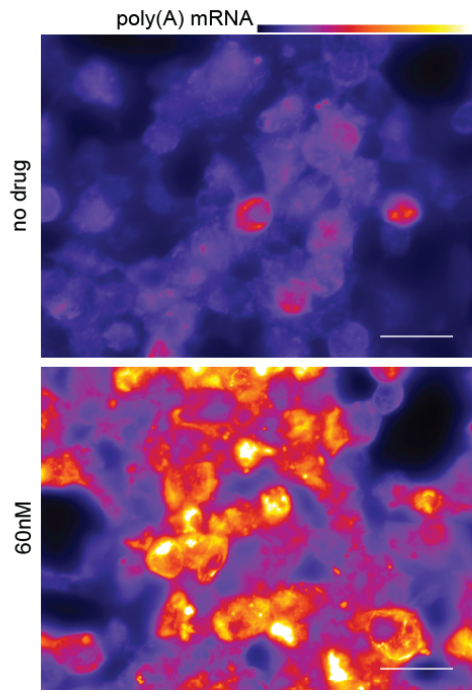


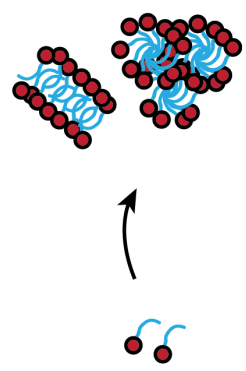
Figure 8. RG3039 treatment increases poly(A) RNA signal in treated cells

Cells were treated for 24 hours with different concentrations of RG3039.

Poly(A) FISH was performed and signal was quantified over the volume of cells. Example images are heat maps of the poly(A) signal. One way

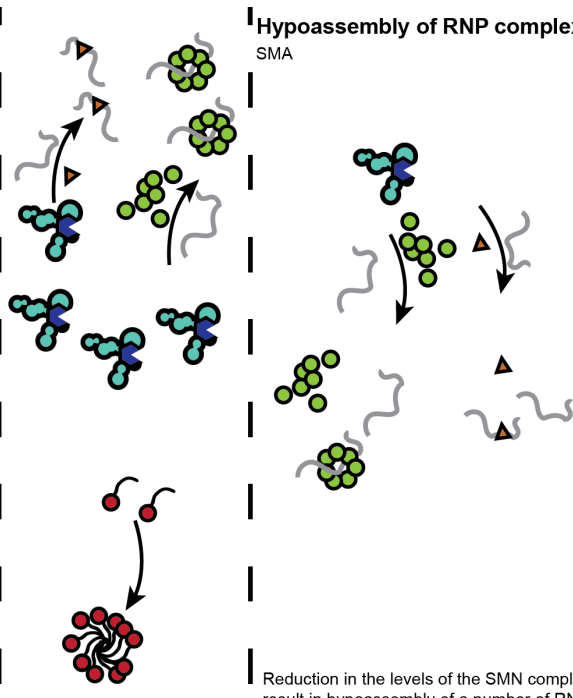
ANOVA multiple comparisons (to mean of 0nM), all except 20nM 1&2 days significant. In HEK293 cells, n= 3

Hyperassembly of RNA bodies
ALS



Mutations within RNA binding proteins found within RNA bodies lead to low complexity domain mediated hyperassembly and aggregation in disease.

Hypoassembly of RNP complexes
SMA



Reduction in the levels of the SMN complex result in hypoassembly of a number of RNP complexes.

Figure 9: Widespread disruptions in a number of RNP mediated processes contribute to SMA pathology.

Similar to SMA, ALS is a motoneuron disease characterized by widespread alterations in RNP homeostasis. Unlike SMA, ALS is a disease characterized of aggregation or hyper assembly of RNP complexes as opposed to the hypo assembly seen in SMA. These opposing processes, both resulting in motoneuron disease, highlight the importance of proper RNP regulation and homeostasis.

Appendix: mRNA localization and local translation defects in SMN deficiency.

mRNA are mislocalized from axonal compartments with SMN deficiency

The previously described axon outgrowth defect in SMA motor neurons (Fallini et al., 2016; Rossoll et al., 2003) indicates the involvement of other transcripts in addition to *β-actin*, will contribute to the axonal growth defect (Donnelly et al., 2013). We focused on *Gap43* mRNA, a known mRNA whose axonal translation contributes to axonal growth. To assess the effects of SMN deficiency on *Gap43* mRNA and protein localization in wild-type motor neurons SMN levels were acutely reduced by shRNA (Figure 1) and the localization and abundance of *Gap43* and *β-actin* mRNAs were assessed by quantitative fluorescence *in situ* hybridization (Q-FISH). A striking reduction in the levels of both mRNAs was observed in the axons and growth cones of shSMN-transfected motor neurons 5 days after transfection (Figure 3). No difference was detected in the cell bodies. These results are similar to those seen in motor neuron cultures derived from a severe SMA mouse model (Fallini et al., 2016).

GAP43 protein is reduced in SMA growth cones.

To investigate whether reduced *Gap43* mRNA levels in the axon of SMA motor neurons and SMN depleted motor neurons is associated with a decrease in the levels of GAP43 protein; we performed quantitative immunofluorescence for GAP43 protein. We found decreased localization of GAP43 protein levels at the growth cone in the SMA motor neurons

(Figure 2A-B), with no decrease in the cell body. shSMN-transfected motor neurons (Figure 2C, D) show a similar decrease in GAP43 protein localization in the growthcone with no decrease in the cell body. However, no difference in GAP43 protein levels was detected in whole brain and spinal cord lysates by western blotting (Figure 2E). These data suggest that SMN is important for the axonal localization of *Gap43* mRNA and protein.

Overexpression of IMP1 and HuD rescues GAP43 axonal deficiency.

Since *Gap43* mRNA stability, transport, and translation are controlled by the mRNA-binding proteins (mRBPs), HuD and IMP1 (Yoo et al., 2013), we hypothesized that enhancing the levels of these mRBPs could rescue the reduction of GAP43 levels at the growth cone. To test, we expressed GFP-tagged HuD and IMP1 in SMA motor neurons and quantified GAP43 protein (Figure 3A). We observed a significant increase in GAP43 protein at the growth cone to levels similar to wild-type cells, for both IMP1 and HuD. Additionally, the rescue in GAP43 protein levels was accompanied by an increase in the levels of *Gap43* mRNA in the growth cone (Figure 3B). We next investigated whether the rescue of GAP43 protein levels by IMP1 and HuD expression could also restore axon growth in SMA motor neurons. SMA motor neurons were transfected with either IMP1 or HuD and the length of the main axon branch was measured 2 days after transfection. SMA motor neurons had significantly shorter

axons compared to littermate control motor neurons. Expression of HuD or IMP1 was able to fully rescue the axonal defect (Figure 3C). These data suggest that overexpression of these mRBPs rescues the transport and localization of mRNA to mitigate the defects in the SMA motor neurons, indicating that the mislocalization of mRNA and reduced protein levels directly contribute to the axonal pathology.

SMN deficiency affects translation at the growth cone.

These observations led us to hypothesize that reduced axonal transcript levels may cause a compartmentalized reduction in local protein translation. To test this hypothesis, cortical neurons, which, readily grow and project axons across compartmentalized microfluidic chambers, were transfected with shRNA vectors to knock down SMN protein expression (shSMN) (Figure 4A-B) (Fallini et al., 2011). New protein synthesis in the cell body or growth cone compartment were detected using FUNCAT (fluorescent non-canonical amino acid tagging) (Tom Dieck et al., 2012). The methionine analog AHA was added to either the cell body or the axon side. Click-iT chemistry was used to fluorescently tag the incorporated AHA, and newly synthesized proteins were quantified using fluorescence high-resolution microscopy. While no effect was observed on overall protein synthesis in the cell body, a 60% reduction in the levels of AHA-labeled proteins was detected in neuronal growth cones (Figure 4C-E). Although we cannot exclude that subtle changes in the translational levels

in the cell body are below the threshold level of detection due to the abundance of newly synthesized proteins, these data do not suggest any significant global change in protein synthesis, but rather more spatially restricted local changes distally. These data demonstrate that SMN deficiency leads to defective mRNA localization and consequent impairment in local protein synthesis in the distal axon, thus possibly contributing to the axonal phenotype in SMA.

Materials and Methods

Motor Neuron Culture and Transfection.

Primary motor neurons from wild type and SMA (*Smn*^{-/-}; *hSMN2*; Stock number: 005024, Jackson Laboratories) E13.5 mouse embryos of either sex were isolated, cultured, and transfected by magnetofection as previously described (Fallini et al., 2010; Fallini et al., 2011). Cells were fixed at 3-5 DIV or 2-3 days after transfection as indicated, and processed for Q-FISH or immunostaining. Monomeric green (GFP) or red (mCherry) fluorescent proteins were fused to murine SMN (Fallini et al., 2010), human HuD (Fallini et al., 2011), and rat IMP1 (Fallini et al., 2014) cDNAs. A flexible linker [(SGGG)3] was inserted between all the fusion partners to facilitate correct protein folding. The pGIPZ shRNA vectors targeting SMN sequence (shSMN) and a non-silencing control (shCtrl, RHS4346) were obtained from Open Biosystems (Fallini et al., 2011). For axon length analysis, cells were transfected with GFP alone to label the whole axon and identify individual cells.

Fluorescence in situ Hybridization and Immunofluorescence.

Motor neurons were fixed for 15 minutes with 4% paraformaldehyde in PBS. Fluorescence in situ hybridization (FISH) was performed as described previously (Fallini et al., 2011) with some modifications. Briefly, fixed motor neurons were rinsed in PBS containing 5 mM MgCl₂ and equilibrated in 1x SSC buffer for 10'. Cells were then washed in 10%

formamide (Sigma) for 10' before preincubation in hybridization buffer (20% dextran sulfate, 4× SSC, 4 mg/ml BSA, 20 mM ribonucleoside vanadyl complex, and 10 mM sodium phosphate buffer, pH 7.0) at 37°C for 1.5 h. Probes (1µl) were resuspended with 10 µg each of E. coli tRNA and salmon sperm DNA in 50 µl hybridization buffer and incubated with the coverslips at 37°C overnight. Stellaris FISH probes for *Gap43* and β -*actin* directly labeled with Quasar570 and Quasar670 respectively were obtained from Biosearch Technologies. A cy3-labeled oligo dT probe (Biosearch Technologies) was used to detect poly(A)-positive mRNAs. The specificity of the probes was demonstrated using a GFP control probe (Figure 4C). For immunofluorescence assays, fixed motor neurons were incubated overnight at 4°C with GAP43 (Epitomics, 1:250) and SMN (BD Biosciences, 1:500) antibodies in blocking buffer (5% BSA, 1xPBS). Cy3-, Cy2- or Cy5-conjugated secondary antibodies (Jackson Immunoresearch) were incubated for 1 hour at room temperature.

Image Acquisition and Analysis.

For high resolution imaging, a 60x objective (1.4 NA) was used. Z-series (5 to 10 sections, 0.2 µm thickness) were acquired with an epifluorescence microscope (Ti, Nikon) equipped with a cooled CCD camera (HQ2, Photometrics). For low magnification imaging, a 10x or 20x phase objective was used and single optical slices were acquired. Z-stacks were deconvolved (AutoquantX2, Media Cybernetics) and analyzed

using the Imaris software (Bitplane). For the analysis of fluorescence intensity, a 70-80 μm segment of the axon starting at 20 μm distance from the cell body were analyzed. Background fluorescence was subtracted in all channels, and an additional threshold was applied to discriminate between signal and noise. Axon length measurements were performed as described (Fallini et al., 2012a).

Protein Extraction and Western Blot.

Brain and spinal cord tissue isolated from E12 mouse embryos of either sex was homogenized in lysis buffer (50 mM Tris-HCl, 150 mM NaCl, 2% Triton X-100, protease inhibitors) and sonicated on ice 3x10". Proteins were separated on a 10% polyacrylamide-SDS gel and hybridized with primary antibodies directed against SMN (BD Bioscience, 1:500), GAP43 (Epitomics, 1:500), actin (Sigma, 1:1000), and tubulin (Sigma, 1:1000). IRDye-conjugated secondary antibodies (LI-COR) were used for detection. The intensity of the protein bands was quantified using ImageJ.

L-Azidohomoalanine (AHA) labeling.

Primary E18 cortical neurons were transfected via nucleofection (Lonza) with either shCtrl or shSMN plasmids and plated in PDMS microfluidic chambers (Xona) plated on poly-D lysine coated coverglass. Cells were grown until axons crossed into the axonal chamber (DIV4), and methionine free DMEM (Invitrogen) supplemented with B-27 was then

added to both the axonal and cell body compartments for 1 hour. Following methionine starvation, 2mM L-Azidohomoalanine (AHA) was added to only the cell body or axonal compartment, to locally spatially restrict AHA labeling to individual compartments, with or without 40 μ M anisomycin to inhibit protein synthesis. Media volume was higher in compartments without AHA added, to prevent diffusion of AHA from the compartment added. Cells were washed and fixed after 2 hours, and AHA incorporation was detected with Alexa647-conjugated alkyne using Click-iT chemistry (Invitrogen) according to the manufacturer's recommendation.

Statistical analysis

Experimental data were analyzed for statistical significance using the Prism 6 (GraphPad) software. Individual values were normalized to the mean of the control sample (e.g. wild type cells) and measurements from at least three individual experiments were pooled together. For normally distributed data, Student's t test or one-way ANOVA with Dunnet's post *hoc* test were used. For axon length analysis, axon measurements from each individual experiment were normalized to the mean of the control sample (i.e. wild type cells), and values from 4 separate experiments were pooled together. The distribution of the data across the whole population was analyzed using cumulative frequency plots that display the frequency of occurrence (*Y axis*) of axonal length values (*X axis*) that are equal or

less than a reference value. The Kolmogorov-Smirnov test was used to determine if the distributions from the different conditions were significantly different from the control population (i.e. wild type). For all analyses, significance was defined as $p < 0.05$.

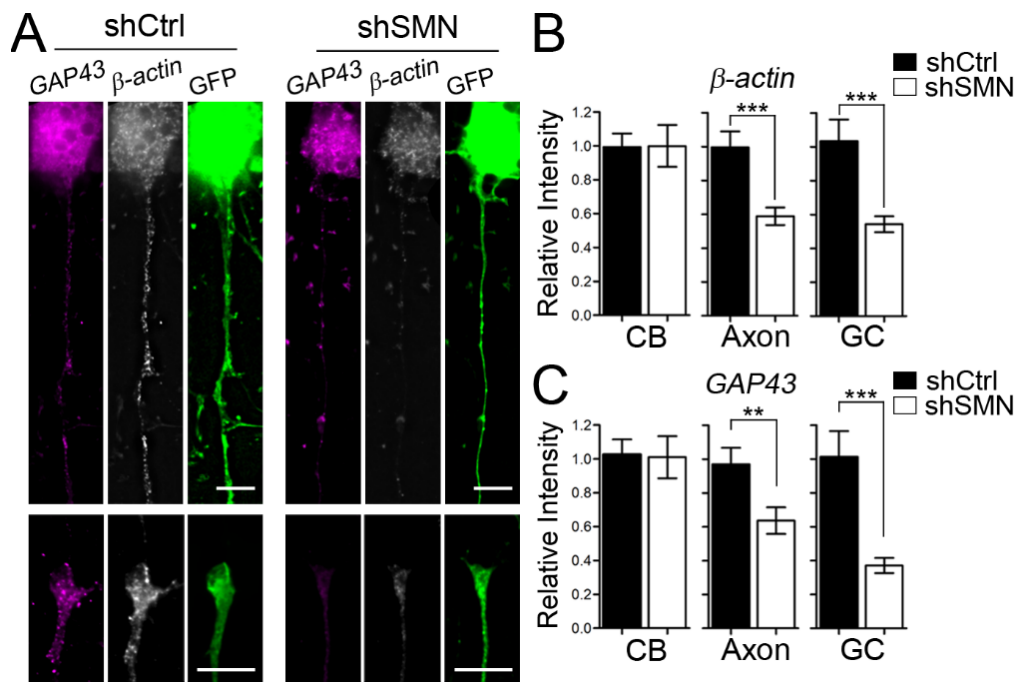


Figure 1. *GAP43* and *β-actin* mRNAs are reduced in axons and growth cones of SMN deficient motor neurons.

A. Primary motor neurons were transfected with an shRNA construct directed against SMN (shSMN) or a control vector (shCtrl). Five days after transfection, cells were fixed and hybridized with probes specific for *GAP43* (magenta) and *β-actin* (white) mRNA. GFP (green) identifies transfected cells.

B-C. Fluorescence intensity was quantified in the cell body, axon, and growth cone and compared between shSMN and shCtrl cells. A significant reduction in both *GAP43* (C) and *β-actin* (B) mRNA levels was observed in the axon and growth cone. Bars are mean and SEM (Student's t test; n=30 from three independent experiments; ** $p < 0.01$, *** $p < 0.001$). Scale bar: 10 μ m.

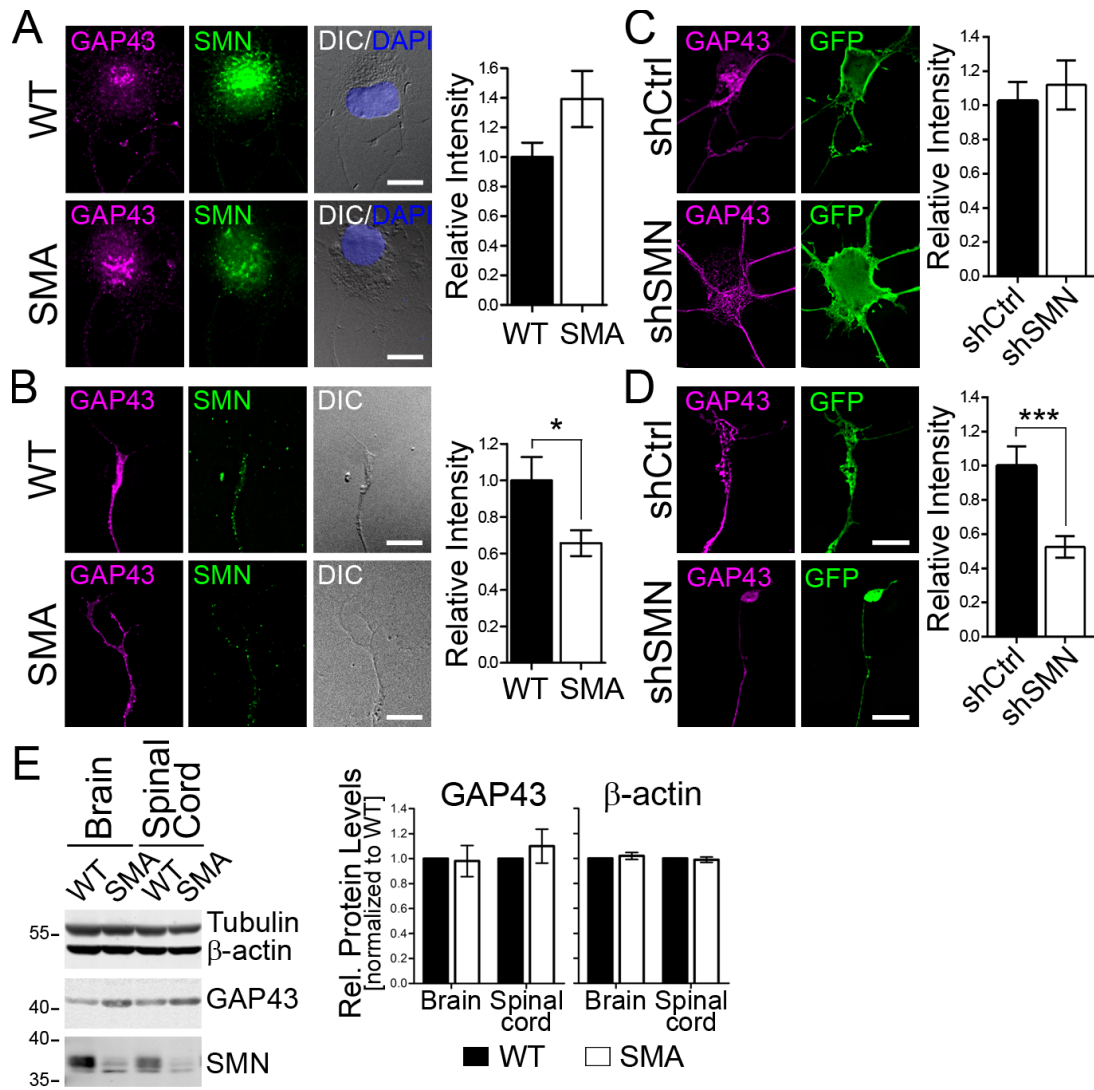


Figure 2. GAP43 protein is reduced in axonal growth cones of SMA MNs.

A-B. Immunostaining and quantification of GAP43 levels (magenta) in the cell body (A) and growth cone (B) of SMA and WT MNs. Bars are mean and SEM (Student's t test; n=43; * $p < 0.05$). C-D. Immunostaining and quantification of GAP43 protein levels (magenta) in the cell body (C) and growth cone (D) of MNs transfected with shRNA constructs. GFP (green) was used to identify transfected cells. Bars are mean and SEM (Student's t test; n=40 from three independent experiments; *** $p < 0.001$). E. Western blot analysis of GAP43 and β -actin protein levels in SMA tissue. SMN and Tubulin were used as controls. Bars are mean and SEM (n=4).

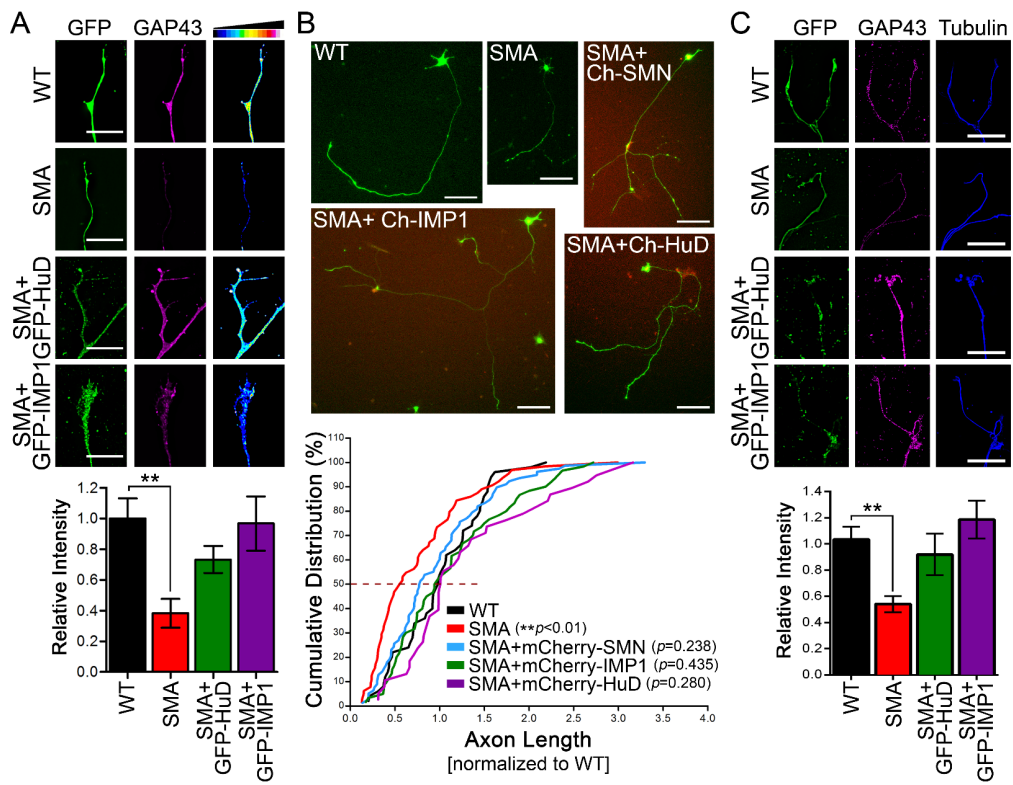


Figure 3. Overexpression of HuD and IMP1 restores GAP43 levels and axon length of SMA MNs.

A. Immunostaining and quantification of GAP43 levels (magenta) in WT and SMA MNs with or without the expression of GFP-tagged HuD and IMP1 (green). Bars are mean and SEM (one-way ANOVA and Dunnett's post hoc test; n=30 from three independent experiments; ** $p < 0.01$). Scale bars: 10 μ m

B. Representative images and cumulative distribution analysis of axonal length of WT and SMA MNs with or without the expression of mCherry-tagged SMN, HuD, and IMP1. The Y axis represent the frequency of the occurrence of axonal length values equal or less than a reference value. For statistical analysis the Komogorov-Smirnov test was used (n=38-70 from three independent experiments). Scale bars: 50 μ m.

C. Fluorescence *in situ* hybridization and quantification of *GAP43* mRNA levels (magenta) in WT and SMA MNs with or without the expression of GFP-tagged HuD and IMP1 (green). Tubulin (blue) was used to label the axons and growth cones. Bars are mean and SEM (one-way ANOVA and Dunnett's post hoc test; n=46-48 from three independent experiments; * $p < 0.05$). Scale bars: 10 μ m

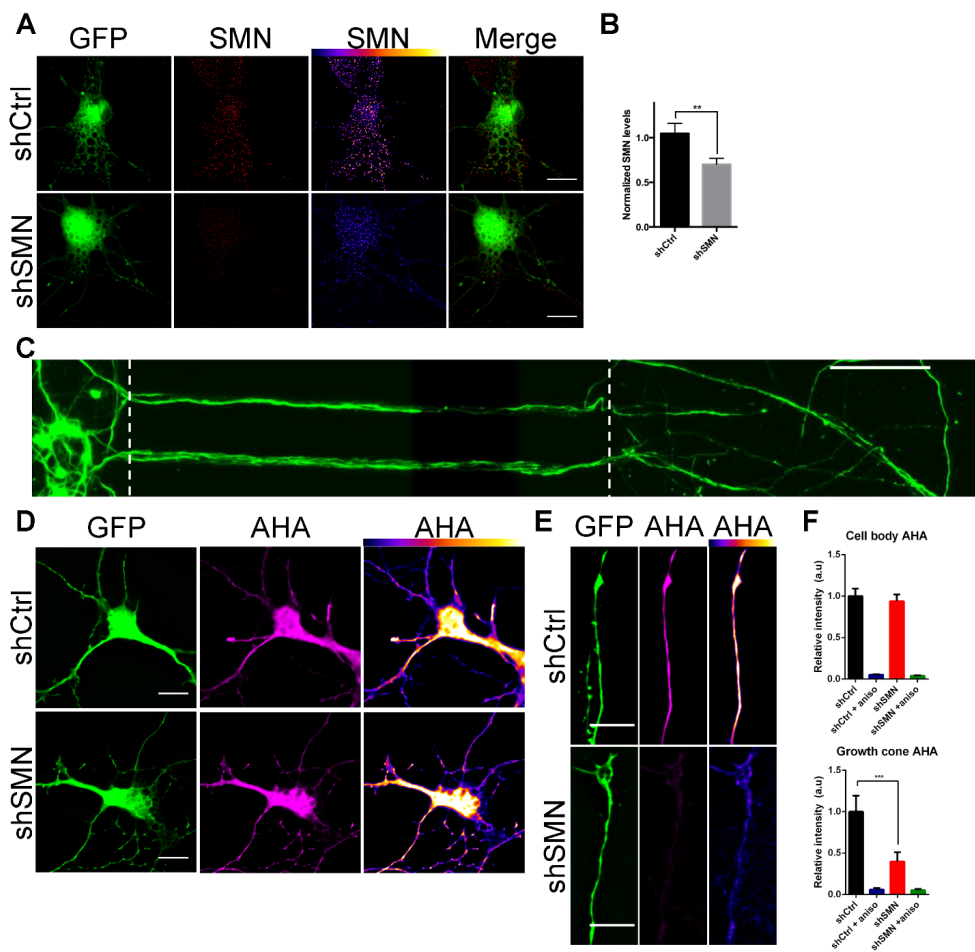


Figure 4. SMN-deficiency causes reduced local protein synthesis in axonal growth cones.

A-B. SMN knock down efficiency (red) was quantified in cortical neurons transfected with a shRNA directed against SMN (shSMN) versus control cells (shCtrl). GFP (green) was used to identify transfected cells. Bars are mean and SEM (Student's t test, $n \geq 30$ cells/condition from three independent experiments, $**p < .001$). C. Cortical neurons grown in microfluidic chambers stained for tubulin, scale bar: $100\mu\text{m}$. D-E. SMN depletion leads to decreased incorporation of AHA in growth cones of cortical neurons with no change in the cell body.

F. Quantification of AHA staining in the cell body and growth cone from shCtrl and shSMN neurons. Bars are mean and SEM (one way ANOVA with Dunnet's post *hoc* test, $n \geq 30$ cells/condition from three independent experiments, $***p < .001$).

References:

Agulhon, C., Charnay, Y., Vallet, P., Abitbol, M., Kobetz, A., Bertrand, D., and Malafosse, A. (1998). Distribution of mRNA for the alpha4 subunit of the nicotinic acetylcholine receptor in the human fetal brain. *Brain Res Mol Brain Res* 58, 123-131.

Akten, B., Kye, M.J., Hao le, T., Wertz, M.H., Singh, S., Nie, D., Huang, J., Merienda, T.T., Twiss, J.L., Beattie, C.E., *et al.* (2011). Interaction of survival of motor neuron (SMN) and HuD proteins with mRNA cpg15 rescues motor neuron axonal deficits. *Proc Natl Acad Sci U S A* 108, 10337-10342.

Alami, N.H., Smith, R.B., Carrasco, M.A., Williams, L.A., Winborn, C.S., Han, S.S., Kiskinis, E., Winborn, B., Freibaum, B.D., Kanagaraj, A., *et al.* (2014). Axonal transport of TDP-43 mRNA granules is impaired by ALS-causing mutations. *Neuron* 81, 536-543.

Alvarez, J., Giuditta, A., and Koenig, E. (2000). Protein synthesis in axons and terminals: significance for maintenance, plasticity and regulation of phenotype. With a critique of slow transport theory. *Prog Neurobiol* 62, 1-62.

Atlas, R., Behar, L., Sapoznik, S., and Ginzburg, I. (2007). Dynamic association with polysomes during P19 neuronal differentiation and an untranslated-region-dependent translation regulation of the tau mRNA by the tau mRNA-associated proteins IMP1, HuD, and G3BP1. *J Neurosci Res* 85, 173-183.

Autilio, L.A., Appel, S.H., Pettis, P., and Gambetti, P.L. (1968). Biochemical studies of synapses in vitro. I. Protein synthesis. *Biochemistry* 7, 2615-2622.

Avila, A.M., Burnett, B.G., Taye, A.A., Gabanella, F., Knight, M.A., Hartenstein, P., Cizman, Z., Di Prospero, N.A., Pellizzoni, L., Fischbeck, K.H., and Sumner, C.J. (2007). Trichostatin A increases SMN expression and survival in a mouse model of spinal muscular atrophy. *J Clin Invest* 117, 659-671.

Azzouz, T.N., Pillai, R.S., Dapp, C., Chari, A., Meister, G., Kambach, C., Fischer, U., and Schumperli, D. (2005). Toward an assembly line for U7 snRNPs: interactions of U7-specific Lsm proteins with PRMT5 and SMN complexes. *J Biol Chem* 280, 34435-34440.

Baleriola, J., and Hengst, U. (2015). Targeting axonal protein synthesis in neuroregeneration and degeneration. *Neurotherapeutics* 12, 57-65.

Baleriola, J., Walker, C.A., Jean, Y.Y., Crary, J.F., Troy, C.M., Nagy, P.L., and Hengst, U. (2014). Axonally synthesized ATF4 transmits a neurodegenerative signal across brain regions. *Cell* 158, 1159-1172.

Bassell, G.J., and Warren, S.T. (2008). Fragile X syndrome: loss of local mRNA regulation alters synaptic development and function. *Neuron* 60, 201-214.

Bassell, G.J., Zhang, H., Byrd, A.L., Femino, A.M., Singer, R.H., Taneja, K.L., Lifshitz, L.M., Herman, I.M., and Kosik, K.S. (1998). Sorting of beta-actin mRNA and protein to neurites and growth cones in culture. *J Neurosci* 18, 251-265.

Battle, D.J., Kasim, M., Yong, J., Lotti, F., Lau, C.K., Mouaikel, J., Zhang, Z., Han, K., Wan, L., and Dreyfuss, G. (2006). The SMN complex: an assembly machine for RNPs. *Cold Spring Harb Symp Quant Biol* 71, 313-320.

Baumer, D., Lee, S., Nicholson, G., Davies, J.L., Parkinson, N.J., Murray, L.M., Gillingwater, T.H., Ansorge, O., Davies, K.E., and Talbot, K. (2009). Alternative splicing events are a late feature of pathology in a mouse model of spinal muscular atrophy. *PLoS genetics* 5, e1000773.

Bechade, C., Rostaing, P., Cisterni, C., Kalisch, R., La Bella, V., Pettmann, B., and Triller, A. (1999). Subcellular distribution of survival motor neuron (SMN) protein: possible involvement in nucleocytoplasmic and dendritic transport. *Eur J Neurosci* 11, 293-304.

Bertrand, E., Chartrand, P., Schaefer, M., Shenoy, S.M., Singer, R.H., and Long, R.M. (1998). Localization of ASH1 mRNA particles in living yeast. *Mol Cell* 2, 437-445.

Bill, B.R., Lowe, J.K., Dybuncio, C.T., and Fogel, B.L. (2013). Orchestration of neurodevelopmental programs by RBFOX1: implications for autism spectrum disorder. *Int Rev Neurobiol* 113, 251-267.

Bolduc, F.V., Bell, K., Cox, H., Broadie, K.S., and Tully, T. (2008). Excess protein synthesis in *Drosophila* fragile X mutants impairs long-term memory. *Nat Neurosci* 11, 1143-1145.

Boulisfane, N., Choleza, M., Rage, F., Neel, H., Soret, J., and Bordonne, R. (2011). Impaired minor tri-snRNP assembly generates differential splicing defects of U12-type introns in lymphoblasts derived from a type I SMA patient. *Hum Mol Genet* 20, 641-648.

Bowerman, M., Murray, L.M., Beauvais, A., Pinheiro, B., and Kothary, R. (2012). A critical smn threshold in mice dictates onset of an intermediate spinal muscular atrophy phenotype associated with a distinct neuromuscular junction pathology. *Neuromuscular disorders : NMD* 22, 263-276.

Brahms, H., Meheus, L., de Brabandere, V., Fischer, U., and Luhrmann, R. (2001). Symmetrical dimethylation of arginine residues in spliceosomal Sm protein B/B' and the Sm-like protein LSm4, and their interaction with the SMN protein. *Rna* 7, 1531-1542.

Bramham, C.R., and Wells, D.G. (2007). Dendritic mRNA: transport, translation and function. *Nat Rev Neurosci* 8, 776-789.

Briese, M., Esmaili, B., and Sattelle, D.B. (2005). Is spinal muscular atrophy the result of defects in motor neuron processes? *Bioessays* 27, 946-957.

Browder, L.W., Wilkes, J., and Rodenhiser, D.I. (1992). Preparative labeling of proteins with [35S]methionine. *Anal Biochem* 204, 85-89.

Buhler, D., Raker, V., Luhrmann, R., and Fischer, U. (1999). Essential role for the tudor domain of SMN in spliceosomal U snRNP assembly: implications for spinal muscular atrophy. *Hum Mol Genet* 8, 2351-2357.

Burghes, A.H., and Beattie, C.E. (2009). Spinal muscular atrophy: why do low levels of survival motor neuron protein make motor neurons sick? *Nat Rev Neurosci* 10, 597-609.

Buxbaum, A.R., Haimovich, G., and Singer, R.H. (2015). In the right place at the right time: visualizing and understanding mRNA localization. *Nat Rev Mol Cell Biol* 16, 95-109.

Buxbaum, A.R., Wu, B., and Singer, R.H. (2014). Single beta-actin mRNA detection in neurons reveals a mechanism for regulating its translatability. *Science* 343, 419-422.

Caillet-Boudin, M.L., Fernandez-Gomez, F.J., Tran, H., Dhaenens, C.M., Buee, L., and Sergeant, N. (2014). Brain pathology in myotonic dystrophy: when tauopathy meets spliceopathy and RNAopathy. *Front Mol Neurosci* 6, 57.

Cajigas, I.J., Tushev, G., Will, T.J., tom Dieck, S., Fuerst, N., and Schuman, E.M. (2012). The local transcriptome in the synaptic neuropil revealed by deep sequencing and high-resolution imaging. *Neuron* 74, 453-466.

Carrel, T.L., McWhorter, M.L., Workman, E., Zhang, H., Wolstencroft, E.C., Lorson, C., Bassell, G.J., Burghes, A.H., and Beattie, C.E. (2006). Survival motor neuron function in motor axons is independent of functions required for small nuclear ribonucleoprotein biogenesis. *J Neurosci* 26, 11014-11022.

Castello, A., Fischer, B., Frese, C.K., Horos, R., Alleaume, A.M., Foehr, S., Curk, T., Krijgsveld, J., and Hentze, M.W. (2016a). Comprehensive Identification of RNA-Binding Domains in Human Cells. *Mol Cell* 63, 696-710.

Castello, A., Hentze, M.W., and Preiss, T. (2015). Metabolic Enzymes Enjoying New Partnerships as RNA-Binding Proteins. *Trends Endocrinol Metab* 26, 746-757.

Castello, A., Horos, R., Strein, C., Fischer, B., Eichelbaum, K., Steinmetz, L.M., Krijgsveld, J., and Hentze, M.W. (2013). System-wide identification of RNA-binding proteins by interactome capture. *Nat Protoc* 8, 491-500.

Castello, A., Horos, R., Strein, C., Fischer, B., Eichelbaum, K., Steinmetz, L.M., Krijgsveld, J., and Hentze, M.W. (2016b). Comprehensive Identification of RNA-Binding Proteins by RNA Interactome Capture. *Methods Mol Biol* 1358, 131-139.

Chao, J.A., Patskovsky, Y., Patel, V., Levy, M., Almo, S.C., and Singer, R.H. (2010). ZBP1 recognition of beta-actin zipcode induces RNA looping. *Genes Dev* 24, 148-158.

Chartron, J.W., Hunt, K.C., and Frydman, J. (2016). Cotranslational signal-independent SRP preloading during membrane targeting. *Nature* 536, 224-228.

Chen, A.K., Rhee, W.J., Bao, G., and Tsourkas, A. (2011). Delivery of molecular beacons for live-cell imaging and analysis of RNA. *Methods Mol Biol* 714, 159-174.

Chen, E., Sharma, M.R., Shi, X., Agrawal, R.K., and Joseph, S. (2014). Fragile X mental retardation protein regulates translation by binding directly to the ribosome. *Mol Cell* 54, 407-417.

Chen, F., Wassie, A.T., Cote, A.J., Sinha, A., Alon, S., Asano, S., Daugharthy, E.R., Chang, J.B., Marblestone, A., Church, G.M., *et al.* (2016). Nanoscale imaging of RNA with expansion microscopy. *Nat Methods* 13, 679-684.

Chen, K.H., Boettiger, A.N., Moffitt, J.R., Wang, S., and Zhuang, X. (2015). RNA imaging. Spatially resolved, highly multiplexed RNA profiling in single cells. *Science* 348, aaa6090.

Cifuentes-Diaz, C., Nicole, S., Velasco, M.E., Borra-Cebrian, C., Panozzo, C., Frugier, T., Millet, G., Roblot, N., Joshi, V., and Melki, J. (2002). Neurofilament accumulation at the motor endplate and lack of axonal sprouting in a spinal muscular atrophy mouse model. *Hum Mol Genet* 11, 1439-1447.

Coyne, A.N., Yamada, S.B., Siddegowda, B.B., Estes, P.S., Zaepfel, B.L., Johannesmeyer, J.S., Lockwood, D.B., Pham, L.T., Hart, M.P., Cassel, J.A., *et al.* (2015). Fragile X protein mitigates TDP-43 toxicity by remodeling RNA granules and restoring translation. *Hum Mol Genet* 24, 6886-6898.

Custer, S.K., Gilson, T.D., Li, H., Todd, A.G., Astroski, J.W., Lin, H., Liu, Y., and Androphy, E.J. (2016). Altered mRNA Splicing in SMN-Depleted Motor Neuron-Like Cells. *PloS one* 11, e0163954.

Darnell, J.C., and Klann, E. (2013). The translation of translational control by FMRP: therapeutic targets for FXS. *Nat Neurosci* 16, 1530-1536.

Darnell, J.C., Van Driesche, S.J., Zhang, C., Hung, K.Y., Mele, A., Fraser, C.E., Stone, E.F., Chen, C., Fak, J.J., Chi, S.W., *et al.* (2011). FMRP stalls ribosomal translocation on mRNAs linked to synaptic function and autism. *Cell* 146, 247-261.

Darnell, R.B. (2010). HITS-CLIP: panoramic views of protein-RNA regulation in living cells. *Wiley Interdiscip Rev RNA* 1, 266-286.

David, A., Dolan, B.P., Hickman, H.D., Knowlton, J.J., Clavarino, G., Pierre, P., Bennink, J.R., and Yewdell, J.W. (2012). Nuclear translation visualized by ribosome-bound nascent chain puromycylation. *J Cell Biol* 197, 45-57.

Dayangac-Erden, D., Bora, G., Ayhan, P., Kocaefe, C., Dalkara, S., Yelekci, K., Demir, A.S., and Erdem-Yurter, H. (2009). Histone deacetylase inhibition activity and molecular docking of (e)-resveratrol: its therapeutic potential in spinal muscular atrophy. *Chem Biol Drug Des* 73, 355-364.

De Gendt, K., Verhoeven, G., Amieux, P.S., and Wilkinson, M.F. (2014). Genome-wide identification of AR-regulated genes translated in Sertoli cells in vivo using the RiboTag approach. *Mol Endocrinol* 28, 575-591.

- De Rubeis, S., He, X., Goldberg, A.P., Poultney, C.S., Samocha, K., Cicek, A.E., Kou, Y., Liu, L., Fromer, M., Walker, S., *et al.* (2014). Synaptic, transcriptional and chromatin genes disrupted in autism. *Nature* 515, 209-215.
- Deshler, J.O., Highett, M.I., Abramson, T., and Schnapp, B.J. (1998). A highly conserved RNA-binding protein for cytoplasmic mRNA localization in vertebrates. *Curr Biol* 8, 489-496.
- Dieterich, D.C., Hodas, J.J., Gouzer, G., Shadrin, I.Y., Ngo, J.T., Triller, A., Tirrell, D.A., and Schuman, E.M. (2010). In situ visualization and dynamics of newly synthesized proteins in rat hippocampal neurons. *Nat Neurosci* 13, 897-905.
- Doktor, T.K., Hua, Y., Andersen, H.S., Broner, S., Liu, Y.H., Wieckowska, A., Dembic, M., Bruun, G.H., Krainer, A.R., and Andresen, B.S. (2016). RNA-sequencing of a mouse-model of spinal muscular atrophy reveals tissue-wide changes in splicing of U12-dependent introns. *Nucleic Acids Res.*
- Dombert, B., Sivadasan, R., Simon, C.M., Jablonka, S., and Sendtner, M. (2014). Presynaptic localization of Smn and hnRNP R in axon terminals of embryonic and postnatal mouse motoneurons. *PLoS one* 9, e110846.
- Donlin-Asp, P.G., Bassell, G.J., and Rossoll, W. (2016). A role for the survival of motor neuron protein in mRNP assembly and transport. *Curr Opin Neurobiol* 39, 53-61.
- Donnelly, C.J., Park, M., Spillane, M., Yoo, S., Pacheco, A., Gomes, C., Vuppalachchi, D., McDonald, M., Kim, H.H., Merianda, T.T., *et al.* (2013). Axonally synthesized beta-actin and GAP-43 proteins support distinct modes of axonal growth. *J Neurosci* 33, 3311-3322.
- Donnelly, C.J., Willis, D.E., Xu, M., Tep, C., Jiang, C., Yoo, S., Schanen, N.C., Kirn-Safran, C.B., van Minnen, J., English, A., *et al.* (2011). Limited availability of ZBP1 restricts axonal mRNA localization and nerve regeneration capacity. *The EMBO journal* 30, 4665-4677.
- Doron-Mandel, E., Fainzilber, M., and Terenzio, M. (2015). Growth control mechanisms in neuronal regeneration. *FEBS Lett* 589, 1669-1677.
- Doyle, J.P., Dougherty, J.D., Heiman, M., Schmidt, E.F., Stevens, T.R., Ma, G., Bupp, S., Shrestha, P., Shah, R.D., Doughty, M.L., *et al.* (2008). Application of a translational profiling approach for the comparative analysis of CNS cell types. *Cell* 135, 749-762.

Ebert, A.D., Yu, J., Rose, F.F., Jr., Mattis, V.B., Lorson, C.L., Thomson, J.A., and Svendsen, C.N. (2009). Induced pluripotent stem cells from a spinal muscular atrophy patient. *Nature* 457, 277-280.

Edstrom, A., and Sjostrand, J. (1969). Protein synthesis in the isolated Mauthner nerve fibre of goldfish. *Journal of neurochemistry* 16, 67-81.

Eirin, A., Riester, S.M., Zhu, X.Y., Tang, H., Evans, J.M., O'Brien, D., van Wijnen, A.J., and Lerman, L.O. (2014). MicroRNA and mRNA cargo of extracellular vesicles from porcine adipose tissue-derived mesenchymal stem cells. *Gene* 551, 55-64.

Elbaum-Garfinkle, S., and Brangwynne, C.P. (2015). Liquids, Fibers, and Gels: The Many Phases of Neurodegeneration. *Dev Cell* 35, 531-532.

Eliyahu, E., Pnueli, L., Melamed, D., Scherrer, T., Gerber, A.P., Pines, O., Rapaport, D., and Arava, Y. (2010). Tom20 mediates localization of mRNAs to mitochondria in a translation-dependent manner. *Mol Cell Biol* 30, 284-294.

Eom, T., Antar, L.N., Singer, R.H., and Bassell, G.J. (2003). Localization of a beta-actin messenger ribonucleoprotein complex with zipcode-binding protein modulates the density of dendritic filopodia and filopodial synapses. *J Neurosci* 23, 10433-10444.

Evans, M.C., Cherry, J.J., and Androphy, E.J. (2011). Differential regulation of the SMN2 gene by individual HDAC proteins. *Biochem Biophys Res Commun* 414, 25-30.

Fallini, C., Bassell, G.J., and Rossoll, W. (2010). High-efficiency transfection of cultured primary motor neurons to study protein localization, trafficking, and function. *Mol Neurodegener* 5, 17.

Fallini, C., Bassell, G.J., and Rossoll, W. (2012a). The ALS disease protein TDP-43 is actively transported in motor neuron axons and regulates axon outgrowth. *Hum Mol Genet* 21, 3703-3718.

Fallini, C., Bassell, G.J., and Rossoll, W. (2012b). Spinal muscular atrophy: the role of SMN in axonal mRNA regulation. *Brain research* 1462, 81-92.

Fallini, C., Donlin-Asp, P.G., Rouanet, J.P., Bassell, G.J., and Rossoll, W. (2016). Deficiency of the Survival of Motor Neuron Protein Impairs mRNA Localization and Local Translation in the Growth Cone of Motor Neurons. *J Neurosci* 36, 3811-3820.

Fallini, C., Rouanet, J.P., Donlin-Asp, P.G., Guo, P., Zhang, H., Singer, R.H., Rossoll, W., and Bassell, G.J. (2013). Dynamics of survival of motor neuron (SMN) protein interaction with the mRNA-binding protein IMP1 facilitates its trafficking into motor neuron axons. *Developmental neurobiology*.

Fallini, C., Rouanet, J.P., Donlin-Asp, P.G., Guo, P., Zhang, H., Singer, R.H., Rossoll, W., and Bassell, G.J. (2014). Dynamics of survival of motor neuron (SMN) protein interaction with the mRNA-binding protein IMP1 facilitates its trafficking into motor neuron axons. *Developmental neurobiology* 74, 319-332.

Fallini, C., Zhang, H., Su, Y., Silani, V., Singer, R.H., Rossoll, W., and Bassell, G.J. (2011). The survival of motor neuron (SMN) protein interacts with the mRNA-binding protein HuD and regulates localization of poly(A) mRNA in primary motor neuron axons. *J Neurosci* 31, 3914-3925.

Fan, L., and Simard, L.R. (2002). Survival motor neuron (SMN) protein: role in neurite outgrowth and neuromuscular maturation during neuronal differentiation and development. *Hum Mol Genet* 11, 1605-1614.

Faravelli, I., Nizzardo, M., Comi, G.P., and Corti, S. (2015). Spinal muscular atrophy--recent therapeutic advances for an old challenge. *Nat Rev Neurol* 11, 351-359.

Farina, K.L., Huttelmaier, S., Musunuru, K., Darnell, R., and Singer, R.H. (2003). Two ZBP1 KH domains facilitate beta-actin mRNA localization, granule formation, and cytoskeletal attachment. *J Cell Biol* 160, 77-87.

Femino, A.M., Fogarty, K., Lifshitz, L.M., Carrington, W., and Singer, R.H. (2003). Visualization of single molecules of mRNA in situ. *Methods Enzymol* 361, 245-304.

Francesca, G., Cinzia, P., Antonella, B., Stefano, F.V., Teresa, C.M., Tiziano, I., Annalisa, O., Martine, A.T., Nicoletta, C., Nadia, C., *et al.* (2016). SMN affects membrane remodelling and anchoring of the protein synthesis machinery. *Journal of cell science*.

Freibaum, B.D., Chitta, R.K., High, A.A., and Taylor, J.P. (2010). Global analysis of TDP-43 interacting proteins reveals strong association with RNA splicing and translation machinery. *J Proteome Res* 9, 1104-1120.

- Friesen, W.J., and Dreyfuss, G. (2000). Specific sequences of the Sm and Sm-like (Lsm) proteins mediate their interaction with the spinal muscular atrophy disease gene product (SMN). *J Biol Chem* 275, 26370-26375.
- Friesen, W.J., Massenet, S., Paushkin, S., Wyce, A., and Dreyfuss, G. (2001). SMN, the product of the spinal muscular atrophy gene, binds preferentially to dimethylarginine-containing protein targets. *Mol Cell* 7, 1111-1117.
- Fritzsche, R., Karra, D., Bennett, K.L., Ang, F.Y., Heraud-Farlow, J.E., Tolino, M., Doyle, M., Bauer, K.E., Thomas, S., Panyavsky, M., *et al.* (2013). Interactome of two diverse RNA granules links mRNA localization to translational repression in neurons. *Cell Rep* 5, 1749-1762.
- Gabanella, F., Butchbach, M.E., Saieva, L., Carissimi, C., Burghes, A.H., and Pellizzoni, L. (2007). Ribonucleoprotein assembly defects correlate with spinal muscular atrophy severity and preferentially affect a subset of spliceosomal snRNPs. *PloS one* 2, e921.
- Garcia, E.L., Wen, Y., Praveen, K., and Matera, A.G. (2016). Transcriptomic comparison of *Drosophila* snRNP biogenesis mutants reveals mutant-specific changes in pre-mRNA processing: implications for spinal muscular atrophy. *Rna* 22, 1215-1227.
- Garcia, J.F., and Parker, R. (2016). Ubiquitous accumulation of 3' mRNA decay fragments in *Saccharomyces cerevisiae* mRNAs with chromosomally integrated MS2 arrays. *Rna* 22, 657-659.
- Gaynes, J.A., Otsuna, H., Campbell, D.S., Manfredi, J.P., Levine, E.M., and Chien, C.B. (2015). The RNA Binding Protein Igf2bp1 Is Required for Zebrafish RGC Axon Outgrowth In Vivo. *PloS one* 10, e0134751.
- Gkogkas, C.G., Khoutorsky, A., Ran, I., Rampakakis, E., Nevarko, T., Weatherill, D.B., Vasuta, C., Yee, S., Truitt, M., Dallaire, P., *et al.* (2013). Autism-related deficits via dysregulated eIF4E-dependent translational control. *Nature* 493, 371-377.
- Goetz, S.C., and Anderson, K.V. (2010). The primary cilium: a signalling centre during vertebrate development. *Nat Rev Genet* 11, 331-344.
- Gogliotti, R.G., Cardona, H., Singh, J., Bail, S., Emery, C., Kuntz, N., Jorgensen, M., Durens, M., Xia, B., Barlow, C., *et al.* (2013). The DcpS inhibitor RG3039 improves survival, function and motor unit pathologies in two SMA mouse models. *Hum Mol Genet* 22, 4084-4101.

Gogliotti, R.G., Quinlan, K.A., Barlow, C.B., Heier, C.R., Heckman, C.J., and Didonato, C.J. (2012). Motor neuron rescue in spinal muscular atrophy mice demonstrates that sensory-motor defects are a consequence, not a cause, of motor neuron dysfunction. *J Neurosci* 32, 3818-3829.

Gonsalvez, G.B., Rajendra, T.K., Wen, Y., Praveen, K., and Matera, A.G. (2010). Sm proteins specify germ cell fate by facilitating oskar mRNA localization. *Development* 137, 2341-2351.

Goulet, B.B., Kothary, R., and Parks, R.J. (2013). At the "junction" of spinal muscular atrophy pathogenesis: the role of neuromuscular junction dysfunction in SMA disease progression. *Current molecular medicine* 13, 1160-1174.

Graber, T.E., Hebert-Seropian, S., Khoutorsky, A., David, A., Yewdell, J.W., Lacaille, J.C., and Sossin, W.S. (2013). Reactivation of stalled polyribosomes in synaptic plasticity. *Proc Natl Acad Sci U S A* 110, 16205-16210.

Grimmler, M., Otter, S., Peter, C., Muller, F., Chari, A., and Fischer, U. (2005). Unrip, a factor implicated in cap-independent translation, associates with the cytosolic SMN complex and influences its intracellular localization. *Hum Mol Genet* 14, 3099-3111.

Groen, E.J., Fumoto, K., Blokhuis, A.M., Engelen-Lee, J., Zhou, Y., van den Heuvel, D.M., Koppers, M., van Diggelen, F., van Heest, J., Demmers, J.A., *et al.* (2013). ALS-associated mutations in FUS disrupt the axonal distribution and function of SMN. *Hum Mol Genet* 22, 3690-3704.

Gross, C., Nakamoto, M., Yao, X., Chan, C.B., Yim, S.Y., Ye, K., Warren, S.T., and Bassell, G.J. (2010). Excess phosphoinositide 3-kinase subunit synthesis and activity as a novel therapeutic target in fragile X syndrome. *J Neurosci* 30, 10624-10638.

Gross, C., Yao, X., Pong, D.L., Jeromin, A., and Bassell, G.J. (2011). Fragile X mental retardation protein regulates protein expression and mRNA translation of the potassium channel Kv4.2. *J Neurosci* 31, 5693-5698.

Gu, W., Katz, Z., Wu, B., Park, H.Y., Li, D., Lin, S., Wells, A.L., and Singer, R.H. (2012). Regulation of local expression of cell adhesion and motility-related mRNAs in breast cancer cells by IMP1/ZBP1. *Journal of cell science* 125, 81-91.

- Gubitz, A.K., Feng, W., and Dreyfuss, G. (2004). The SMN complex. *Exp Cell Res* 296, 51-56.
- Guo, W., Chen, Y., Zhou, X., Kar, A., Ray, P., Chen, X., Rao, E.J., Yang, M., Ye, H., Zhu, L., *et al.* (2011). An ALS-associated mutation affecting TDP-43 enhances protein aggregation, fibril formation and neurotoxicity. *Nat Struct Mol Biol* 18, 822-830.
- Gupta, K., Martin, R., Sharp, R., Sarachan, K.L., Ninan, N.S., and Van Duyne, G.D. (2015). Oligomeric Properties of Survival Motor Neuron Gemin2 Complexes. *J Biol Chem* 290, 20185-20199.
- Gustafsson, M.G. (2000). Surpassing the lateral resolution limit by a factor of two using structured illumination microscopy. *J Microsc* 198, 82-87.
- Gustafsson, M.G., Shao, L., Carlton, P.M., Wang, C.J., Golubovskaya, I.N., Cande, W.Z., Agard, D.A., and Sedat, J.W. (2008). Three-dimensional resolution doubling in wide-field fluorescence microscopy by structured illumination. *Biophys J* 94, 4957-4970.
- Hansen, T.V., Hammer, N.A., Nielsen, J., Madsen, M., Dalbaeck, C., Wewer, U.M., Christiansen, J., and Nielsen, F.C. (2004). Dwarfism and impaired gut development in insulin-like growth factor II mRNA-binding protein 1-deficient mice. *Mol Cell Biol* 24, 4448-4464.
- Hao le, T., Duy, P.Q., Jontes, J.D., and Beattie, C.E. (2015). Motoneuron development influences dorsal root ganglia survival and Schwann cell development in a vertebrate model of spinal muscular atrophy. *Hum Mol Genet* 24, 346-360.
- Hao le, T., Duy, P.Q., Jontes, J.D., Wolman, M., Granato, M., and Beattie, C.E. (2013). Temporal requirement for SMN in motoneuron development. *Hum Mol Genet* 22, 2612-2625.
- Hauke, J., Riessland, M., Lunke, S., Eyupoglu, I.Y., Blumcke, I., El-Osta, A., Wirth, B., and Hahnen, E. (2009). Survival motor neuron gene 2 silencing by DNA methylation correlates with spinal muscular atrophy disease severity and can be bypassed by histone deacetylase inhibition. *Hum Mol Genet* 18, 304-317.
- Heiman, M., Schaefer, A., Gong, S., Peterson, J.D., Day, M., Ramsey, K.E., Suarez-Farinas, M., Schwarz, C., Stephan, D.A., Surmeier, D.J., *et al.* (2008). A

translational profiling approach for the molecular characterization of CNS cell types. *Cell* 135, 738-748.

Hocine, S., Raymond, P., Zenklusen, D., Chao, J.A., and Singer, R.H. (2013). Single-molecule analysis of gene expression using two-color RNA labeling in live yeast. *Nat Methods* 10, 119-121.

Holt, C.E., and Schuman, E.M. (2013). The central dogma decentralized: new perspectives on RNA function and local translation in neurons. *Neuron* 80, 648-657.

Hu, C.D., Grinberg, A.V., and Kerppola, T.K. (2006). Visualization of protein interactions in living cells using bimolecular fluorescence complementation (BiFC) analysis. *Curr Protoc Cell Biol* Chapter 21, Unit 21 23.

Hua, Y., Sahashi, K., Rigo, F., Hung, G., Horev, G., Bennett, C.F., and Krainer, A.R. (2011). Peripheral SMN restoration is essential for long-term rescue of a severe spinal muscular atrophy mouse model. *Nature* 478, 123-126.

Hua, Y., and Zhou, J. (2004). Survival motor neuron protein facilitates assembly of stress granules. *FEBS Lett* 572, 69-74.

Huber, K.M., Kayser, M.S., and Bear, M.F. (2000). Role for rapid dendritic protein synthesis in hippocampal mGluR-dependent long-term depression. *Science* 288, 1254-1257.

Huber, K.M., Klann, E., Costa-Mattioli, M., and Zukin, R.S. (2015). Dysregulation of Mammalian Target of Rapamycin Signaling in Mouse Models of Autism. *J Neurosci* 35, 13836-13842.

Hubers, L., Valderrama-Carvajal, H., Laframboise, J., Timbers, J., Sanchez, G., and Cote, J. (2011). HuD interacts with survival motor neuron protein and can rescue spinal muscular atrophy-like neuronal defects. *Hum Mol Genet* 20, 553-579.

Huppertz, I., Attig, J., D'Ambrogio, A., Easton, L.E., Sibley, C.R., Sugimoto, Y., Tajnik, M., Konig, J., and Ule, J. (2014). iCLIP: protein-RNA interactions at nucleotide resolution. *Methods* 65, 274-287.

Huttelmaier, S., Zenklusen, D., Lederer, M., Dichtenberg, J., Lorenz, M., Meng, X., Bassell, G.J., Condeelis, J., and Singer, R.H. (2005). Spatial regulation of beta-actin translation by Src-dependent phosphorylation of ZBP1. *Nature* 438, 512-515.

Huynh, T.N., Shah, M., Koo, S.Y., Faraud, K.S., Santini, E., and Klann, E. (2015). eIF4E/Fmr1 double mutant mice display cognitive impairment in addition to ASD-like behaviors. *Neurobiol Dis* 83, 67-74.

Ifrim, M.F., Williams, K.R., and Bassell, G.J. (2015). Single-Molecule Imaging of PSD-95 mRNA Translation in Dendrites and Its Dysregulation in a Mouse Model of Fragile X Syndrome. *J Neurosci* 35, 7116-7130.

Imlach, W.L., Beck, E.S., Choi, B.J., Lotti, F., Pellizzoni, L., and McCabe, B.D. (2012). SMN is required for sensory-motor circuit function in *Drosophila*. *Cell* 151, 427-439.

Ishiguro, A., Kimura, N., Watanabe, Y., Watanabe, S., and Ishihama, A. (2016). TDP-43 binds and transports G-quadruplex-containing mRNAs into neurites for local translation. *Genes Cells* 21, 466-481.

Jablonka, S., Dombert, B., Asan, E., and Sendtner, M. (2014). Mechanisms for axon maintenance and plasticity in motoneurons: alterations in motoneuron disease. *Journal of anatomy* 224, 3-14.

Jakobsen, K.R., Sorensen, E., Brondum, K.K., Daugaard, T.F., Thomsen, R., and Nielsen, A.L. (2013). Direct RNA sequencing mediated identification of mRNA localized in protrusions of human MDA-MB-231 metastatic breast cancer cells. *J Mol Signal* 8, 9.

Kalinski, A.L., Sachdeva, R., Gomes, C., Lee, S.J., Shah, Z., Houle, J.D., and Twiss, J.L. (2015). mRNAs and Protein Synthetic Machinery Localize into Regenerating Spinal Cord Axons When They Are Provided a Substrate That Supports Growth. *J Neurosci* 35, 10357-10370.

Kalous, A., Stake, J.I., Yisraeli, J.K., and Holt, C.E. (2014). RNA-binding protein Vg1RBP regulates terminal arbor formation but not long-range axon navigation in the developing visual system. *Developmental neurobiology* 74, 303-318.

Kariya, S., Park, G.H., Maeno-Hikichi, Y., Leykekhman, O., Lutz, C., Arkovitz, M.S., Landmesser, L.T., and Monani, U.R. (2008). Reduced SMN protein impairs maturation of the neuromuscular junctions in mouse models of spinal muscular atrophy. *Hum Mol Genet* 17, 2552-2569.

Katz, Z.B., English, B.P., Lionnet, T., Yoon, Y.J., Monnier, N., Ovrzyn, B., Bathe, M., and Singer, R.H. (2016). Mapping translation 'hot-spots' in live cells by tracking single molecules of mRNA and ribosomes. *Elife* 5.

Katz, Z.B., Wells, A.L., Park, H.Y., Wu, B., Shenoy, S.M., and Singer, R.H. (2012). beta-Actin mRNA compartmentalization enhances focal adhesion stability and directs cell migration. *Genes Dev* 26, 1885-1890.

Keene, J.D., Komisarow, J.M., and Friedersdorf, M.B. (2006). RIP-Chip: the isolation and identification of mRNAs, microRNAs and protein components of ribonucleoprotein complexes from cell extracts. *Nat Protoc* 1, 302-307.

Keil, J.M., Seo, J., Howell, M.D., Hsu, W.H., Singh, R.N., and DiDonato, C.J. (2014). A short antisense oligonucleotide ameliorates symptoms of severe mouse models of spinal muscular atrophy. *Mol Ther Nucleic Acids* 3, e174.

Kernochan, L.E., Russo, M.L., Woodling, N.S., Huynh, T.N., Avila, A.M., Fischbeck, K.H., and Sumner, C.J. (2005). The role of histone acetylation in SMN gene expression. *Hum Mol Genet* 14, 1171-1182.

Kerppola, T.K. (2013). Bimolecular fluorescence complementation (BiFC) analysis of protein interactions in live cells. *Cold Spring Harb Protoc* 2013, 727-731.

Kim, Y.E., Hipp, M.S., Bracher, A., Hayer-Hartl, M., and Hartl, F.U. (2013). Molecular chaperone functions in protein folding and proteostasis. *Annu Rev Biochem* 82, 323-355.

Kim, Y.J., Maizel, A., and Chen, X. (2014). Traffic into silence: endomembranes and post-transcriptional RNA silencing. *The EMBO journal* 33, 968-980.

Kislauskis, E.H., Zhu, X., and Singer, R.H. (1994). Sequences responsible for intracellular localization of beta-actin messenger RNA also affect cell phenotype. *J Cell Biol* 127, 441-451.

Klann, E., and Sweatt, J.D. (2008). Altered protein synthesis is a trigger for long-term memory formation. *Neurobiol Learn Mem* 89, 247-259.

Klein, M.E., Younts, T.J., Castillo, P.E., and Jordan, B.A. (2013). RNA-binding protein Sam68 controls synapse number and local beta-actin mRNA metabolism in dendrites. *Proc Natl Acad Sci U S A* 110, 3125-3130.

Koenig, E. (1967). Synthetic mechanisms in the axon. IV. In vitro incorporation of [3H]precursors into axonal protein and RNA. *Journal of neurochemistry* 14, 437-446.

- Kong, L., Wang, X., Choe, D.W., Polley, M., Burnett, B.G., Bosch-Marce, M., Griffin, J.W., Rich, M.M., and Sumner, C.J. (2009). Impaired synaptic vesicle release and immaturity of neuromuscular junctions in spinal muscular atrophy mice. *J Neurosci* 29, 842-851.
- Konig, J., Zarnack, K., Rot, G., Curk, T., Kayikci, M., Zupan, B., Turner, D.J., Luscombe, N.M., and Ule, J. (2010). iCLIP reveals the function of hnRNP particles in splicing at individual nucleotide resolution. *Nat Struct Mol Biol* 17, 909-915.
- Konig, J., Zarnack, K., Rot, G., Curk, T., Kayikci, M., Zupan, B., Turner, D.J., Luscombe, N.M., and Ule, J. (2011). iCLIP--transcriptome-wide mapping of protein-RNA interactions with individual nucleotide resolution. *J Vis Exp*.
- Kraut-Cohen, J., Afanasieva, E., Haim-Vilmovsky, L., Slobodin, B., Yosef, I., Bibi, E., and Gerst, J.E. (2013). Translation- and SRP-independent mRNA targeting to the endoplasmic reticulum in the yeast *Saccharomyces cerevisiae*. *Mol Biol Cell* 24, 3069-3084.
- Kroiss, M., Schultz, J., Wiesner, J., Chari, A., Sickmann, A., and Fischer, U. (2008). Evolution of an RNP assembly system: a minimal SMN complex facilitates formation of UsnRNPs in *Drosophila melanogaster*. *Proc Natl Acad Sci U S A* 105, 10045-10050.
- Kugler, J.M., and Lasko, P. (2009). Localization, anchoring and translational control of oskar, gurken, bicoid and nanos mRNA during *Drosophila* oogenesis. *Fly (Austin)* 3, 15-28.
- Kwon, D.Y., Motley, W.W., Fischbeck, K.H., and Burnett, B.G. (2011). Increasing expression and decreasing degradation of SMN ameliorate the spinal muscular atrophy phenotype in mice. *Hum Mol Genet* 20, 3667-3677.
- Kye, M.J., Niederst, E.D., Wertz, M.H., Goncalves Ido, C., Akten, B., Dover, K.Z., Peters, M., Riessland, M., Neveu, P., Wirth, B., *et al.* (2014). SMN regulates axonal local translation via miR-183/mTOR pathway. *Hum Mol Genet* 23, 6318-6331.
- Lam, S.S., Martell, J.D., Kamer, K.J., Deerinck, T.J., Ellisman, M.H., Mootha, V.K., and Ting, A.Y. (2015). Directed evolution of APEX2 for electron microscopy and proximity labeling. *Nat Methods* 12, 51-54.

- Lambert, J.D., and Nagy, L.M. (2002). Asymmetric inheritance of centrosomally localized mRNAs during embryonic cleavages. *Nature* 420, 682-686.
- Lasko, P. (2012). mRNA localization and translational control in *Drosophila* oogenesis. *Cold Spring Harb Perspect Biol* 4.
- Latham, V.M., Jr., Kislauskis, E.H., Singer, R.H., and Ross, A.F. (1994). Beta-actin mRNA localization is regulated by signal transduction mechanisms. *J Cell Biol* 126, 1211-1219.
- Le Borgne, M., Chartier, N., Buchet-Poyau, K., Destaing, O., Faurobert, E., Thibert, C., Rouault, J.P., Courchet, J., Negre, D., Bouvard, D., *et al.* (2014). The RNA-binding protein Mex3b regulates the spatial organization of the Rap1 pathway. *Development* 141, 2096-2107.
- Lecuyer, E., Yoshida, H., Parthasarathy, N., Alm, C., Babak, T., Cerovina, T., Hughes, T.R., Tomancak, P., and Krause, H.M. (2007). Global analysis of mRNA localization reveals a prominent role in organizing cellular architecture and function. *Cell* 131, 174-187.
- Lee, J.A., Damianov, A., Lin, C.H., Fontes, M., Parikshak, N.N., Anderson, E.S., Geschwind, D.H., Black, D.L., and Martin, K.C. (2016). Cytoplasmic Rbfox1 Regulates the Expression of Synaptic and Autism-Related Genes. *Neuron* 89, 113-128.
- Lepelletier, L., Langlois, S.D., Kent, C.B., Welshhans, K., Morin, S., Bassell, G.J., Yam, P.T., and Charron, F. (2017). Sonic Hedgehog guides axons via Zipcode Binding Protein 1-mediated local translation. *J Neurosci*.
- Lesiak, A.J., Brodsky, M., and Neumaier, J.F. (2015). RiboTag is a flexible tool for measuring the translational state of targeted cells in heterogeneous cell cultures. *Biotechniques* 58, 308-317.
- Lesnik, C., Golani-Armon, A., and Arava, Y. (2015). Localized translation near the mitochondrial outer membrane: An update. *RNA Biol* 12, 801-809.
- Leung, K.M., and Holt, C.E. (2008). Live visualization of protein synthesis in axonal growth cones by microinjection of photoconvertible Kaede into *Xenopus* embryos. *Nat Protoc* 3, 1318-1327.

- Leung, K.M., van Horck, F.P., Lin, A.C., Allison, R., Standart, N., and Holt, C.E. (2006). Asymmetrical beta-actin mRNA translation in growth cones mediates attractive turning to netrin-1. *Nat Neurosci* 9, 1247-1256.
- Levsky, J.M., and Singer, R.H. (2003). Fluorescence in situ hybridization: past, present and future. *Journal of cell science* 116, 2833-2838.
- Li, D.K., Tisdale, S., Lotti, F., and Pellizzoni, L. (2014a). SMN control of RNP assembly: from post-transcriptional gene regulation to motor neuron disease. *Seminars in cell & developmental biology* 32, 22-29.
- Li, D.K., Tisdale, S., Lotti, F., and Pellizzoni, L. (2014b). SMN control of RNP assembly: From post-transcriptional gene regulation to motor neuron disease. *Seminars in cell & developmental biology*.
- Li, H., Custer, S.K., Gilson, T., Hao, L.T., Beattie, C.E., and Androphy, E.J. (2015). alpha-COP binding to the survival motor neuron protein SMN is required for neuronal process outgrowth. *Hum Mol Genet*.
- Li, Y.R., King, O.D., Shorter, J., and Gitler, A.D. (2013). Stress granules as crucibles of ALS pathogenesis. *J Cell Biol* 201, 361-372.
- Lin, A.C., and Holt, C.E. (2007). Local translation and directional steering in axons. *The EMBO journal* 26, 3729-3736.
- Lin, Y., Protter, D.S., Rosen, M.K., and Parker, R. (2015). Formation and Maturation of Phase-Separated Liquid Droplets by RNA-Binding Proteins. *Mol Cell* 60, 208-219.
- Ling, K.K., Gibbs, R.M., Feng, Z., and Ko, C.P. (2012). Severe neuromuscular denervation of clinically relevant muscles in a mouse model of spinal muscular atrophy. *Hum Mol Genet* 21, 185-195.
- Ling, S.C., Polymenidou, M., and Cleveland, D.W. (2013). Converging mechanisms in ALS and FTD: disrupted RNA and protein homeostasis. *Neuron* 79, 416-438.
- Lionnet, T., Czaplinski, K., Darzacq, X., Shav-Tal, Y., Wells, A.L., Chao, J.A., Park, H.Y., de Turriz, V., Lopez-Jones, M., and Singer, R.H. (2011). A transgenic mouse for in vivo detection of endogenous labeled mRNA. *Nat Methods* 8, 165-170.

Little, D., Valori, C.F., Mutsaers, C.A., Bennett, E.J., Wyles, M., Sharrack, B., Shaw, P.J., Gillingwater, T.H., Azzouz, M., and Ning, K. (2015). PTEN depletion decreases disease severity and modestly prolongs survival in a mouse model of spinal muscular atrophy. *Mol Ther* 23, 270-277.

Liu, H., Yazdani, A., Murray, L.M., Beauvais, A., and Kothary, R. (2014). The Smn-independent beneficial effects of trichostatin A on an intermediate mouse model of spinal muscular atrophy. *PloS one* 9, e101225.

Livak, K.J., and Schmittgen, T.D. (2001). Analysis of relative gene expression data using real-time quantitative PCR and the 2(-Delta Delta C(T)) Method. *Methods* 25, 402-408.

Lorson, C.L., Hahnen, E., Androphy, E.J., and Wirth, B. (1999a). A single nucleotide in the SMN gene regulates splicing and is responsible for spinal muscular atrophy. *Proc Natl Acad Sci U S A* 96, 6307-6311.

Lorson, C.L., Hahnen, E., Androphy, E.J., and Wirth, B. (1999b). A single nucleotide in the SMN gene regulates splicing and is responsible for spinal muscular atrophy. *Proc Natl Acad Sci U S A* 96, 6307-6311.

Lotti, F., Imlach, W.L., Saieva, L., Beck, E.S., Hao le, T., Li, D.K., Jiao, W., Mentis, G.Z., Beattie, C.E., McCabe, B.D., and Pellizzoni, L. (2012). An SMN-dependent U12 splicing event essential for motor circuit function. *Cell* 151, 440-454.

Luo, Y., Blechingberg, J., Fernandes, A.M., Li, S., Fryland, T., Borglum, A.D., Bolund, L., and Nielsen, A.L. (2015). EWS and FUS bind a subset of transcribed genes encoding proteins enriched in RNA regulatory functions. *BMC Genomics* 16, 929.

Lutz, C.M., Kariya, S., Patruni, S., Osborne, M.A., Liu, D., Henderson, C.E., Li, D.K., Pellizzoni, L., Rojas, J., Valenzuela, D.M., *et al.* (2011). Postsymptomatic restoration of SMN rescues the disease phenotype in a mouse model of severe spinal muscular atrophy. *J Clin Invest* 121, 3029-3041.

Ma, H., Tu, L.C., Naseri, A., Huisman, M., Zhang, S., Grunwald, D., and Pederson, T. (2016). Multiplexed labeling of genomic loci with dCas9 and engineered sgRNAs using CRISPRainbow. *Nat Biotechnol* 34, 528-530.

Mahdavi, A., Hamblin, G.D., Jindal, G.A., Bagert, J.D., Dong, C., Sweredoski, M.J., Hess, S., Schuman, E.M., and Tirrell, D.A. (2016). Engineered Aminoacyl-tRNA Synthetase for Cell-Selective Analysis of Mammalian Protein Synthesis. *J Am Chem Soc* 138, 4278-4281.

- Majumder, P., Chu, J.F., Chatterjee, B., Swamy, K.B., and Shen, C.J. (2016). Co-regulation of mRNA translation by TDP-43 and Fragile X Syndrome protein FMRP. *Acta Neuropathol* 132, 721-738.
- Mardakheh, F.K., Paul, A., Kumper, S., Sadok, A., Paterson, H., McCarthy, A., Yuan, Y., and Marshall, C.J. (2015). Global Analysis of mRNA, Translation, and Protein Localization: Local Translation Is a Key Regulator of Cell Protrusions. *Dev Cell* 35, 344-357.
- Martin, K.C., and Ephrussi, A. (2009). mRNA localization: gene expression in the spatial dimension. *Cell* 136, 719-730.
- Martin, R., Gupta, K., Ninan, N.S., Perry, K., and Van Duyne, G.D. (2012). The survival motor neuron protein forms soluble glycine zipper oligomers. *Structure* 20, 1929-1939.
- Marzluff, W.F., Wagner, E.J., and Duronio, R.J. (2008). Metabolism and regulation of canonical histone mRNAs: life without a poly(A) tail. *Nat Rev Genet* 9, 843-854.
- McKinlay, C.J., Vargas, J.R., Blake, T.R., Hardy, J.W., Kanada, M., Contag, C.H., Wender, P.A., and Waymouth, R.M. (2017). Charge-altering releasable transporters (CARTs) for the delivery and release of mRNA in living animals. *Proc Natl Acad Sci U S A* 114, E448-E456.
- McMahon, A.C., Rahman, R., Jin, H., Shen, J.L., Fieldsend, A., Luo, W., and Rosbash, M. (2016). TRIBE: Hijacking an RNA-Editing Enzyme to Identify Cell-Specific Targets of RNA-Binding Proteins. *Cell* 165, 742-753.
- McWhorter, M.L., Monani, U.R., Burghes, A.H., and Beattie, C.E. (2003). Knockdown of the survival motor neuron (Smn) protein in zebrafish causes defects in motor axon outgrowth and pathfinding. *J Cell Biol* 162, 919-931.
- Medioni, C., Ramialison, M., Ephrussi, A., and Besse, F. (2014). Imp promotes axonal remodeling by regulating profilin mRNA during brain development. *Curr Biol* 24, 793-800.
- Meister, G., Buhler, D., Pillai, R., Lottspeich, F., and Fischer, U. (2001). A multiprotein complex mediates the ATP-dependent assembly of spliceosomal U snRNPs. *Nat Cell Biol* 3, 945-949.

- Meola, G., and Cardani, R. (2015). Myotonic dystrophies: An update on clinical aspects, genetic, pathology, and molecular pathomechanisms. *Biochim Biophys Acta* 1852, 594-606.
- Merianda, T.T., Coleman, J., Kim, H.H., Kumar Sahoo, P., Gomes, C., Brito-Vargas, P., Rauvala, H., Blesch, A., Yoo, S., and Twiss, J.L. (2015). Axonal amphoterin mRNA is regulated by translational control and enhances axon outgrowth. *J Neurosci* 35, 5693-5706.
- Merianda, T.T., Gomes, C., Yoo, S., Vuppalachchi, D., and Twiss, J.L. (2013). Axonal localization of neuritin/CPG15 mRNA in neuronal populations through distinct 5' and 3' UTR elements. *J Neurosci* 33, 13735-13742.
- Michaevlevski, I., Medzihradzsky, K.F., Lynn, A., Burlingame, A.L., and Fainzilber, M. (2010). Axonal transport proteomics reveals mobilization of translation machinery to the lesion site in injured sciatic nerve. *Mol Cell Proteomics* 9, 976-987.
- Miley, M.P., Brown, C.M., and Mouland, A.J. (2010). Live cell visualization of the interactions between HIV-1 Gag and the cellular RNA-binding protein Staufen1. *Retrovirology* 7, 41.
- Mili, S., Moissoglu, K., and Macara, I.G. (2008). Genome-wide screen reveals APC-associated RNAs enriched in cell protrusions. *Nature* 453, 115-119.
- Miller, S., Yasuda, M., Coats, J.K., Jones, Y., Martone, M.E., and Mayford, M. (2002). Disruption of dendritic translation of CaMKIIalpha impairs stabilization of synaptic plasticity and memory consolidation. *Neuron* 36, 507-519.
- Moffitt, J.R., Hao, J., Wang, G., Chen, K.H., Babcock, H.P., and Zhuang, X. (2016). High-throughput single-cell gene-expression profiling with multiplexed error-robust fluorescence in situ hybridization. *Proc Natl Acad Sci U S A* 113, 11046-11051.
- Monani, U.R. (2005). Spinal muscular atrophy: a deficiency in a ubiquitous protein; a motor neuron-specific disease. *Neuron* 48, 885-895.
- Monani, U.R., Sendtner, M., Coover, D.D., Parsons, D.W., Andreassi, C., Le, T.T., Jablonka, S., Schrank, B., Rossoll, W., Prior, T.W., *et al.* (2000). The human centromeric survival motor neuron gene (SMN2) rescues embryonic lethality in *Smn(-/-)* mice and results in a mouse with spinal muscular atrophy. *Hum Mol Genet* 9, 333-339.

Morgan, I.G., and Austin, L. (1968). Synaptosomal protein synthesis in a cell-free system. *Journal of neurochemistry* 15, 41-51.

Morgan, I.G., and Austin, L. (1969). Ion effects and protein synthesis in synaptosomal fraction. *J Neurobiol* 1, 155-167.

Morisaki, T., Lyon, K., DeLuca, K.F., DeLuca, J.G., English, B.P., Zhang, Z., Lavis, L.D., Grimm, J.B., Viswanathan, S., Looger, L.L., *et al.* (2016). Real-time quantification of single RNA translation dynamics in living cells. *Science* 352, 1425-1429.

Murakami, T., Qamar, S., Lin, J.Q., Schierle, G.S., Rees, E., Miyashita, A., Costa, A.R., Dodd, R.B., Chan, F.T., Michel, C.H., *et al.* (2015). ALS/FTD Mutation-Induced Phase Transition of FUS Liquid Droplets and Reversible Hydrogels into Irreversible Hydrogels Impairs RNP Granule Function. *Neuron* 88, 678-690.

Nagaoka, K., Udagawa, T., and Richter, J.D. (2012). CPEB-mediated ZO-1 mRNA localization is required for epithelial tight-junction assembly and cell polarity. *Nat Commun* 3, 675.

Nelles, D.A., Fang, M.Y., O'Connell, M.R., Xu, J.L., Markmiller, S.J., Doudna, J.A., and Yeo, G.W. (2016). Programmable RNA Tracking in Live Cells with CRISPR/Cas9. *Cell* 165, 488-496.

Ning, K., Drepper, C., Valori, C.F., Ahsan, M., Wyles, M., Higginbottom, A., Herrmann, T., Shaw, P., Azzouz, M., and Sendtner, M. (2010). PTEN depletion rescues axonal growth defect and improves survival in SMN-deficient motor neurons. *Hum Mol Genet* 19, 3159-3168.

Nizzardo, M., Simone, C., Dametti, S., Salani, S., Ulzi, G., Pagliarani, S., Rizzo, F., Frattini, E., Pagani, F., Bresolin, N., *et al.* (2015). Spinal muscular atrophy phenotype is ameliorated in human motor neurons by SMN increase via different novel RNA therapeutic approaches. *Sci Rep* 5, 11746.

Nizzardo, M., Simone, C., Salani, S., Ruepp, M.D., Rizzo, F., Ruggieri, M., Zanetta, C., Brajkovic, S., Moulton, H.M., Muehlemann, O., *et al.* (2014). Effect of combined systemic and local morpholino treatment on the spinal muscular atrophy Delta7 mouse model phenotype. *Clin Ther* 36, 340-356 e345.

O'Connell, M.R., Oakes, B.L., Sternberg, S.H., East-Seletsky, A., Kaplan, M., and Doudna, J.A. (2014). Programmable RNA recognition and cleavage by CRISPR/Cas9. *Nature* 516, 263-266.

Osman, E.Y., Miller, M.R., Robbins, K.L., Lombardi, A.M., Atkinson, A.K., Brehm, A.J., and Lorson, C.L. (2014). Morpholino antisense oligonucleotides targeting intronic repressor Element1 improve phenotype in SMA mouse models. *Hum Mol Genet* 23, 4832-4845.

Osterweil, E.K., Krueger, D.D., Reinhold, K., and Bear, M.F. (2010). Hypersensitivity to mGluR5 and ERK1/2 leads to excessive protein synthesis in the hippocampus of a mouse model of fragile X syndrome. *J Neurosci* 30, 15616-15627.

Otter, S., Grimmmler, M., Neuenkirchen, N., Chari, A., Sickmann, A., and Fischer, U. (2007). A comprehensive interaction map of the human survival of motor neuron (SMN) complex. *J Biol Chem* 282, 5825-5833.

Pagliardini, S., Giavazzi, A., Setola, V., Lizier, C., Di Luca, M., DeBiasi, S., and Battaglia, G. (2000). Subcellular localization and axonal transport of the survival motor neuron (SMN) protein in the developing rat spinal cord. *Hum Mol Genet* 9, 47-56.

Patel, V.L., Mitra, S., Harris, R., Buxbaum, A.R., Lionnet, T., Brenowitz, M., Girvin, M., Levy, M., Almo, S.C., Singer, R.H., and Chao, J.A. (2012). Spatial arrangement of an RNA zipcode identifies mRNAs under post-transcriptional control. *Genes Dev* 26, 43-53.

Pellizzoni, L. (2007). Chaperoning ribonucleoprotein biogenesis in health and disease. *EMBO Rep* 8, 340-345.

Pellizzoni, L., Yong, J., and Dreyfuss, G. (2002). Essential role for the SMN complex in the specificity of snRNP assembly. *Science* 298, 1775-1779.

Penagarikano, O., Mulle, J.G., and Warren, S.T. (2007). The pathophysiology of fragile x syndrome. *Annu Rev Genomics Hum Genet* 8, 109-129.

Peritz, T., Zeng, F., Kannanayakal, T.J., Kilk, K., Eiriksdottir, E., Langel, U., and Eberwine, J. (2006). Immunoprecipitation of mRNA-protein complexes. *Nat Protoc* 1, 577-580.

Peter, C.J., Evans, M., Thayanithy, V., Taniguchi-Ishigaki, N., Bach, I., Kolpak, A., Bassell, G.J., Rossoll, W., Lorson, C.L., Bao, Z.Z., and Androphy, E.J. (2011). The COPI vesicle complex binds and moves with survival motor neuron within axons. *Hum Mol Genet* 20, 1701-1711.

Phan, H.C., Taylor, J.L., Hannon, H., and Howell, R. (2015). Newborn screening for spinal muscular atrophy: Anticipating an imminent need. *Semin Perinatol* 39, 217-229.

Piazzon, N., Rage, F., Schlotter, F., Moine, H., Branlant, C., and Massenet, S. (2008). In vitro and in cellulo evidences for association of the survival of motor neuron complex with the fragile X mental retardation protein. *J Biol Chem* 283, 5598-5610.

Pichon, X., Bastide, A., Safieddine, A., Chouaib, R., Samacoits, A., Basyuk, E., Peter, M., Mueller, F., and Bertrand, E. (2016). Visualization of single endogenous polysomes reveals the dynamics of translation in live human cells. *J Cell Biol* 214, 769-781.

Pillai, R.S., Grimmmler, M., Meister, G., Will, C.L., Luhrmann, R., Fischer, U., and Schumperli, D. (2003). Unique Sm core structure of U7 snRNPs: assembly by a specialized SMN complex and the role of a new component, Lsm11, in histone RNA processing. *Genes Dev* 17, 2321-2333.

Pineiro, D., Fernandez, N., Ramajo, J., and Martinez-Salas, E. (2013). Gemin5 promotes IRES interaction and translation control through its C-terminal region. *Nucleic Acids Res* 41, 1017-1028.

Pineiro, D., Fernandez-Chamorro, J., Francisco-Velilla, R., and Martinez-Salas, E. (2015). Gemin5: A Multitasking RNA-Binding Protein Involved in Translation Control. *Biomolecules* 5, 528-544.

Porensky, P.N., Mitrpant, C., McGovern, V.L., Bevan, A.K., Foust, K.D., Kaspar, B.K., Wilton, S.D., and Burghes, A.H. (2012). A single administration of morpholino antisense oligomer rescues spinal muscular atrophy in mouse. *Hum Mol Genet* 21, 1625-1638.

Praveen, K., Wen, Y., and Matera, A.G. (2012). A Drosophila model of spinal muscular atrophy uncouples snRNP biogenesis functions of survival motor neuron from locomotion and viability defects. *Cell Rep* 1, 624-631.

Preitner, N., Quan, J., Nowakowski, D.W., Hancock, M.L., Shi, J., Tcherkezian, J., Young-Pearse, T.L., and Flanagan, J.G. (2014). APC is an RNA-binding protein, and its interactome provides a link to neural development and microtubule assembly. *Cell* 158, 368-382.

Prescott, A.R., Bales, A., James, J., Trinkle-Mulcahy, L., and Sleeman, J.E. (2014). Time-resolved quantitative proteomics implicates the core snRNP

protein SmB together with SMN in neural trafficking. *Journal of cell science* 127, 812-827.

Prior, T.W. (2010). Perspectives and diagnostic considerations in spinal muscular atrophy. *Genet Med* 12, 145-152.

Pyhtila, B., Zheng, T., Lager, P.J., Keene, J.D., Reedy, M.C., and Nicchitta, C.V. (2008). Signal sequence- and translation-independent mRNA localization to the endoplasmic reticulum. *Rna* 14, 445-453.

Rackham, O., and Brown, C.M. (2004). Visualization of RNA-protein interactions in living cells: FMRP and IMP1 interact on mRNAs. *The EMBO journal* 23, 3346-3355.

Rage, F., Boulisfane, N., Rihan, K., Neel, H., Gostan, T., Bertrand, E., Bordonne, R., and Soret, J. (2013). Genome-wide identification of mRNAs associated with the protein SMN whose depletion decreases their axonal localization. *Rna* 19, 1755-1766.

Ray, D., Kazan, H., Cook, K.B., Weirauch, M.T., Najafabadi, H.S., Li, X., Gueroussov, S., Albu, M., Zheng, H., Yang, A., *et al.* (2013). A compendium of RNA-binding motifs for decoding gene regulation. *Nature* 499, 172-177.

Renton, A.E., Chio, A., and Traynor, B.J. (2014). State of play in amyotrophic lateral sclerosis genetics. *Nat Neurosci* 17, 17-23.

Richter, J.D., Bassell, G.J., and Klann, E. (2015). Dysregulation and restoration of translational homeostasis in fragile X syndrome. *Nat Rev Neurosci* 16, 595-605.

Riessland, M., Ackermann, B., Forster, A., Jakubik, M., Hauke, J., Garbes, L., Fritzsche, I., Mende, Y., Blumcke, I., Hahnen, E., and Wirth, B. (2010). SAHA ameliorates the SMA phenotype in two mouse models for spinal muscular atrophy. *Hum Mol Genet* 19, 1492-1506.

Rishal, I., and Fainzilber, M. (2014). Axon-soma communication in neuronal injury. *Nat Rev Neurosci* 15, 32-42.

Romano, M., Feiguin, F., and Buratti, E. (2016). TBPH/TDP-43 modulates translation of *Drosophila futsch* mRNA through an UG-rich sequence within its 5'UTR. *Brain research* 1647, 50-56.

Ross, A.F., Oleynikov, Y., Kislauskis, E.H., Taneja, K.L., and Singer, R.H. (1997). Characterization of a beta-actin mRNA zipcode-binding protein. *Mol Cell Biol* 17, 2158-2165.

Rossoll, W., and Bassell, G.J. (2009a). Spinal Muscular Atrophy and a Model for Survival of Motor Neuron Protein Function in Axonal Ribonucleoprotein Complexes. *Results Probl Cell Differ*.

Rossoll, W., and Bassell, G.J. (2009b). Spinal muscular atrophy and a model for survival of motor neuron protein function in axonal ribonucleoprotein complexes. *Results Probl Cell Differ* 48, 289-326.

Rossoll, W., Jablonka, S., Andreassi, C., Kroning, A.K., Karle, K., Monani, U.R., and Sendtner, M. (2003). Smn, the spinal muscular atrophy-determining gene product, modulates axon growth and localization of beta-actin mRNA in growth cones of motoneurons. *J Cell Biol* 163, 801-812.

Rossoll, W., Kroning, A.K., Ohndorf, U.M., Steegborn, C., Jablonka, S., and Sendtner, M. (2002). Specific interaction of Smn, the spinal muscular atrophy determining gene product, with hnRNP-R and gry-rbp/hnRNP-Q: a role for Smn in RNA processing in motor axons? *Hum Mol Genet* 11, 93-105.

Roux, K.J., Kim, D.I., and Burke, B. (2013). BioID: a screen for protein-protein interactions. *Curr Protoc Protein Sci* 74, Unit 19 23.

Saal, L., Briese, M., Kneitz, S., Glinka, M., and Sendtner, M. (2014). Subcellular transcriptome alterations in a cell culture model of spinal muscular atrophy point to widespread defects in axonal growth and presynaptic differentiation. *Rna* 20, 1789-1802.

Sachdeva, R., Farrell, K., McMullen, M.K., Twiss, J.L., and Houle, J.D. (2016). Dynamic Changes in Local Protein Synthetic Machinery in Regenerating Central Nervous System Axons after Spinal Cord Injury. *Neural Plast* 2016, 4087254.

Sanchez, G., Bondy-Chorney, E., Laframboise, J., Paris, G., Didillon, A., Jasmin, B.J., and Cote, J. (2015). A novel role for CARM1 in promoting nonsense-mediated mRNA decay: potential implications for spinal muscular atrophy. *Nucleic Acids Res*.

Sanchez, G., Dury, A.Y., Murray, L.M., Biondi, O., Tadesse, H., El Fatimy, R., Kothary, R., Charbonnier, F., Khandjian, E.W., and Cote, J. (2013). A novel

function for the survival motoneuron protein as a translational regulator. *Hum Mol Genet* 22, 668-684.

Santini, E., and Klann, E. (2014). Reciprocal signaling between translational control pathways and synaptic proteins in autism spectrum disorders. *Sci Signal* 7, re10.

Santoro, M.R., Bray, S.M., and Warren, S.T. (2012). Molecular mechanisms of fragile X syndrome: a twenty-year perspective. *Annu Rev Pathol* 7, 219-245.

Sanz, E., Evanoff, R., Quintana, A., Evans, E., Miller, J.A., Ko, C., Amieux, P.S., Griswold, M.D., and McKnight, G.S. (2013). RiboTag analysis of actively translated mRNAs in Sertoli and Leydig cells in vivo. *PloS one* 8, e66179.

Sanz, E., Yang, L., Su, T., Morris, D.R., McKnight, G.S., and Amieux, P.S. (2009). Cell-type-specific isolation of ribosome-associated mRNA from complex tissues. *Proc Natl Acad Sci U S A* 106, 13939-13944.

Sasaki, Y., Welshhans, K., Wen, Z., Yao, J., Xu, M., Goshima, Y., Zheng, J.Q., and Bassell, G.J. (2010). Phosphorylation of zipcode binding protein 1 is required for brain-derived neurotrophic factor signaling of local beta-actin synthesis and growth cone turning. *J Neurosci* 30, 9349-9358.

Schmidt, E.K., Clavarino, G., Ceppi, M., and Pierre, P. (2009). SUnSET, a nonradioactive method to monitor protein synthesis. *Nat Methods* 6, 275-277.

Schrank, B., Gotz, R., Gunnensen, J.M., Ure, J.M., Toyka, K.V., Smith, A.G., and Sendtner, M. (1997). Inactivation of the survival motor neuron gene, a candidate gene for human spinal muscular atrophy, leads to massive cell death in early mouse embryos. *Proc Natl Acad Sci U S A* 94, 9920-9925.

Schwartz, T.U. (2007). Origins and evolution of cotranslational transport to the ER. *Adv Exp Med Biol* 607, 52-60.

See, K., Yadav, P., Giegerich, M., Cheong, P.S., Graf, M., Vyas, H., Lee, S.G., Mathavan, S., Fischer, U., Sendtner, M., and Winkler, C. (2014). SMN deficiency alters *Nrxn2* expression and splicing in zebrafish and mouse models of spinal muscular atrophy. *Hum Mol Genet* 23, 1754-1770.

Selth, L.A., Gilbert, C., and Svejstrup, J.Q. (2009). RNA immunoprecipitation to determine RNA-protein associations in vivo. *Cold Spring Harb Protoc* 2009, pdb prot5234.

Shababi, M., Lorson, C.L., and Rudnik-Schoneborn, S.S. (2013). Spinal muscular atrophy: a motor neuron disorder or a multi-organ disease? *Journal of anatomy*.

Shababi, M., Lorson, C.L., and Rudnik-Schoneborn, S.S. (2014). Spinal muscular atrophy: a motor neuron disorder or a multi-organ disease? *Journal of anatomy* 224, 15-28.

Shafey, D., Boyer, J.G., Bhanot, K., and Kothary, R. (2010). Identification of novel interacting protein partners of SMN using tandem affinity purification. *J Proteome Res* 9, 1659-1669.

Sharma, A., Lyashchenko, A.K., Lu, L., Nasrabady, S.E., Elmaleh, M., Mendelsohn, M., Nemes, A., Tapia, J.C., Mentis, G.Z., and Shneider, N.A. (2016). ALS-associated mutant FUS induces selective motor neuron degeneration through toxic gain of function. *Nat Commun* 7, 10465.

Shestakova, E.A., Singer, R.H., and Condeelis, J. (2001). The physiological significance of beta -actin mRNA localization in determining cell polarity and directional motility. *Proc Natl Acad Sci U S A* 98, 7045-7050.

Shigeoka, T., Jung, H., Jung, J., Turner-Bridger, B., Ohk, J., Lin, J.Q., Amieux, P.S., and Holt, C.E. (2016). Dynamic Axonal Translation in Developing and Mature Visual Circuits. *Cell* 166, 181-192.

Shukla, S., and Parker, R. (2016). Hypo- and Hyper-Assembly Diseases of RNA-Protein Complexes. *Trends Mol Med* 22, 615-628.

Singh, N.N., Lee, B.M., DiDonato, C.J., and Singh, R.N. (2015). Mechanistic principles of antisense targets for the treatment of spinal muscular atrophy. *Future Med Chem* 7, 1793-1808.

So, B.R., Wan, L., Zhang, Z., Li, P., Babiash, E., Duan, J., Younis, I., and Dreyfuss, G. (2016). A U1 snRNP-specific assembly pathway reveals the SMN complex as a versatile hub for RNP exchange. *Nat Struct Mol Biol*.

Staropoli, J.F., Li, H., Chun, S.J., Allaire, N., Cullen, P., Thai, A., Fleet, C.M., Hua, Y., Bennett, C.F., Krainer, A.R., *et al.* (2015). Rescue of gene-expression changes in an induced mouse model of spinal muscular atrophy by an antisense oligonucleotide that promotes inclusion of SMN2 exon 7. *Genomics* 105, 220-228.

Steward, O., and Levy, W.B. (1982). Preferential localization of polyribosomes under the base of dendritic spines in granule cells of the dentate gyrus. *J Neurosci* 2, 284-291.

Steward, O., and Schuman, E.M. (2001). Protein synthesis at synaptic sites on dendrites. *Annu Rev Neurosci* 24, 299-325.

Steward, O., and Worley, P. (2001). Localization of mRNAs at synaptic sites on dendrites. *Results Probl Cell Differ* 34, 1-26.

Sun, S., Ling, S.C., Qiu, J., Albuquerque, C.P., Zhou, Y., Tokunaga, S., Li, H., Qiu, H., Bui, A., Yeo, G.W., *et al.* (2015). ALS-causative mutations in FUS/TLS confer gain and loss of function by altered association with SMN and U1-snRNP. *Nat Commun* 6, 6171.

Swanger, S.A., and Bassell, G.J. (2013). Dendritic protein synthesis in the normal and diseased brain. *Neuroscience* 232, 106-127.

Sylwestrak, E.L., Rajasethupathy, P., Wright, M.A., Jaffe, A., and Deisseroth, K. (2016). Multiplexed Intact-Tissue Transcriptional Analysis at Cellular Resolution. *Cell* 164, 792-804.

Tadesse, H., Deschenes-Furry, J., Boisvenue, S., and Cote, J. (2008). KH-type splicing regulatory protein interacts with survival motor neuron protein and is misregulated in spinal muscular atrophy. *Hum Mol Genet* 17, 506-524.

Taliaferro, J.M., Vidaki, M., Oliveira, R., Olson, S., Zhan, L., Saxena, T., Wang, E.T., Graveley, B.R., Gertler, F.B., Swanson, M.S., and Burge, C.B. (2016). Distal Alternative Last Exons Localize mRNAs to Neural Projections. *Mol Cell* 61, 821-833.

Tanenbaum, M.E., Gilbert, L.A., Qi, L.S., Weissman, J.S., and Vale, R.D. (2014). A protein-tagging system for signal amplification in gene expression and fluorescence imaging. *Cell* 159, 635-646.

Tatavarty, V., Ifrim, M.F., Levin, M., Korza, G., Barbarese, E., Yu, J., and Carson, J.H. (2012). Single-molecule imaging of translational output from individual RNA granules in neurons. *Mol Biol Cell* 23, 918-929.

Tcherkezian, J., Brittis, P.A., Thomas, F., Roux, P.P., and Flanagan, J.G. (2010). Transmembrane receptor DCC associates with protein synthesis machinery and regulates translation. *Cell* 141, 632-644.

- Terns, M.P., and Terns, R.M. (2001). Macromolecular complexes: SMN--the master assembler. *Curr Biol* 11, R862-864.
- Tkach, M., and Thery, C. (2016). Communication by Extracellular Vesicles: Where We Are and Where We Need to Go. *Cell* 164, 1226-1232.
- Todd, A.G., Lin, H., Ebert, A.D., Liu, Y., and Androphy, E.J. (2013). COPI transport complexes bind to specific RNAs in neuronal cells. *Hum Mol Genet* 22, 729-736.
- tom Dieck, S., Kochen, L., Hanus, C., Heumuller, M., Bartnik, I., Nassim-Assir, B., Merk, K., Mosler, T., Garg, S., Bunse, S., *et al.* (2015). Direct visualization of newly synthesized target proteins in situ. *Nat Methods* 12, 411-414.
- Tom Dieck, S., Muller, A., Nehring, A., Hinz, F.I., Bartnik, I., Schuman, E.M., and Dieterich, D.C. (2012). Metabolic labeling with noncanonical amino acids and visualization by chemoselective fluorescent tagging. *Curr Protoc Cell Biol* Chapter 7, Unit7 11.
- Twiss, J.L., Kalinski, A.L., Sachdeva, R., and Houle, J.D. (2016). Intra-axonal protein synthesis - a new target for neural repair? *Neural Regen Res* 11, 1365-1367.
- Ule, J., Jensen, K., Mele, A., and Darnell, R.B. (2005). CLIP: a method for identifying protein-RNA interaction sites in living cells. *Methods* 37, 376-386.
- Vangipuram, M., Ting, D., Kim, S., Diaz, R., and Schule, B. (2013). Skin punch biopsy explant culture for derivation of primary human fibroblasts. *J Vis Exp*, e3779.
- Wang, C., Han, B., Zhou, R., and Zhuang, X. (2016a). Real-Time Imaging of Translation on Single mRNA Transcripts in Live Cells. *Cell* 165, 990-1001.
- Wang, E.T., Cody, N.A., Jog, S., Biancolella, M., Wang, T.T., Treacy, D.J., Luo, S., Schroth, G.P., Housman, D.E., Reddy, S., *et al.* (2012). Transcriptome-wide regulation of pre-mRNA splicing and mRNA localization by muscleblind proteins. *Cell* 150, 710-724.
- Wang, E.T., Taliaferro, J.M., Lee, J.A., Sudhakaran, I.P., Rossoll, W., Gross, C., Moss, K.R., and Bassell, G.J. (2016b). Dysregulation of mRNA Localization and Translation in Genetic Disease. *J Neurosci* 36, 11418-11426.

- Wang, H., Dichtenberg, J.B., Ku, L., Li, W., Bassell, G.J., and Feng, Y. (2008a). Dynamic Association of the Fragile X Mental Retardation Protein as a Messenger Ribonucleoprotein between Microtubules and Polyribosomes. *Mol Biol Cell* 19, 105-114.
- Wang, I.F., Wu, L.S., Chang, H.Y., and Shen, C.K. (2008b). TDP-43, the signature protein of FTL-D-U, is a neuronal activity-responsive factor. *Journal of neurochemistry* 105, 797-806.
- Welshhans, K., and Bassell, G.J. (2011). Netrin-1-induced local beta-actin synthesis and growth cone guidance requires zipcode binding protein 1. *J Neurosci* 31, 9800-9813.
- Weyn-Vanhentenryck, S.M., Mele, A., Yan, Q., Sun, S., Farny, N., Zhang, Z., Xue, C., Herre, M., Silver, P.A., Zhang, M.Q., *et al.* (2014). HITS-CLIP and integrative modeling define the Rbfox splicing-regulatory network linked to brain development and autism. *Cell Rep* 6, 1139-1152.
- Wheway, G., Schmidts, M., Mans, D.A., Szymanska, K., Nguyen, T.M., Racher, H., Phelps, I.G., Toedt, G., Kennedy, J., Wunderlich, K.A., *et al.* (2015). An siRNA-based functional genomics screen for the identification of regulators of ciliogenesis and ciliopathy genes. *Nat Cell Biol* 17, 1074-1087.
- Williams, K.R., McAninch, D.S., Stefanovic, S., Xing, L., Allen, M., Li, W., Feng, Y., Mihailescu, M.R., and Bassell, G.J. (2016). hnRNP-Q1 represses nascent axon growth in cortical neurons by inhibiting Gap-43 mRNA translation. *Mol Biol Cell* 27, 518-534.
- Willis, D.E., and Twiss, J.L. (2010). Regulation of protein levels in subcellular domains through mRNA transport and localized translation. *Mol Cell Proteomics* 9, 952-962.
- Willis, D.E., van Niekerk, E.A., Sasaki, Y., Mesngon, M., Merianda, T.T., Williams, G.G., Kendall, M., Smith, D.S., Bassell, G.J., and Twiss, J.L. (2007). Extracellular stimuli specifically regulate localized levels of individual neuronal mRNAs. *J Cell Biol* 178, 965-980.
- Workman, E., Kalda, C., Patel, A., and Battle, D.J. (2015). Gemin5 Binds to the Survival Motor Neuron mRNA to Regulate SMN Expression. *J Biol Chem* 290, 15662-15669.
- Wu, B., Eliscovich, C., Yoon, Y.J., and Singer, R.H. (2016). Translation dynamics of single mRNAs in live cells and neurons. *Science* 352, 1430-1435.

- Xing, L., and Bassell, G.J. (2013). mRNA localization: an orchestration of assembly, traffic and synthesis. *Traffic* 14, 2-14.
- Xing, L., Yao, X., Williams, K.R., and Bassell, G.J. (2012). Negative regulation of RhoA translation and signaling by hnRNP-Q1 affects cellular morphogenesis. *Mol Biol Cell* 23, 1500-1509.
- Yamazaki, T., Chen, S., Yu, Y., Yan, B., Haertlein, T.C., Carrasco, M.A., Tapia, J.C., Zhai, B., Das, R., Lalancette-Hebert, M., *et al.* (2012). FUS-SMN protein interactions link the motor neuron diseases ALS and SMA. *Cell Rep* 2, 799-806.
- Yan, X., Hoek, T.A., Vale, R.D., and Tanenbaum, M.E. (2016). Dynamics of Translation of Single mRNA Molecules In Vivo. *Cell* 165, 976-989.
- Yao, J., Sasaki, Y., Wen, Z., Bassell, G.J., and Zheng, J.Q. (2006). An essential role for beta-actin mRNA localization and translation in Ca²⁺-dependent growth cone guidance. *Nat Neurosci* 9, 1265-1273.
- Yasuda, K., Zhang, H., Loiselle, D., Haystead, T., Macara, I.G., and Mili, S. (2013). The RNA-binding protein Fus directs translation of localized mRNAs in APC-RNP granules. *J Cell Biol* 203, 737-746.
- Yi, S., Zhang, H., Gong, L., Wu, J., Zha, G., Zhou, S., Gu, X., and Yu, B. (2015). Deep Sequencing and Bioinformatic Analysis of Lesioned Sciatic Nerves after Crush Injury. *PloS one* 10, e0143491.
- Yin, J., Zhu, D., Zhang, Z., Wang, W., Fan, J., Men, D., Deng, J., Wei, H., Zhang, X.E., and Cui, Z. (2013). Imaging of mRNA-protein interactions in live cells using novel mCherry trimolecular fluorescence complementation systems. *PloS one* 8, e80851.
- Yoo, S., Kim, H.H., Kim, P., Donnelly, C.J., Kalinski, A.L., Vuppalachchi, D., Park, M., Lee, S.J., Merianda, T.T., Perrone-Bizzozero, N.I., and Twiss, J.L. (2013). A HuD-ZBP1 ribonucleoprotein complex localizes GAP-43 mRNA into axons through its 3' untranslated region AU-rich regulatory element. *Journal of neurochemistry* 126, 792-804.
- Yoon, B.C., Zivraj, K.H., and Holt, C.E. (2009). Local translation and mRNA trafficking in axon pathfinding. *Results Probl Cell Differ* 48, 269-288.
- Zhang, H., Xing, L., Rossoll, W., Wichterle, H., Singer, R.H., and Bassell, G.J. (2006). Multiprotein complexes of the survival of motor neuron protein SMN

with Gemins traffic to neuronal processes and growth cones of motor neurons. *J Neurosci* 26, 8622-8632.

Zhang, H.L., Pan, F., Hong, D., Shenoy, S.M., Singer, R.H., and Bassell, G.J. (2003). Active transport of the survival motor neuron protein and the role of exon-7 in cytoplasmic localization. *J Neurosci* 23, 6627-6637.

Zhang, H.L., Singer, R.H., and Bassell, G.J. (1999). Neurotrophin regulation of beta-actin mRNA and protein localization within growth cones. *J Cell Biol* 147, 59-70.

Zhang, Z., Lotti, F., Dittmar, K., Younis, I., Wan, L., Kasim, M., and Dreyfuss, G. (2008). SMN deficiency causes tissue-specific perturbations in the repertoire of snRNAs and widespread defects in splicing. *Cell* 133, 585-600.

Zhang, Z., Pinto, A.M., Wan, L., Wang, W., Berg, M.G., Oliva, I., Singh, L.N., Dengler, C., Wei, Z., and Dreyfuss, G. (2013). Dysregulation of synaptogenesis genes antecedes motor neuron pathology in spinal muscular atrophy. *Proc Natl Acad Sci U S A* 110, 19348-19353.

Zivraj, K.H., Tung, Y.C., Piper, M., Gumy, L., Fawcett, J.W., Yeo, G.S., and Holt, C.E. (2010). Subcellular profiling reveals distinct and developmentally regulated repertoire of growth cone mRNAs. *J Neurosci* 30, 15464-15478.

Zou, T., Yang, X., Pan, D., Huang, J., Sahin, M., and Zhou, J. (2011). SMN deficiency reduces cellular ability to form stress granules, sensitizing cells to stress. *Cell Mol Neurobiol* 31, 541-550.